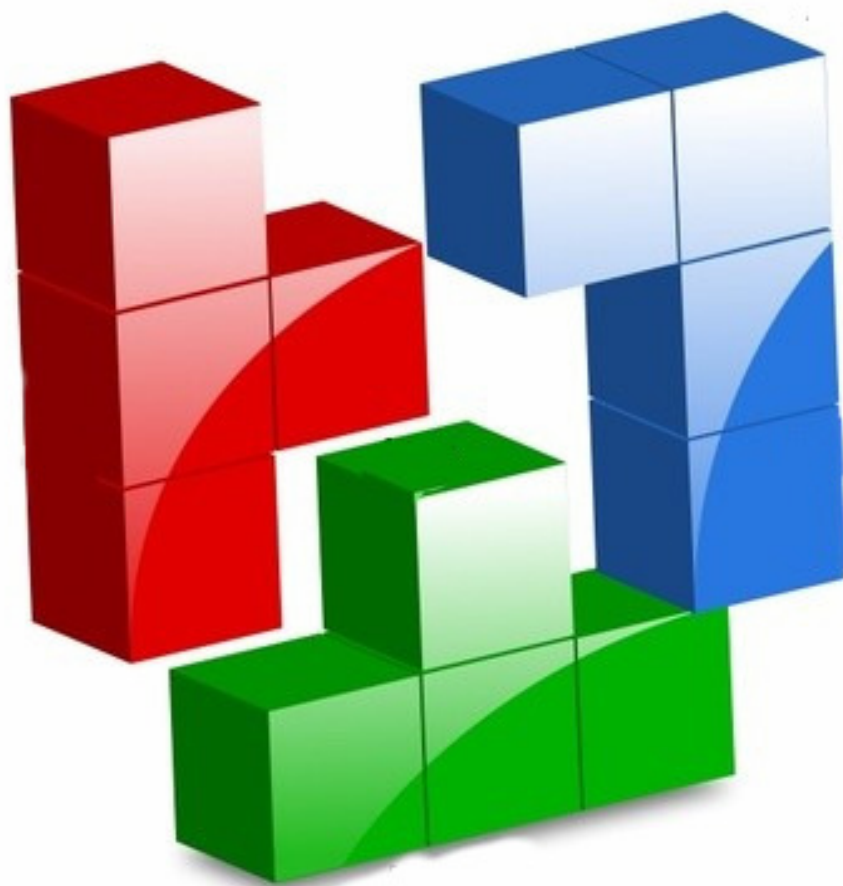


Doctoral Thesis in Chemical Sciences

Valentina Bambagioni



**DESIGN AND DEVELOPMENT OF
PALLADIUM-BASED ELECTROCATALYSTS
FOR DIRECT ALCOHOL FUEL CELLS:
THE CONVERSION OF RENEWABLES INTO
ENERGY AND CHEMICALS**



UNIVERSITA' DEGLI STUDI DI FIRENZE

Dottorato di Ricerca in Scienze Chimiche - Ciclo XXIII
Settore CHIM / 03 – Chimica generale e inorganica

**DESIGN AND DEVELOPMENT OF PALLADIUM-
BASED ELECTROCATALYSTS
FOR DIRECT ALCOHOL FUEL CELLS:
THE CONVERSION OF RENEWABLES INTO ENERGY
AND CHEMICALS**

Doctoral Thesis

Submitted by

VALENTINA BAMBAGIONI

Coordinator:
Prof. Andrea Goti

Tutor:
Dr. Claudio Bianchini

Table of contents

Frequently used abbreviations	V
Chapter 1: Introduction	1
1.1 Overview	1
1.2 The planet Earth safety	2
1.3 H ₂ : a fuel possible solution?	3
1.4 Other renewable fuels	8
1.5 The Direct Alcohol Fuel Cell (DAFC)	12
1.5.1 Cathode electrocatalysts	13
1.5.2 Polymer electrolyte membrane	14
1.5.3 Anode electrocatalysts	15
1.5.4 Synthetic strategies and characterization of electrocatalysts for DAFCs	18
1.6 Scope	20
1.7 References	21
Chapter 2: Palladium onto Nickel-Zinc supports	31
2.1 Overview	31
2.2 Introduction	32
2.3 Results and discussion	36
2.3.1 Catalyst synthesis	36
2.3.2 Catalyst characterization	37
2.3.3 Electrochemical characterization of the Pd-based catalysts in alkaline environment	45
2.3.4 Half-cell studies of ethanol oxidation on the Pd-based catalysts in alkaline environment	49
2.3.5 Direct Ethanol Fuel Cells (DEFCs) with Pd-based anode electrocatalysts	54
2.3.6 NaBH ₄ : an additive that improves the DEFC performance	59
2.3.7 Half-cell studies of ethylene glycol oxidation on the Pd-based catalysts in alkaline environment	65
2.3.7.1 In situ FTIR study in alkaline environment with ethylene glycol on Pd-based catalysts	71

2.3.8 Direct Ethylene Glycol Fuel Cells (DEGFCs) with Pd-based anode electrocatalysts	74
2.3.9 Half-cell studies of glycerol oxidation on the Pd-based catalysts in alkaline environment	78
2.3.10 Direct Glycerol Fuel Cells (DEGFCs) with Pd-based anode electrocatalysts	82
2.3.11 Half-cell studies of methanol oxidation on the Pd-based catalysts in alkaline environment	86
2.3.12 Direct Methanol Fuel Cells (DMFCs) with Pd-based anode electrocatalysts	90
2.4 Conclusions	93
2.5 Experimental section	97
2.5.1 Catalyst synthesis	97
2.5.2 Physical material characterization	98
2.5.3 Electrochemical studies	99
2.5.4 Fuel cell assembly	102
2.5.5 IC and NMR analysis	105
2.6 References	106
Chapter 3: Modified Palladium electrocatalysts	113
3.1 Overview	113
3.2 Introduction	114
3.3 Results and discussion	117
3.3.1 Catalyst synthesis	117
3.3.2 Catalyst characterization	118
3.3.3 Electrochemical characterization of the Pd-based catalysts in alkaline environment	122
3.3.4 Half-cell studies of ethanol oxidation on the Pd-based catalysts in alkaline environment	126
3.3.5 Direct Ethanol Fuel Cells (DEFCs) with Pd-based anode electrocatalysts	130
3.4 Conclusions	133
3.5 Experimental section	134
3.5.1 Catalyst synthesis	134
3.5.2 Physical material characterization	135
3.5.3 Electrochemical studies	136

3.5.4 Fuel Cell Assembly	137
3.5.5 IC and NMR analysis	138
3.6 References	139
Chapter 4: Technological Applications	145
4.1 Overview	145
4.2 Technological applications of a DAFC	146
4.3 References	148
Curriculum Vitae	151
Ringraziamenti	159

Frequently used abbreviations

FC	Fuel Cell
DAFC	Direct Alcohol Fuel Cell
DEFC	Direct Ethanol Fuel Cell
DEGFC	Direct Ethylene Glycol Fuel Cell
DGFC	Direct Glycerol Fuel Cell-Direct Glucose Fuel Cell
DMFC	Direct Methanol Fuel Cell
Gly	Glycerol
EG	Ethylene Glycol
MeOH	Methanol
EtOH	Ethanol
CV	Cyclic Voltammetry
MEA	Membrane Electrode Assembly
ORR	Oxygen Reduction Reaction
GFCs	Gas Flow Channels, cooling channels, bipolar plates
GDLs/MPLs	Gas Diffusion Layers, micro-porous layers
CLs	Catlyst Layers
AE	Alkaline Electrolizer
PME	Polymeric Membrane Electrolizer
EOR	Ethanol Oxidation Reaction
ETR	Electron Transfer Rate
Kj	Ketjen black carbon
EGOR	Ethylene Glycol Oxidation Reaction

To whoever works for a better world

1.1 Overview

The depletion of fossil fuels and climate changes caused by greenhouse gases are boosting increasing research efforts to find out alternative energy sources and technologies. Among these, fuel cells are receiving much attention for their efficiency as well as the capability to use, besides hydrogen, a variety of renewable fuels such as alcohols and carbohydrates. Fuel cells of which there exist different types according to the electrolyte employed, working temperature and fuel, are electrochemical devices that directly convert the chemical energy stored in a fuel into electrical energy with little or no emission of greenhouse gases, no noise and with high energy efficiency. In this doctorate thesis, we have focused our attention on Direct Alcohol Fuel Cells (DAFC), i. e. low temperature fuel cells that make use of renewable alcohols as fuel. We have synthesized several new anode electrocatalysts and have also developed a new type of DAFC where alcohols are partially and selectively oxidized to carboxylic acids.

1.2 The planet Earth safety

Climatic changes, rapidly growing world population and increasing energy shortage are current dramatic issues. Over the last two centuries, fossil fuels have been the primary source for the generation of electricity, domestic heating and transportation vehicles. Nowadays, this type of development is not allowed as fossil fuels are rapidly declining in quantity and quality. On the other hand, the Society's demand needs to be satisfied but this is possible only by safeguarding the environment to provide the future generations with a decent life standard. Establishing an equilibrium between mankind's needs and environment is a challenging task for all scientists.

In 1983 was established the Bruntland Commission (ONU) for the Environment and Development and in 1987 a document entitled "Our common future" appeared reporting on the Earth environment. During the Kyoto congress (1997), all industrialized countries agreed to limit remarkably the greenhouse emissions within 2012 by more than 5%. This year, in Cancun (Mexico) a further commitment to reduce the emission by 20% has been decided.

Chemistry can largely contribute to establish a real sustainable development: all new chemical processes must be selective and make use of nontoxic and recyclable reagents. Likewise, fossil fuels must be replaced, whenever possible, by renewable resources and energy produced by more efficient processes than the plain combustion of the resources themselves. In this doctorate thesis work, we have considered direct alcohol fuel cells as a tool to produce simultaneously energy and selective chemicals from renewable resources.

1.3 H₂ fuel: a possible solution?

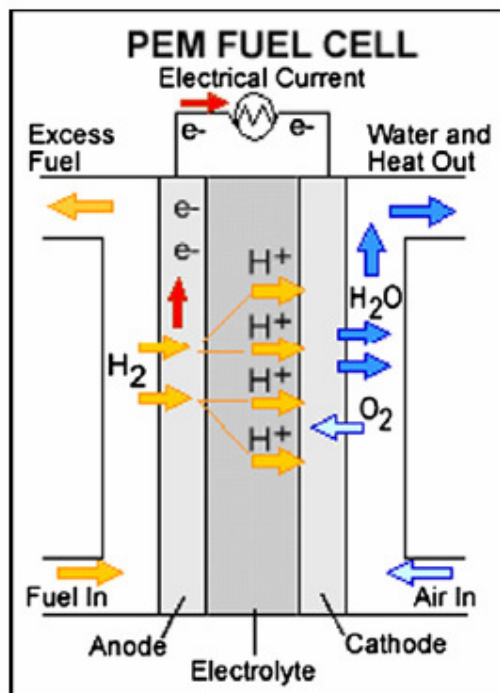
A fuel cell represents an attractive technology as tomorrow's energy vector, because it converts the chemical energy of a chemical compound (fuel) directly into electrical energy. Since fuel cells generate electricity through a chemical process, they are not subjected to the Carnot Limit, so they can extract more energy from fuel (40-70% efficiency) than traditional internal combustion engines (30% efficiency). If fed with H₂, no CO₂ is emitted by fuel cells. In addition a fuel cell can be recharge quickly with an amount of fresh fuel giving the same performances, while a common battery (lithium-battery, f.i.) stops working when it reaches the chemical equilibrium of the redox reaction ¹.

Fuel cells have been discovered in 1839 by William Grove, but the first practical applications appeared more than a century later with the advent of the space age (1950)² then the General Electric Company (GE) started developing fuel cells and was awarded a contract for the Gemini fuel space mission ³. Nowadays different kinds of fuel cells exist depending on the working temperature, type of fuel and electrolyte (Table 1). PEM fuel cells contain polymer electrolyte membranes (generally Nafion[®]) as proton exchange medium and platinum (Pt)-based materials as electrocatalysts. Their main features include low operating temperature, high power density, and easy scale-up, making PEM fuel cell a promising candidate as the next generation power sources for transportation, stationary, and portable applications. Scheme 1 shows a schematic of a PEM fuel cell. Furthermore the hydrogen is the most abundant element of the universe, as it is the simplest molecule and the energy request for breaking the H-H bond is (453 kJ/mol). The major application of PEM fuel cells is for automotive in city centers where pollution is more important than elsewhere ⁴.

	PEMFC	PAFC	MCFC	AFC	SOFC
Electrolyte	Polymer Electrolyte	Phosphoric Acid	Molten Carbonate	Alkaline solutions	Solid Oxide
Temperature	25-100°C	160-220°C	600-650°C	25-75°C 100-250°C	800-1000°C
Fuels	H ₂ , alcohols, light hydrocarbons	H ₂ , light hydrocarbons	H ₂ , light hydrocarbons	H ₂	H ₂ , hydrocarbons
Applications	Residential Portable Transport	Distribution	Industrial Distribution	Portable	Industrial

Table 1. Different kind of fuel cells for different electrolytes.

Other applications include distributed/stationary and portable power generators. The major motor companies are prevalently considering PEM fuel cells due to their high power density and excellent dynamic characteristics as compared with other kind of fuel cells ⁵. Auto makers such as Toyota, Honda, Hyudai, Daimler, and General Motors (GM) have announced plans of commercializing their fuel-cell vehicles by 2015 ⁶. Distributed PEM fuel cell power system is primarily focused on small scale (50–250 kW for decentralized use or <10 kW for households) ⁷. Early design of fuel cells was for residential power supply, in which the waste heat can be utilized for household usage ⁸. However, the high cost of PEM fuel cells remains a major barrier hindering their widespread application in this area. Indeed in general the world-wide commercialization barriers of PEMFCs are durability and cost of electrocatalysts and membrane ⁶. Fuel cell components, such as the MEA (membrane electrode assembly) ⁹, suffer degradation during long-term operations. The lifetime required by a commercial fuel cell is over 5000 operating hours for light-weight vehicles and over 40,000 h for stationary power generation with less than a 10% performance decay ^{10,11}. Various interrelated and complex phenomena occur during fuel cell operation, including mass/heat transfer, electrochemical reactions, and ionic/electronic transport, which governs fuel cell operation. For example, avoiding electrode flooding is of critical importance for optimal fuel-cell performance and durability; however this phenomenon is not well understood. The ability to model fuel and reactant transport and electrochemical reactions in



Scheme 1. A simplified and dissected view of the basic components of a proton exchange membrane hydrogen/oxygen fuel cell ¹².

electrodes is critical, particularly at the cathode side in which the oxygen reduction reaction (ORR) is sluggish and inefficient and water is generated. The fundamental understanding of the electrochemical activity at the triple-phase boundaries is a key to breakthroughs of further Pt-loading reduction ⁵. Specifically, as schematically shown in Figure 1, the following multi-physics, highly coupled and nonlinear transport and electrochemical phenomena take place during fuel cell operation ⁵: (1) hydrogen gas and air are forced (by pumping) to flow down the anode and cathode GFCs (Gas flow channels, cooling channels, and bipolar plates), respectively; (2) H₂ and O₂ flow through the respective porous GDLs/MPLs (Gas Diffusion Layers and micro-porous layers) and diffuse into the respective CLs (Catalyst layers); (3) H₂ is oxidized at the anode CL, forming protons and electrons; (4) protons migrate and water is transported through the membrane; (5) electrons are conducted via carbon support to the anode current collector, and then to the cathode current collector via an external circuit; (6) O₂ is reduced with protons and electrons at the cathode CL to form water; (7) product water is transported out of the cathode CL, through cathode GDL/MPL, and eventually out of the cathode GFC; and (8) heat is generated due to inefficiencies, mainly in the cathode

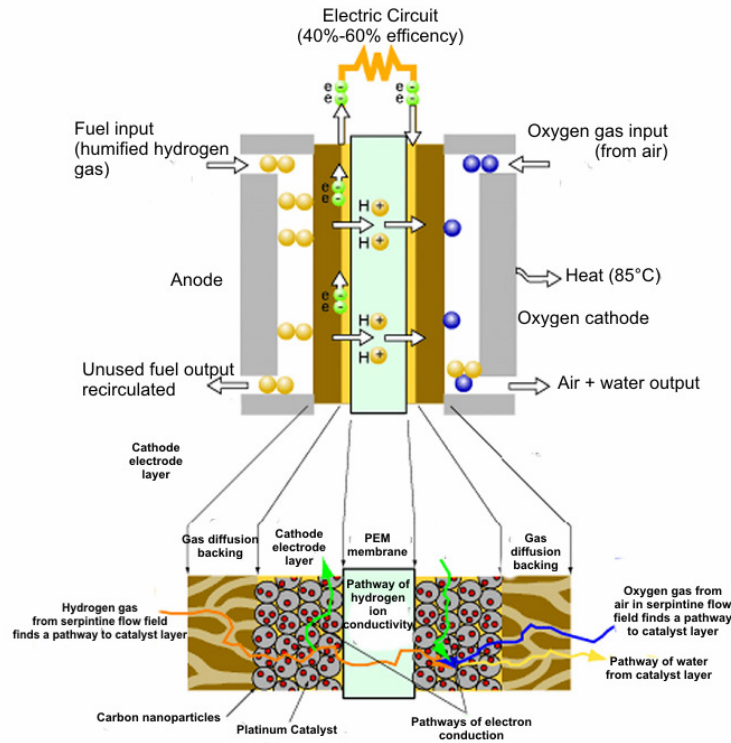
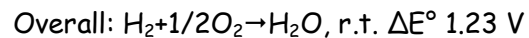


Figure 1. Phenomena in a PEMFC¹³.

CL due to the sluggish oxygen reduction reaction (ORR), and is conducted out of the cell via carbon support and BPs. The transport phenomena are three-dimensional because the flows of fuel (H_2) and oxidant (O_2) in the anode and cathode GFCs are usually normal to proton transport through the membrane and gas transport through the respective GDLs/MPLs and CLs. When operating under practical current loads, relatively high inlet humidity, liquid water is present within the fuel cell. Fundamental models have been developed to examine the transport processes based on the laws of conservation of mass, momentum, energy, species and charges and the multiphase mixture formulation^{14,15,16}. The reactions that occur in a PEMFC are shown below:



On the other hand, there are other important aspects to consider to overcome the barriers to the commercialization of PEMFCs. The hydrogen production from water electrolysis represents an alternative to the production of hydrogen from fossil fuels

(reforming of hydrocarbons), and the only way where renewable energy can be exploited to produce highly pure hydrogen (99.999%)¹⁷. Unfortunately this process requires too much energy (ΔE° 1.228V energy request).

Botte et al.^{18,19,20} studied the aqueous ammonia electrolysis on Pt-Ir catalysts in alkaline electrolyzer (AE) needs of 0.36V at 60°C. Other authors used methanol in anode compartment of a PME (Polymeric Membrane Electrolyzer) containing cation-exchange membrane on a Pt catalyst^{21,22}. The oxidation reaction produces CO₂ and the anode material slowly gets poisoned by CO coordination on active sites, which leads to high overpotentials²³. Recently in our lab a PME which electrolyzes renewable alcohols-water to chemicals and pure hydrogen was prepared (ΔE° 0.127V)²⁴. In addition to other issues, efficient hydrogen storage is still an unresolved problem to consider in the hydrogen economy.

1.4 Other renewable fuels

An interesting alternative to the hydrogen-fuel is represented by liquid fuels such as renewable alcohols. The devices which use this kind of fuel are named Direct Alcohol Fuel Cells (DAFCs). Compared to gaseous fuels, liquid fuels have the advantage of high energy density as well as easy transportation and handling. On the other hand the oxidation kinetics of any alcohol are much slower and still H₂-fueled PEMFCs exhibit superior electrical performance as compared to DAFCs with comparable electroactive surface areas^{25,26}.

Methanol (MeOH) is a highly attractive fuel for mobile applications such as electric vehicles^{27,28} as it has a theoretical cell voltage of 1.2 V and a theoretical energy density of 6094 Wh Kg⁻¹ (5x that of the best battery couples). Surely its practical energy density is only 1500-3100 Wh kg⁻¹ while its operating cell voltage is 0.4 V⁵. Further methanol is an easy available product, but it is toxic. Usually the DMFC (Direct Methanol Fuel Cell) contains a MEA constituted by an anode catalyst based on Pt/C, a Nafion® membrane (cationic membrane) and a Pt/C cathode. The main potential losses are due to anode side overvoltages caused by slow oxidation kinetic and by irreversible poisoning^{1,29} and to cathode side overvoltage caused by methanol cross-over, which competes with ORR (Oxygen Reduction Reaction). Indeed platinum itself is known to be rapidly poisoned on its surface by strongly adsorbed species coming from the dissociative adsorption of methanol^{30,31}. In the literature many efforts to mitigate the Pt poisoning have been concentrated on the addition of co-catalysts, particularly ruthenium^{32,33,34,29c,d} and tin^{35,36,37}, to platinum; or on the influence of the carbon support on the Pt poisoning (multi and single walled carbon nanotubes^{38,39}, polyaniline nanofibres⁴⁰, carbon nanofibres³⁹, carbon nanowires³⁹ and so on). On the other hand also the methanol cross-over represents a serious problem, as it influenced the ORR (Oxygen Reduction Reaction)^{41,42,43}. Metalloporphyrins^{44,45} and Platinum Group Metal (PGM) alloys⁴⁶ have been used to design catalysts for the 4e⁻ reduction of O₂ to water and many studies are directed to understand the mechanism of oxygen reduction on Pt-Fe, Pt-Ni, Pt-Co⁴⁷, including CO or methanol tolerance⁴⁸. Several methods have been proposed to reduce methanol crossover in DMFCs, such as adding ZrO₂ to the membrane⁴⁹, using a PTFE improved

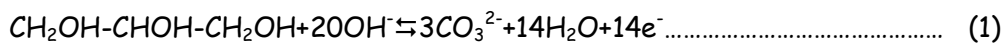
Nafion® as the electrolyte membrane⁵⁰, adding a thin layer of palladium^{51,52} etc. All of these methods are capable of reducing methanol crossover to a certain extent, but none can prevent methanol crossover and all of these methods also increase the impedance for proton transport through the membrane.

For all of these reasons ethanol (EtOH) offers an attractive alternative as fuel in low temperature fuel cells, because it can be produced in large quantities as it is the major renewable biofuel from the fermentation of biomass⁵³ from agricultural products (first generation ethanol). Nowadays it is also produced from the organic urban waste (second generation ethanol). Moreover EtOH copes with the toxicity problem of MeOH, its boiling point (64.7°C) and its low energy density²⁷. By comparing the performance of fuel cells employing Pt-Ru anode catalyst, H₃PO₄-doped polybenzimidazole membrane on various methanol-alternative fuels, Wang et al.⁵⁴ found that ethanol is a promising alternative fuel with an electrochemical activity comparable to that of methanol. Further pure Pt is not the most efficient anode catalyst for DEFC (Direct Ethanol Fuel Cell)^{53,55}, the ethanol permeation through the Nafion® membrane towards cathode is not so appreciable as well as for MeOH and EtOH reaction kinetic on Pt/C cathode is slower than for MeOH⁵⁶. The latter evidences make possible a development of DEFC working with cationic membrane using Pt-Sn anode catalysts that improve EOR (Ethanol Oxidation Reaction) notwithstanding C-C bond cleavage inhibition⁵⁷, or Pt-Sn-based ternary catalysts^{58,59,60}, or in the presence of Sn or Ru oxides^{59,60}, which promote water dissociation at a lower potential than Pt-Ru systems and cathode containing Pt-Pd (9:1) catalysts more tolerant to ethanol cross-over.

In alkaline media Pd-based anode electrocatalysts show better activity towards EOR for better electrochemical performances and poison tolerance⁶¹. Recent studies have shown that the oxidation of alcohols in general in alkaline media proceeds with enhanced kinetics for both anode and cathode reactions than in acidic environment^{62,63,64}. This is due to a major concentration of -OH groups at the surface in alkaline media, which plays a key role in the removal of electrode poisoning species⁶⁵. The increased performances in alkaline media for DAFCs is also due to the favourable direction of the electro-osmotic drag, which goes from the cathode side to the anode side, slowing the alcohol cross-over. For ethanol in alkaline environment, acetaldehyde, acetic acid and carbon dioxide (pH<13⁶⁶) are discussed as products^{65b}. In order to use the full energy density of an alcohol, the fuel needs to be completely oxidized to carbon

dioxide. However, in the case of ethanol this involves the breaking of the C-C bond, known to be difficult, and its product in the highest oxidation state in alkaline medium is acetate which means an electron transfer of four electrons or a Faradic efficiency of 33%.

Other higher molecular weight alcohols can be used as fuels in DAFCs: Ehtylene glycol (EG) and glycerol (Gly). Both of them are renewables as EG can be produced by heterogeneous hydrogenation of cellulose, while Gly is a byproduct of biodiesel production and, as such, is inexpensive and largely available⁶⁷. EG has also a higher electron transfer rate (ETR) than EtOH and the higher theoretical capacity than methanol (EG 4.8 Ah/mL; MeOH 4 Ah/mL)^{68,69,70}. It has been demonstrated that the main product of EG oxidation is oxalic acid/oxalate^{71,72} which leads to the electron transfer of 8 electrons, hence the ETR of EG is 80%⁷³. These alcohols, however, are difficult to oxidize on platinum or platinum alloys. In particular, no known anode catalyst based on platinum has demonstrated the capacity to produce acceptable power densities in either DEGFC^{53,74,75} or DGFC^{53,74,75,55}, unless a partially inorganic solid electrolyte is used at temperatures >130°C⁷⁶. The Glycerol is also an interesting fuel as it has a high theoretical energy density of 5.0 kWh/kg and its complete oxidation leads to 14e⁻ (according to Eq [1]).



Coutanceau et al. have demonstrated that Pd_xAu_{1-x}/C and Pd_{0.5}Ni_{0.5}/C electrocatalysts have a higher activity towards glycerol oxidation close to Pt/C and that the catalyst composition and structure affect the Gly oxidation product distribution⁷⁷ in alkaline media. Indeed Au and PdAu catalysts do not show selectivity to C-C cleavage, at the opposite that for Pt and Pd catalysts. At the same time Gly gives high current density in alkaline media also in half-cell study on Pd/MWCNT electrode respect to Pt-Ru/MWCNT electrode in acidic media⁷⁸.

Glucose can also be used as fuel in DAFCs operating in alkaline environment^{79,80}. Usually this sugar is employed in enzymatic bio-fuel cells for applications in medical implants such as pacemaker and glucose-sensor^{81,82}, giving low power density. Nowadays it represents a potential fuel for DAFCs because it is renewable, abundant, non-toxic, easy handle and store and its complete oxidation leads to 24e⁻⁸¹. For these reasons Chan et al

⁸³ measured the cell performance of a glucose-air fuel cell with PtCo and Pt as the anode and the cathode catalysts. Fujiwara et al. ⁸⁴ compared the cell performances of an AEM-DGFC and a PEM-DGFC using the PtRu black and Pt black as the anode and cathode catalysts, obtaining best results in alkaline media.

In conclusion the DAFs can use a lot of renewable alcohols for producing energy and chemicals, but it is necessary to design and develop catalysts with specific structures for each of them for reaching H₂-fuel PEMFC performances and getting possible their global commercialization respecting the sustainability concept.

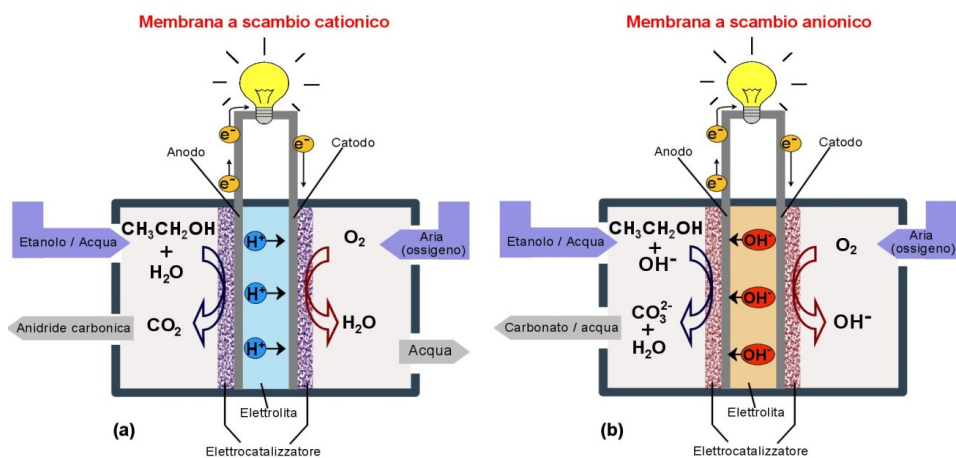
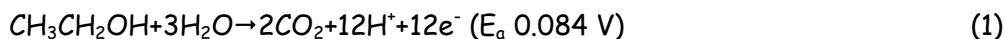


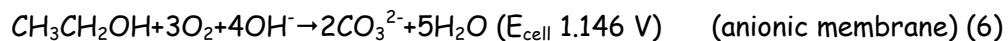
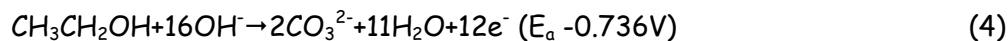
Figure 2. DAFCs with anionic and cationic polymeric membranes.

1.5 The Direct Alcohol Fuel Cell (DAFC)

The Direct Alcohol Fuel Cell (DAFC) is an electrochemical device which converts the chemical energy of a fuel (alcohol) into electrical energy and eventually chemicals of industrial interest. The performance of a fuel cell depends on the catalyst activity/lifetime. DAFCs contains Membrane Electrolyte Assemblies (MEAs) constituted by anode, polymeric electrolyte membrane and cathode mechanically pressed onto each other. In general, DAFCs cannot operate at temperatures higher than to 80°C due to the low thermal stability of the membrane . In Figure 2 are illustrated the two type of DAFCs operating with either anionic or cationic exchange polymeric membrane (Tokuyama Corporation membranes, Morgane by Solvay and Nafion™ by Du Pont).

Eq[(1-6)] report single electrode and overall reactions occurring in a direct ethanol fuel cell in either acidic or alkaline media. The reactions below refer to the total oxidation of ethanol to CO_2 or CO_3^{2-} , but there are DEFCs (largely presented in this thesis work) where the partial oxidation of ethanol (as well as of other alcohols) occurs selectively.

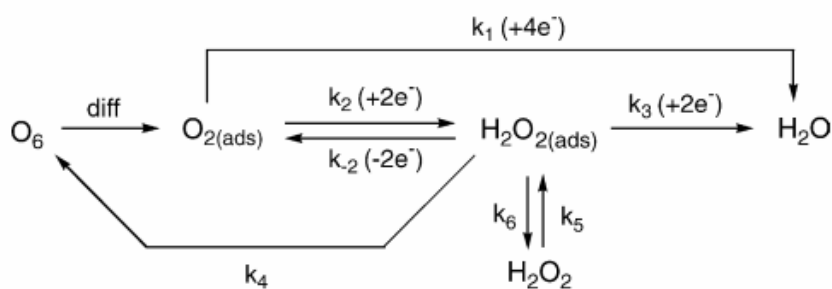




The oxidation potentials of alcohols are favourable in alkaline environment⁶¹⁻⁶⁵.

1.5.1 Cathode electrocatalysts

The slow oxygen reduction reaction (ORR) kinetics on Pt catalysts is among a limiting factor in the energy conversion efficiency of PEMFCs. Also, Pt is scarcely available and its price increases constantly. Alternative catalytic materials are therefore necessary for fuel cell applications. ORR process includes several individual reactions (Scheme 2). For electrochemical catalytic ORR analysis, two general processes are examined mostly. One is the production of water through a four-electron pathway, and the other is the production of hydrogen peroxide through a two-electron pathway. The desired feature for a successful ORR catalyst would reduce oxygen molecules to water through the four-electron route. Incomplete reduction of oxygen to hydrogen peroxide not only leads to low energy conversion efficiency, but also produces reactive intermediates that can further convert to harmful free radical species⁸⁸, deteriorating the cathode catalysts.



Scheme 2. ORR mechanism⁸⁸.

Since 1964⁸⁵ cobalt and iron complexes with phthalocyanines (Pc) or similar *N*-macrocycles, supported on carbon blacks, have been largely used as electrocatalysts for the oxygen reduction reaction (ORR), either in the molecular form^{86,87,88,89} and or after thermal treatment under inert atmosphere^{90,91}. This has been possible working in DAFCs operating in alkaline environment (anionic polymer electrolyte membrane), where one may use no noble metals^{91b,92}. As a matter of fact, MPc-derived electrocatalysts are the best materials for alkaline direct alcohol fuel cells (DAFCs), in terms of both cost and performances^{92b}.

Considering catalysts treated under inert atmosphere, the pyrolysis temperature has been found to be a crucial parameter to determine the structure of metallophthalocyanine-derived electrocatalysts and, consequently, their electrochemical performance⁹³. It is now apparent that pyrolysis temperatures around 600 °C lead to the prevalent formation of M-N₄ units with the metals predominantly in the +2 oxidation state, while metal particles are obtained at higher temperatures, around 800 °C^{91,94,95}. An other important aspect is that these kind of metal complexes do not oxidize alcohols, reducing the problem correlated to their cross-over which can occur in DAFCs⁹³. For bettering ORR performances of MPc-derived electrocatalysts, the influence of the carbon support has been investigated and it has been understood that also its nature influences the ORR activity of the cathode electrocatalysts^{93,96,97}. During this Doctoral thesis work all of the passive and active fuel cell tests were performed using FeCo/Kj black cathode electrocatalysts, before synthesized and characterized in our labs⁹³.

1.5.2 Polymer electrolyte membrane

The electrolyte is fundamental for the correct working of a fuel cell, as it keeps in contact the two anode and cathode compartments through a ionic flux, but resisting to cross-over of fuels from one side to an other and to the oxidative environment of anode or the reductive environment of the cathode. In the DAFC operating in acid media also the water management can be a problem, as it is attracted to the cathode side for polarization and water is frequently introduced in the feed stream to the fuel cell^{98,99}. In

addition interfacial transport across the membrane/gas boundary diffusion layer swells all contribute resistances to water transport and sorption¹⁰⁰. This affects the local proton conductivity. The most common used membrane for fuel cell operating at low temperature is the cationic Nafion® by DuPont. It is based on perfluorosulfonic acid made of polytetrafluoroethylene which provides membrane with physical strength. The sulfonic acid functional groups provide charge sites for proton transport. Additionally other perfluorinated membrane such as Neosepta-F™ (Tokuyama), Gore-Select™ (W. L. Gore and Associates, Inc.), Flemion™ (Asahi Glass Company) and Asiplex™ (Asahi Chemical Industry) are also adopted for fuel cells⁵. On the other hand in the alkaline environment the water management is a less serious problem, as water is formed at the anode side and the electroosmotic flux goes from cathode to anode. In the last years the increasing interest in DAFCs operating in alkaline condition permits to develop and produce anion exchange membranes (AEMs)^{101,102}. The drawback of traditional alkaline fuel cells (AFCs) to undergo electrolyte carbonation is strongly minimized by the use of an anion conductive polymeric membrane.

In this Doctoral thesis Tokuyama A006 (Tokuyama Corporation) anion exchange membrane was used for all the electrochemical measurements for active and passive monoplanar DAFCs^{103,78,104} (perfluorinated membrane in its quaternary ammonium form).

1.5.3 Anode electrocatalysts

The most used anode electrocatalysts for DAFCs are based on Pt. They still present many problems. Further they are not so efficient for oxidizing superior alcohols as ethanol, ethylene glycol or glycerol. For all of these reasons the real attraction is to develop Pd-based electrocatalysts. This metal is less expensive and more abundant than platinum, it is efficient for alcohol oxidation in alkaline media where it is usable also diluted with no noble metal at the anode or cathode side^{92b}. For getting good catalysts one may pay attention to the morphology, shape, dispersion and to the support material. The support is generally constituted by carbon matrix, recently utilized in a lot of nanostructures (tubes, wires, fibers..). The large availability and the low cost make the Vulcan-type

materials the most used support for electrocatalysts in low temperature fuel cells. It has a high surface area, good electrical and thermal conductivity, suitable porosity and high stability in the FC environment. The large majority of carbon-supported electrocatalysts are prepared by reduction of physical and chemisorbed metal salts or metal complexes with chemical reductant (NaBH_4 , ethylene glycol, hydrazine, tannic acid, formic acid, formaldehyde, hydrogen gas) that may also act as templating agent to favour the formation of nanosized metal particles¹⁰⁵. It is also possible to reduce metal salts making surfactant stabilized colloidal Pd particles via the Bönnerman method and then mix with carbon support¹⁰⁶. Binary electrocatalysts of PtPd/C or PtPdBi/C have been prepared by water-in-oil microemulsion method successively added to a conductive carbon¹⁰⁷. Another actual and fast method for synthesizing metal nanoparticles is through intermittent microwave irradiation (IMH). Indeed in literature there are an increasing number of publications dealt with this technique¹⁰⁸.

Carbon nanotubes (CNTs) are widely used as support for electrocatalysts for DAFCs as their properties of having higher surface area, higher electric conductivity and porosity than common Vulcan or Ketjen black carbon¹⁰⁹. As a matter of fact it has been demonstrated that increasing the graphitization degree of carbon materials, the π -sites grows up and so the metal particles interaction with the present support, disfavoring the metal sintering and at the same time favouring the stability of the electrocatalysts^{110,78}. Multiwalled carbon nanotubes (MWCNTs) and their functionalized derivatives are already a widespread support for FC (Fuel Cell) catalysts. Sulfonated MWCNTs for depositing Pd showed good activity towards methanol oxidation¹¹¹ as well as treated MWCNTs with hydrofluoric acid towards stability in EOR¹¹². Li and co-workers developed MWCNTs functionalized with mercaptobenzene moieties for anchoring palladium later tested for the oxidation of formaldehyde in alkaline solution¹¹³. Often they can be used for depositing two metal species and realize a binary electrocatalyst¹¹² (PdNi¹¹⁴). In addition TiO_2 ¹¹⁵ nanotubes, vanadium oxide nanotubes¹¹⁶ and $\beta\text{-MnO}_2$ nanotubes¹¹⁷, carbon microspheres (CMSs)¹¹⁸, coinlike hollow carbons (CHCs)¹¹⁹ and ultrahigh-surface hollow carbon spheres (HCSs)¹²⁰ can replace MWCNTs as support for FC catalysts. Tungsten carbide (WC) nanocrystals, prepared by the IMH method, have been recently employed as supports for Pd nanoparticles¹²¹ with better activity towards EOR reaction in alkaline media than Pd/C, as they have higher surface area and there is a synergistic effect between Pd and WC^{121b}. Recently transition metal oxides are

employed for supporting Pd particles as they have a co-catalytic role on Pd activity for alcohol oxidation^{105c}. Indeed Shen and Xu obtained active materials in terms of onset oxidation potential and peak current density and also stability towards EOR^{105c}. In the Chapter 3 of this work it is possible to find a similar material based on CeO₂/C (vide infra). Finally spontaneous deposition (SD) of noble metals onto less noble metal particles or metal surface is emerging¹²². The electrocatalysts shown in the Chapter 2 of this Doctoral thesis represent an example of this kind of deposition technique¹²³. The materials obtained show the best performances never shown before in the literature¹²³ towards EOR and EGOR in DAFCs operating with an anion exchange membrane (vide infra), as palladium particles are very little (1-2 nm) and well-dispersed. A technique similar to SD is the redox replacement reaction between sacrificial cobalt nanoparticles and Pt(IV) and/or Pd(II)¹²⁴ (see Chapter 3) which can give materials with a particular structure such as hollow nanospheres. Although essentially used for laboratory tests in half cells, unsupported Pd electrocatalysts for alcohol oxidation have been reported in the literature. Usually they are prepared through electrochemical methods which involve the electrodeposition technique of one or two metals by cyclic potential sweep¹²⁵ or using templating agents¹²⁶ such as a porous aluminium oxide.

All known Pd-based catalysts are unable to completely oxidize alcohols to CO₂ (CO₃²⁻). Ethanol is almost exclusively oxidized to the corresponding carboxylic acid (carboxylate), while polyalcohols (EG, Gly..) may undergo C-C bond cleavage with formation of carbonate in a minor path as compared to the partial oxidation to carboxylates. Our experimental evidence highlights the sustainability of DAFCs that can simultaneously produce energy with no CO₂ emission and chemicals from renewables.

1.5.4 Synthetic strategies and characterization of electrocatalysts for DAFCs

The most common synthetic routes to obtain metallic nanostructured electrocatalysts can be divided in two approaches: *bottom-up (from molecular scale to nanoscale)* and *top-down (from large to smaller dimensions)*. Further they can be classified as chemical or physical methods. The physical techniques include the thermal evaporation¹²⁷ or the sputtering¹²⁸ in high vacuum of metals. The main disadvantages of physical techniques are the little dimensional check on nanostructure formations and on their distribution onto the surface. Lithography techniques have also been applied to achieve better control of size in vacuum methods¹²⁹. On the other hand a large variety of chemical methods have been reported for the synthesis of metal nanoparticles for FC applications. The common starting point of chemical methods is the molecular or ionic precursor dissolution in water or organic liquid phase. Sometimes the precursors can be carried in supercritical carbon dioxide¹³⁰ or can be itself the gas carrier in the case of metal organic chemical vapour deposition¹³¹. Then a reducing agent is used to obtain metal particles directly on the support to form a larger area electrocatalyst. Other chemical steps such as decomposition, displacement or electrochemical reactions are possible. A crucial step is the nucleation of metal nanoparticles as its control determines the activity of the material. To this aim in Figure 3 some dimensional control strategies are illustrated¹³².

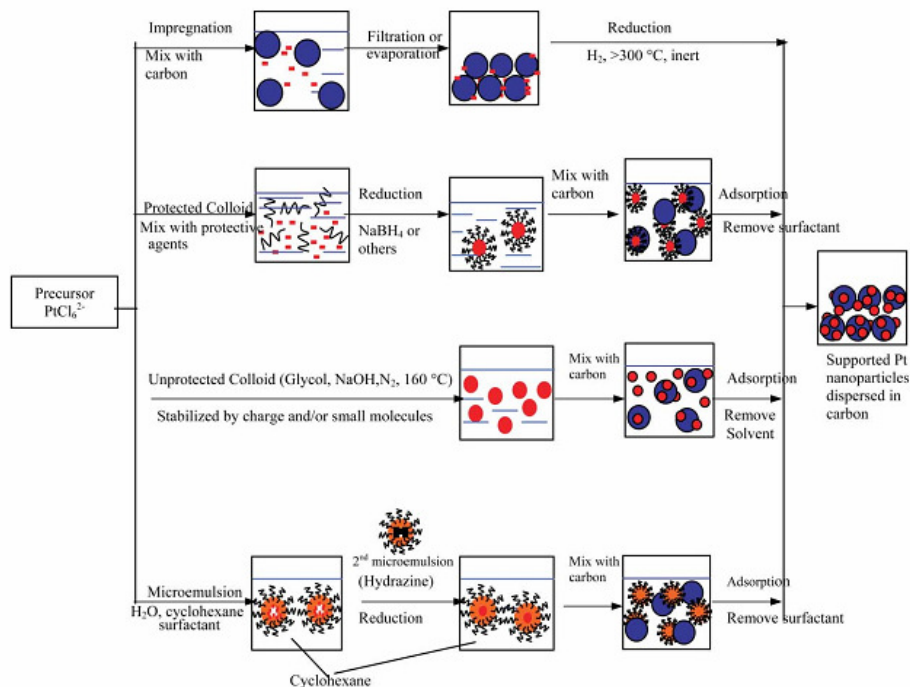


Figure 3. Chemical methods to synthesize supported platinum nanoparticles with different size control methodologies ¹³².

The colloidal method (Figure 3) uses an organic agent (PVP, PVA, PPh₃...) to protect the metal nanoparticles in organic phase (organosol) or in aqueous phase (hydrosol), stabilizing either by steric hindrance or by electrostatic charges. A narrow size of the metal particles is reached, but at the same time the surfactant agent must be removed to ensure the good catalytic action of nanoparticles ¹³³. It would be preferable using appropriate combination of precursor, solvent, reducing agent and electrolyte, as f.i. Wang et al. ¹³⁴ have used ethylene glycol as solvent/surfactant in the appropriate alkaline condition to produce nanoparticles of a lot of metal species. In the Chapter 2 of this work Pd/C synthesis is reported through the latter strategy.

On the contrary the impregnation method illustrated in Figure 3 consists in soaking up of a dissolved metal precursor into pores of a support (Vulcan XC 72, f.i.) and then reducing it into metal particles by chemical or electrochemical strategies. The major drawback is the scarce dimensional control of metal particles except when the support has a definite ordered mesoporous structure ^{118,119,120}. On the other hand the electrochemical method reduction can be a method for controlling this parameter through the amount of current passed ¹³⁵. Finally the microemulsion method ¹³⁶ consists in mixing the metallic precursor liquid phase in an immiscible liquid (surfactant phase) creating an emulsion.

The reducing agent can be introduced itself as a microemulsion and often a co-surfactant can be used for modifying the dimension of metal particles.

Physical methods for the electrocatalyst characterization include high resolution electron microscopy (HRTEM), extended X-ray absorption fine structure spectroscopy (EXAFS), energy dispersive spectroscopy (EDS), inductively coupled plasma atomic emission spectroscopy (ICP-AES), near edge X-ray absorption spectroscopy (XANES), X-ray powder diffraction (XRPD), and infrared and Raman spectroscopy (IR, RS). All of these techniques show morphological and structural information about electrocatalysts. Electrochemical characterization methods include cyclic voltammetry (CV), chronopotentiometry, chronoamperometry, AC impedance spectroscopy, in situ spectroelectro-chemistry, and electrochemical scanning tunnelling microscope. Fast electrocatalyst screening has been achieved by scanning electrochemical microscopy. The latter electrochemical techniques represent a preliminary study about the oxidation/reaction activity of the FC electrocatalysts.

Finally electrochemical tests on the whole activity of a DAFC are effectuated by specific potentiostat-galvanostat for FC (Arbin or Scribner instruments), often after mechanical hot-pressing the MEAs.

1.6 Scope

In this Doctoral thesis, we have developed and characterized Pd-based anode catalysts for DAFCs with aim of producing high current density at relatively low temperature. In the course of our studies we have also developed catalysts that selectively convert renewable alcohols into the corresponding alkali metal carboxylates.

The choice to synthesize Pd-based electrocatalysts is exhaustively discussed in the Introduction as well as in Chapter 2. In Chapter 3 are reported our efforts to improve the first catalysts synthesized, by varying metal particle morphology and dimensions, support materials as well as combining other metals with Pd.

The primary goal of this work is indeed the design and development of Pd-based electrocatalysts and their use as anode materials in DAFCs equipped with anion exchange membranes.

1.7 References

- ¹C.-J. Zhong, J. Luo, P.N. Njoki, D. Mott, B. Wanjala, R. Loukrakpam, S. Lim, L. Wang, B. Fang, Z. Xu *Energy Environmental Science*, **2008**, *1*, 454.
- ²G. A. Olgh "A life of a magic chemistry" autobiographical Reflections of a Nobel Prize Winner" John Wiley and Sons.
- ³G. Wand *Fuel cell history*, part one 14.
- ⁴<http://environmentalchemistry.com/yogi/environmental/200608hydrogenfuelcells.htm>
- ⁵Y. Wang, K.S. Chen, J. Mishler, S.C. Cho, X. C. Adroher *Applied Energy* **2010**, doi: 10.1016/j.apenergy.2010.09.030.
- ⁶C. Gittleman, S. Joergensen, J. Waldecker, S. Hirano, M. Mehall, *Automotive fuel cells R&D needs*. In: DOE fuel cell pre-solicitation workshop. Department of energy, Lakewood, Colorado; **2010**.
- ⁷J. Garche, L. Jorissen *PEMFC fuel cell*, In: W. Vielstich, H. Gasteiger, A. Lamm, editors. *Handbook of fuel cells: fundamentals, technology and applications*, John Wiley & Sons, Ltd.; **2003**.
- ⁸S. Geiger, M.A.J. Copper. *Fuel Cell Today* , **2003**.
- ⁹S. Zhang, et al. *International Journal of Hydrogen Energy* **2009**; 34, 388.
- ¹⁰R. Borup, et al., <http://www.hydrogen.energy.gov/pdfs/review08/fc_26_borup.pdf>.
- ¹¹W. Schmittinger, A. Vahidi, *Journal of Power Sources* **2008**;180, 1.
- ¹²DOE-EERE. FCT fuel cells: types of fuel cells; 2009 https://www1.eere.energy.gov/hydrogenandfuelcells/fuelcells/fc_types.html [05.28.10].
- ¹³NIST. PEM Fuel Cells. 2006. <<http://www.physics.nist.gov/MajResFac/NIF/pemFuelCells.html>>.
- ¹⁴C-Y. Wang *Chemistry Review* **2004**;104, 4727.
- ¹⁵C. Siegel *Energy* **2008**, *33*, 1331.
- ¹⁶Y. Wang, S. Basu, C.Y. Wang, *Journal of Power Sources* **2008**,179, 603.
- ¹⁷W. Kreuter, W. H. Hofmann *International Journal of Hydrogen Energy*, **1998**, *23*, 661.
- ¹⁸F. Vitse, M. Cooper, G. G. Botte *Journal of Power Sources*, **2005**, *142*, 18.
- ¹⁹M. Cooper, G. G. Botte *Journal of Electrochemical Society* **2006**, *153*, A1894.
- ²⁰F. Vitse, M. Cooper, G. G. Botte US PATENT 2005/0211569A1.

- ²¹T. Take, K. Tsuritani, M. Umeda, *Journal of Power Sources*, **2007**, 164, 9.
- ²²Z. Hu, M. Wu, Z. Wei, S. Song, P.K. Shen *Journal of Power Sources*, **2007**, 166, 458.
- ²³H. Igarashi, T. Fujino, Y. Zhu, H. Huchida, M. Watanabe *Physical Chemistry Chemical Physics* **2001**, 3, 306.
- ²⁴C. Bianchini, F. Vizza, A. Lavacchi, V. Bambagioni, M. Bevilacqua, A. Marchionni, J. Filippi, P.K. Shen *ChemSusChem* **2010**, 3, 851.
- ²⁵R. Borup, J. Meyers, B. Pivovar, Y. S.Kim, R. Mukundan, N. Garland, D. Myers, M. Wilson, F. Garzon, D. Wood, P. Zelenay, K. More K. Stroh, T. Zawodzinski, J. Boncella, J. E. McGrath, M. Inaba, K. Miyatake, M. Hori, K. Ota, Z. Ogumi, S. Miyata, A. Nishikata, Z. Siroma, Y. Uchimoto, K. Yasuda, K. C. Kimjima, N. Iwashita *Chemistry Review* **2007**, 107, 3904.
- ²⁶X. B. Cheng, Z. A. Shi, N. A. Glass, L. Zhang, J. J. Zhang, D. Song, Z. S. Liu, H. J. Wang, J. Shen *Journal of Power Sources* **2007**, 165, 739.
- ²⁷C. Lamy, E.M. Belgsir, J.-M. Léger *Journal of Applied Electrochemistry* **2001**, 31, 799.
- ²⁸E. Peled, T. Duvdevani, A. Aharon, A. Melman *Electrochemistry Solid State Letters* **2001**, 4, A38.
- ²⁹(a) G. J. K. Acres, J. C. Frost, G. A. Hards, R.J. Potter, T. R. Ralph, D. Thompsett, G. T. Burstein, G. J. Hutchings *Catalysis Today*, **1997**, 38, 393; (b) S. Wasmus, A. Kuever *Journal of Electroanalytical Chemistry* **1999**, 461, 14; (c) G. Q. Lu, A. Wieckowski *Current Opinion in Colloid and Interface Science* **2000**, 5, 95; (d) A Roucoux, J. Schulz, H. Patin *Chemistry Review*, **2002**, 102, 3757.
- ³⁰J. Divisek, H.F. Oetjen, V. Peinecke, V.M. Schmidt, U. Stimming *Electrochimica Acta* **1998**, 43, 3811.
- ³¹H.M. Yu, Z.J. Hou, B.L. Yi, Z.Y. Lin *Journal of Power Sources* **2002**, 105, 52.
- ³²S. Oke, K. Higashi, K. Shinohara, Y. Izumi, H. Takikawa, T. Sakakibara, S. Itoh, T. Yamaura, G. Xu, K. Miura, K. Yoshikawa, T. Sakakibara, S. Sugawara, T. Okawa, N. Aoyagi *Chemical Engineering Journal*, **2008**, 142, 225.
- ³³M.C. Denis, M. Lefèvre, D. Guay, J.P. Dodelet *Electrochimica Acta*, **2008**, 53, 5142.
- ³⁴Z. B. Wang, G. P. Yin, P. F. Shi *Journal of Alloys and Compounds* **2006**, 420, 126.
- ³⁵D.M. Han, Z.P. Guo, R. Zeng, C.J. Kim, Y.Z. Meng, H.K. Liu *International Journal of Hydrogen Energy*, **2009**, 34, 2426.
- ³⁶E. Antolini, E.R. Gonzalez *Catalysis Today*, 2010 In Press, Corrected Proof.

-
- ³⁷E. Antolini, E.R. Gonzalez *Electrochimica Acta*, **2010**, *56*, 1.
- ³⁸G. Wu, B.-Q. Xu *Journal of Power Sources* **2007**, *174*, 148.
- ³⁹S. Basri, S.K. Kamarudin, W.R.W. Daud, Z. Yaakub *International Journal of Hydrogen Energy* **2010**, *35*, 7957.
- ⁴⁰M. Zhiani, B. Rezaei, J. Jalili *International Journal of hydrogen energy*, **2010**, *35*, 9298.
- ⁴¹J. Han, H. Liu *Journal of Power Sources* **2007**, *164*, 166.
- ⁴²T.H. Kin, W.Y. Shieh, C.C. Yang, George Yu *Journal of Power Sources*, **2006**, *161*, 1183.
- ⁴³C.Y. Du, T.S. Zhao, W.W. Yang *Electrochimica Acta* **2007**, *52*, 5266.
- ⁴⁴J. P. Collman, C. S. Bencosme, R.R. Durand, R. P. Kreh, F. C. Anson *Journal of American Chemical Society* **1983**, *105*, 2699.
- ⁴⁵D. Chu, R. Jiang *Solid State Ionics* **2002**, *148*, 591.
- ⁴⁶U. A. Paulus, A. Wokaun, G. G. Scherer, T. J. Schmidt, V. Stamenkovic, V. Radmilovic, N. M. Markovic, P. N. Ross *Journal of Physical Chemistry B* **2002**, *106*, 4181.
- ⁴⁷N. P. Brandon, S. Skinner, B. C. H. Steele *Annual Review of Materials Research* **2003**, *33*, 183.
- ⁴⁸a) A. K. Shukla, R. K. Raman *Annual Review of Materials Research* **2003**, *33*, 155; (b) S. B. Adler *Chemistry Review* **2004**, *104*, 4791.
- ⁴⁹V.S. Silva, J. Schirmer, R. Reissner, B. Ruffmann, H. Silva, A. Mendes, L.M. Madeira, S.P. Nunes *Journal of Power Sources*, **2005**, *140*, 41.
- ⁵⁰H.-L. Lin, T. Leon Yu, L.-N. Huang, L.-C. Chen, K.-S. Shen, G.-B. Jung *Journal of Power Sources*, **2005**, *150*, 11.
- ⁵¹W. Choon Choi, J. Dam Kim, S. Ihl Woo *Journal of Power Sources* **2001**, *96*, 411.
- ⁵²Z.Q. Ma, P. Cheng, T.S. Zhao, *Journal of Membrane Science* **2003**, *215*, 327.
- ⁵³E. Antolini *Journal of Power Sources* **2007**, *170*, 1.
- ⁵⁴J. Wang, S. Wasmus, R.F. Savinelli *Journal of Electrochemical Society* **1995**, *142*, 4218.
- ⁵⁵D. Bayer, S. Berenger, M. Joos, C. Cremers, J. Tübke *International Journal of Hydrogen Energy* **2010**, *35*, 12660.
- ⁵⁶S. Song, W. Zhou, Z. Liang, R. Cai, G. Sun, Q. Xin, V. Stergiopoulos, P. Tsiakaras *Applied Catalysis B: Environmental* **2005**, *55*, 65.
- ⁵⁷F. Colmati, E. Antolini, E.R. Gonzalez *Journal of Alloy Compounds*, **2007**, *434/435*, 756.
- ⁵⁸E.V. Spinacé, M. Linardi, A. Oliveira Neto, *Electrochemistry Communication* **2005**, *7*, 365.

- ⁵⁹S. Rousseau, C. Coutanceau, C. Lamy, J.-M. Legér *Journal of Power Sources*, **2006**, *158*, 18
- ⁶⁰E. Antolini, F. Colmati, E.R. Gonzalez, *Electrochemistry Communication* **2007**, *9*, 398.
- ⁶¹A. Verma, S. Basu, *Journal of Power Sources* **2005**, *145*, 282.
- ⁶²C. Cremers, D. Bayer, B. Kintzel, M. Joos, F. Jung, M. Krausa *ECS Transactions*, **2008**, *16*, 1263.
- ⁶³V. Rao Hariyanto, C. Cremers, U. Stimming *Fuel Cells*, **2007**, *7*, 417.
- ⁶⁴(a) L. Demarconnay, S. Brimaud, C. Coutanceau, J.-M. Legér *Journal of Electroanalytical Chemistry*, **2007**, *601*, 169; (b) K. Matsuoka, Y. Iriyama, T. Abe, M. Matsuoka, Z. Ogumi *Journal of Power Sources*, **2005**, *150*, 27; (c) L. Jiang, A. Hsu, D. Chu, R. Chen *International Journal of Hydrogen Energy*, **2010**, *35*, 365.
- ⁶⁵(a) J. Liu, J. Xe, C. Xu, S.P. Jiang, Y. Tong *Journal of Power Sources* **2008**, *177*, 67; (b) V. Tripkovic, K.D. Popovic, J. D. Lovic *Electrochimica Acta* **2001**, *46*, 3163.
- ⁶⁶X. Fang, L. Wang, P. K. Shen, G. Cui, C. Bianchini *Journal of Power Sources* **2010**, *195*, 1375.
- ⁶⁷J.-M. Clacens, Y. Pouilloux, J. Barrault *Journal Applied Catalysis A: General* **2002**, *227*, 181.
- ⁶⁸E. Peled, V. Livshits, T. Duvdevani *Journal of Power Sources* **2002**, *106*, 245.
- ⁶⁹E. Peled, V. Livshits, M. Philosoph *Journal of Power Sources* **2008**, *178*, 687.
- ⁷⁰E. Peled, V. Livshits *Journal of Power Sources* **2006**, *161*, 1187.
- ⁷¹K. Matsuoka, Y. Iriyama, T. Abe, M. Matsuoka, Z. Ogumi *Electrochimica Acta* **2005**, *51*, 1085.
- ⁷²R. B. Lima, V. Paganin, T. Iwasita *Electrochimica Acta* **2003**, *49*, 85.
- ⁷³L. An, T. S. Zhao, S.Y. Shen, Q.X. Wu, R. Chen *International Journal of Hydrogen Energy*, **2010**, *35*, 4329.
- ⁷⁴C. Lamy, A. Lima, V. LeRhun, F. Delime, C. Coutanceau, J.-M. Legér *Journal of Power Sources* **2002**, *105*, 283.
- ⁷⁵F. Vigier, S. Rousseau, C. Coutanceau, J.-M. Legér, C. Lamy *Topics in Catalysis* **2006**, *40*, 111.
- ⁷⁶E. Peled, V. Livshits, T. Duvdevani *Journal of Power Sources* **2002**, *105*, 245.
- ⁷⁷M. Simões, S. Baraton, C. Coutanceau *Applied Catalysis B: Environmental* **2010**, *93*, 354.

-
- ⁷⁸V. Bambagioni, C. Bianchini, A. Marchionni, J. Filippi, F. Vizza, J. Teddy, Philippe Serp, M. Zhiani *Journal of Power Sources* **2009**, *90*, 241.
- ⁷⁹L. An, T. S. Zhao, S. Y. Shen, Q. X. Wu, R. Chen *Journal of Power Sources* **2011**, *196*, 186.
- ⁸⁰D. Basu, S. Basu *Electrochimica Acta* **2010**, *55*, 5775.
- ⁸¹S. K. Chaudhuri, D.R. Lovley *Nature Biotechnology* **2003**, *21*, 1229.
- ⁸²V. Soukharev, N. Mano, A. Heller *Journal of American Chemical Society* **2004**, *126*, 8368.
- ⁸³Methods and apparatus for the oxidation of glucose molecules, US 7,419,580 B2 (September 15, **2009**).
- ⁸⁴N. Fujiwara, S. Yamazaki, Z. Siroma, T. Ioroi, H. Senoh, K. Yasuda, *Electrochemistry Communications* **2009**, *11*, 390.
- ⁸⁵R. Jasinski, *Nature* **1964**, *201*, 1212.
- ⁸⁶K. Oyazu, H. Murata, H. Yuesa *Macrocycles for Fuel Cell Cathodes*, Springer-Verlag, Berlin, **2009**, 139.
- ⁸⁷B. Wang *Journal of Power Sources* **2005**, *152*, 1.
- ⁸⁸F. Van Den Brink, W. Visscher, E. Barendrecht *Journal of Electroanalytical Chemistry*, **1983**, *157*, 305.
- ⁸⁹(a) F. Van Den Brink, W. Visscher, E. Barendrecht *Journal of Electroanalytical Chemistry*, **1984**, *175*, 279; (b) J.A.R. Van Veen, C. Visser *Electrochimica Acta*, 1979, *24*, 921; (c) E. Yeager *Electrochimica Acta*, **1984**, *29*, 1527; (d) J. Zagal, M. Pàez, *Journal of Electroanalytical Chemistry* **1992**, *339*, 13.
- ⁹⁰H. Kavelage, A. Mecklenburg, U. Kunz, U. Hoffmann *Chemical Engineering and Technology* **2000**, *23*, 803.
- ⁹¹(a) M.C.M. Alves, J.P. Dodelet, D. Guay, M. Ladouceur, G. Tourillon *Journal of Physical Chemistry* **1992**, *96*, 10898; (b) S. Kim, G. Kwag *Bulletin of Korean Chemical Society* **2002**, *23*, 25; (c) M. Ladouceur, G. Lalande, D. Guay, J.P. Dodelet *Journal of Electrochemistry Society* **1993**, *140*, 1974; (d) L.T. Weng, P. Bertrand, G. Lalande, D. Guay, J.P. Dodelet *Applied Surface Science* **1995**, *84*, 9.
- ⁹²(a) X. Li, G. Liu, B.N. Popov *Journal of Power Sources* **2010**, *195*, 6373; (b) J.S. Spendelov, A. Wieckowski *Physical Chemistry Chemical Physics* **2007**, *9*, 2654.

- ⁹³V. Bambagioni, C. Bianchini, J. Filippi, A. Lavacchi, W. Oberhauser, A. Marchionni, S. Moneti, F. Vizza, R. Psaro, V. Dal Santo, A. Gallo, S. Recchia, L. Sordelli *Journal of Power Sources In Press* **2010**.
- ⁹⁴H.J. Zhang, X. Yuan, W. Wen, D.Y. Zhang, L. Sun, Q.Z. Jiang, Z.F. Ma *Electrochemistry Communication* **2009**, *11*, 206.
- ⁹⁵H. Schulenburg, S. Stankov, V. Schunemann, J. Radnik, I. Dourbandt, S. Fiechter, P. Bogdanoff, H. Tributsch *Journal of Physical Chemistry B* **2003**, *107*, 9034.
- ⁹⁶D. Morales-Acosta, L.G. Arriaga, L. Alvarez-Contreras, S. Fraire Luna, F.J. Rodríguez Varala *Electrochemistry Communications* **2009**, *11*, 1414.
- ⁹⁷A. Nozad Golikand, M. Asgari, E. Lohrasbi *International Journal of Hydrogen Energy*, In Press, **2010**.
- ⁹⁸(a) F. Barbir, PEM Fuel Cells: Theory and Practice, Elsevier Academic Press, Burlington, MA, **2005**; (b) J. Larminie, A. Dicks, Fuel Cell Systems Explained, 2nd ed., Wiley, New York, **2003**; (c) S.H.Ge, X. G. Li, B. L. Yi, I. M. Hsing *Journal of Electrochemical Society* **2005**, *152*, A1149.
- ⁹⁹T. Thampan, S. Malhotra, H. Tang, R. Datta *Journal of Electrochemical Society* **2000**, *147*, 3242.
- ¹⁰⁰P. W. Majsztrik, M. B. Satterfield, A. B. Bocarsly, J. B. Benziger *Journal of Membrane Science* **2007**, *301*, 93.
- ¹⁰¹(a) J.R. Varcoe, R. C. T. Slade, E. L. H. Yee *Chemistry Communications* **2006**, 1428; (b) J. R. Varcoe, R. C. T. Slade *Electrochemistry Communications* **2006**, 8,839; (c) J. R. Varcoe, R. C. T. Slade, E. L. H. Yee, D. D. Poynton, D. J. Driscoll *Journal of Powe Sources* **2007**, *173*,194.
- ¹⁰²(a) T. J. Xu *Membrane Science* **2005**, 263,1; (b) J. Fang, P. K. Shen *Journal of Membrane Science* **2006**, 285,317; (c) H. Hou, G. Sun, R. He, Z. Wu, B. Sun, *Journal of Power Sources* **2008**, *182*, 95.
- ¹⁰³C. Bianchini, V. Bambagioni, J. Filippi, A. Marchionni, F. Vizza, P. Bert, A. Tampucci *Electrochemistry Communications* **2009**, *11*, 1077.
- ¹⁰⁴N. Fujiwara et al. *Electrochemistry Communications* **2009**, *11*, 390.
- ¹⁰⁵(a) R. Pattabiraman *Applied Catalysis A: General* **1997**, *153*, 9; (b) H. T. Zheng, Y. Li, S. Chen, P. K. Shen *Journal of Power Sources* **2006**, *163*,371; (c) P. K Shen, C. Xu *Electrochemistry Communications* **2006**, *8*,184.

- ¹⁰⁶C. Coutenceau, L. Demarconnay, C. Lamy, J. M. Léger *Journal of Power Sources* **2006**, *156*, 14.
- ¹⁰⁷L. Demarconnay, S. Brimaud, C. Coutenceau, J. M. Léger *Journal of Electroanalytical Chemistry* **2007**, *601*,169.
- ¹⁰⁸(a) Z. Q. Tian, F.Y Xie, P. K. Shen *Journal of Material Science* **2004**, *39*, 1509; (b) P. K. Shen, Z. Q. Tian *Electrochimica Acta* **2004**, *49*, 3107.
- ¹⁰⁹C. Bianchini, P. K. Shen *Chemical Reviews* **2009**, *109*, 4183.
- ¹¹⁰(a) F. Coloma, A. Sepulvedaescribano, J. L. G. Fierro *Langmuir* **1994**, *10*, 750; (b) Y. Y. Shao, G. P. Yin, Y. Z. Gao *Journal of Power Sources* **2007**, *171*, 558; (c) X. W. Yu, S. Y. Ye *Journal of Power Sources* **2007**, *172*, 14.
- ¹¹¹Z. P. Sun, X. G. Zhang, R. Liu, Y. Y. Liang, H. L. Li *Journal of Power Sources* **2008**, *185*, 801.
- ¹¹²F. P. Hu, P. K. Shen, Y. L. Li, J. Y. Liang, J. Wu, Q. L. Bao, C. M. Li, Z. D. Wei *Fuel Cells* **2008**, *8*,429.
- ¹¹³Z.-Z. Zhu, Z. Wang, H.-L. Li *Journal of Power Sources* **2009**, *186*, 339.
- ¹¹⁴R. N. Singh, A. S. Anindita *Carbon* **2009**, *47*, 271.
- ¹¹⁵M. Wang, D. J. Guo, H. Li *Journal of Solid State Chemistry* **2005**, *178*, 1996.
- ¹¹⁶K. F. Zhang, D. J. Guo, X. Liu, J. Li, H. L. Li, Z. X. Su *Journal of Power Sources* **2006**, *162*, 1077.
- ¹¹⁷M.W. Xu, G.Y. Gao, W.J. Zhou, K.F. Zhang, H.L. Li *Journal of Power Sources* **2008**, *175*, 217.
- ¹¹⁸C. W. Xu, L. Cheng, P. K. Shen, Y. L. Liu, *Electrochemistry Communications* **2007**, *9*, 997.
- ¹¹⁹D. S. Yuan, C. W. Xu, Y. L. Liu, S. Tan, X. Wang, Z. Wei, P. K. Shen *Electrochemistry Communications* **2007**, *9*, 2473.
- ¹²⁰F. P. Hu, Z. Y. Wang, Y. L. Li, C. M. Liu, X. Zhang, P. K. Shen *Journal of Power Sources* **2008**, *177*, 61.
- ¹²¹(a) M. Nie, ,H. L. Tang, Z. D. Wei, S. P. Jiang, P. K. Shen *Electrochemistry Communications* **2007**, *9*, 2375; (b) F. P. Hu, P. K. Shen *Journal of Power Sources* **2007**, *173*, 877; (c) X. D. Hu, F. P. Hu, J. G. Wang, P. K. Shen *Journal of Catalysis* **2008**, *29*, 1027; (d) F. P. Hu, G. F. Cui, Z. D. Wei, P. K. Shen, *Electrochemistry Communications* **2008**, *10*, 1303.

- ¹²²(a) W. Lee, M. G. Kim, J. Choi, J. Park, S. J. Ko, S. J. Oh, J. Cheon *Journal of American Chemical Society* **2005**, *127*, 16090; (b) E. Spinacé, A. O. Neto, A. M. Linardi *Journal of Power Sources* **2004**, *128*, 121.
- ¹²³V. Bambagioni, C. Bianchini, J. Filippi, W. Oberhauser, A. Marchionni, F. Vizza, R. Psaro, L. Sordelli, M. L. Foresti, M. Innocenti *ChemSusChem* **2009**, *2*, 99.
- ¹²⁴(a) J. Ge, W. Xing, X. Xue, C. Liu, T. Lu, J. Liao, *Journal of Physical Chemistry C* **2007**, *111*, 17305; (b) B. Liu, H. Y. Li, X. H. Zhang, Z. Fan, J. H. Chen *Journal of Power Sources* **2009**, *186*, 62.
- ¹²⁵(a) K. S. Kumar, P. Haridoss, S. K. Seshadri *Surface and Coatings Technology* **2008**, *202*, 1764; (b) J. Zhang, M. Huang, H. Ma, F. Tian, W. Pan, S. Chen *Electrochemistry Communications* **2007**, *9*, 1298.
- ¹²⁶(a) C. W. Xu, H. Wang, P. K. Shen, S. P. Jiang *Advanced Materials* **2007**, *19*, 4256; (b) F. L. Cheng, H. Wang, Z. H. Sun, M. X. Ning, Z. Q. Cai, M. Zhang *Electrochemistry Communications* **2008**, *10*, 798; (c) H. Wang, C. Xu, F. Cheng, M. Zhang, S. Wang, S. P. Jiang *Electrochemistry Communications* **2008**, *10*, 1575.
- ¹²⁷(a) J.S. Bradley, in *Clusters and Colloids: from Theory to Applications*, ed. G. Schmid, VCH, Weinheim, **1994**, pp. 459–536; (b) X. M. Yan, J. Ni, M. Robbins, H. J. Park, W. Zhao and J. M. White *Journal of Nanoparticles Research* **2002**, *4*, 525.
- ¹²⁸T. Sasaki, N. Koshizaki, S. Teuchi, H. Umehara, Y. Matsumoto, M. Koinuma, *Nanostructured Materials* **1997**, *8*, 1077.
- ¹²⁹G. A. Somorjai *Applied Surface Science* **1997**, *122*, 1.
- ¹³⁰K. S. Morley, P. C. Marr, P. B. Webb, A. R. Berry, F. J. Alison, G. Moldovan, P. D. Brown and S. M. Howdle *Journal of Material Chemistry* **2002**, *12*, 1898.
- ¹³¹(a) P. Serp, R. Feurer, Y. Kihn, P. Kalck, J. L. Faria and J. L. Figueiredo *Journal of Physical IV* **2002**, *12(PR4)*, 29; (b) P. Serp, R. Feurer, Y. Kihn, P. Kalck, J. L. Faria and J. L. Figueiredo *Journal of Materials Chemistry* **2001**, *11*, 1980.
- ¹³²K.-Y. Chan, J. Ding, J. Ren, S. Cheng, K. Y. Tsang *Journal of Materials Chemistry* **2004**, *14*, 505.
- ¹³³(a) H. Bönemann, R. M. Richards *European Journal of Inorganic Chemistry* **2001**, *10*, 2455; (b) P. V. Kamat *Journal of Physical Chemistry B* **2002**, *106*, 7729; (c) A. Roucoux, J. Schulz and H. Patin *Chemistry Review* **2002**, *102*, 3757.
- ¹³⁴Y. Wang, J. Ren, K. Deng, L. Gui and Y. Tang *Chemistry of Materials* **2000**, *12*, 1622.

¹³⁵J. V. Zoval, J. Lee, S. Gorerand, R. M. Penner *Journal of Physical Chemistry B* **1998**, *102*, 1166.

¹³⁶(a) J. Wang, Lee See Ee, S. C. Ng, C. H. Chewand, L. M. Gan *Materials Letters* **1997**, *30*, 119; (b) M. H. Lee, C. Y. Taiand, C. H. Lu *Journal of European Ceramic Society* **1999**, *19*, 2593.

Chapter 2. Palladium onto Nickel-Zinc supports

2.1 Overview

This chapter provides the synthesis and the characterization of two nanostructured palladium-based electrocatalysts for anodes of DAFCs, where the anolytes are alkaline aqueous solutions of renewable alcohols such ethanol, glycerol and ethylene glycol.

For comparative purposes is also described the synthesis and the characterization of a traditional palladium catalyst supported on Vulcan XC-72. The chemical-physical characterization of all materials was carried out by HRTEM, EXAFS, XANES, ICP-AES, XRPD techniques.

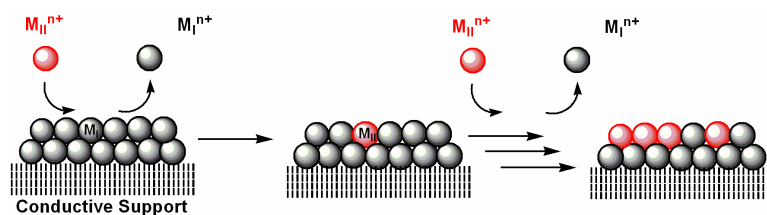
Next, the electrocatalytic activity of all materials towards several fuels was evaluated in both half-cells and monoplanar passive and active fuel cells. To this aim, MEAs were assembled using cathodes comprising in-house Fe-Co electrocatalysts and anion-exchange membranes (from Tokuyama, Japan).

Finally, we focus on the NaBH_4 fuel additive use capable of improving the fuel cell performance, especially in terms of fuel efficiency.

2.2 Introduction

Palladium has recently aroused notable interest in electrocatalysis as it is more abundant in nature, hence less expensive (four times) than platinum and has the capacity to promote the oxidation of several alcohols, including ethanol, in alkaline media. Current synthetic methods for the preparation of Pd-based electrocatalysts for anodes of DAFCs are manifold ¹. There are many aspects to consider for manufacturing electroactive materials. The three major procedures are outlined below.

Electroless procedures generally involve the adsorption of a palladium compounds (PdCl_2 , K_2PdCl_4 or H_2PdCl_4), alone or in conjunction with a salt of another metal, onto a conductive support material, generally carbon black, followed by reduction in aqueous dispersion with an appropriate reducing agent that may also act as templating agent to favor the formation of nanosized metal particles (NaBH_4 , ethylene glycol, hydrazine, tannic acid, formic acid, formaldehyde, hydrogen gas) ². It is also possible that surfactant-stabilizing can be independently prepared and later mixed with a carbon black ³. Following this procedure nanosized Pd particles are obtained with dimension depending on the reducing agent as well as the reaction parameters. An important role in determining the structure of the Pd particles is also provided by the morphological characteristics of the carbon black, in particular specific area, pores and micropores dimension, chemical nature of the surface. So a large variety of conductive materials have been used to support Pd nanoparticles, alone^{2a} or in combination with either nanocrystalline metal oxides (NiO , CeO_2 , Co_3O_4 , Mn_3O_4) ^{4,5} or tungsten carbide nanocrystals ⁶. The two most common supports are Vulcan XC-72 and Ketjen Black, but it is possible also utilize carbon microspheres ⁷, coinlike hollow carbons ⁸, ultrahigh-surface hollow carbon spheres⁹, carbonized porous anode alumina ¹⁰, carbonized TiO_2 nanotubes ¹¹, multiwalled carbon nanotubes ¹² and activated carbon nanofibers ¹². As an alternative to electroless procedure,



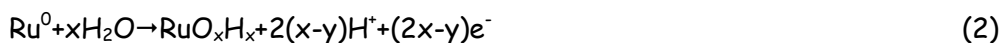
Scheme 1. Deposition of metal MII onto particles of metal MI by redox transmetalation³³.

Pd-electrocatalysts can be synthesized by electrochemical methods. One of the most used is the electrodeposition of one metal at a time, eventually followed by the electrodeposition of other metals, if necessary. Pd nanowire arrays have been prepared by template-electrodeposition on glassy carbon electrodes¹³ with a highly ordered scheme, while cyclic potential sweep techniques have been used to prepare Pd thin films on polycrystalline Pt or Au substrates¹⁴.

A third, less frequent method to synthesize Pd-based electrocatalysts is the spontaneous deposition of noble metals onto less-noble metal particles or metal surfaces^{15,16}. This technique has found some applications for the preparation of anode electrocatalysts for fuel cells^{15c,d,e,16e}, including only one example of an active Pt-Ru anode catalyst in a DEFC^{15c}. The spontaneous deposition is actually considered as a transmetalation reaction, while it is often confused with the electroless deposition technique¹⁷. One of the best definitions has been proposed by Cheon and co-workers^{15b} who wrote: "When a metal-ligand complex in a positive metal oxidation state ($M_{II}^{n+}L_i^{n-}$) approaches an other metal surface (M_I), $M_{II}L_i$ molecules can be reduced through the sacrificial oxidation of the M_I surface atoms to produce M_{II} deposition on the M_I metal surface via a redox transmetalation process". A scheme representing the spontaneous deposition of a high-valent metal through redox transmetalation is shown in the following Scheme 1 for a hypothetical metal phase supported on a conductive material. Using the spontaneous deposition method, Nakashima et al. obtained the formation of a Pt-Ni alloy by treatment of nickel discs with an aqueous solution of H_2PtCl_6 under acidic conditions by the mentioned above mechanism¹⁸. The redox reaction that would occur [Eq. (1)] generates a modified nickel electrode that is active in the catalytic oxidation of methanol.



Certain examples can be lain between the spontaneous and the electroless deposition. This might be the case of the deposition of Pt on either a Ru(001) single surface ^{16d} or Ru nanoparticles supported on Vulcan XC-72R ^{15c}. Indeed, Adzic and co-workers argued that the oxidative dissolution of Ru by action of $[\text{PtCl}_6]^{2-}$ can be excluded because it would occur at a potential more positive than the equilibrium potential of $\text{Pt}/[\text{PtCl}_6]^{2-}$ ^{2,15c}. So they proposed that the reduction of $[\text{PtCl}_6]^{2-}$ to Pt metal is assisted by Ru-OH surface species, easily formed under the specific experimental conditions [Eqs. (2) and (3)].



In this PhD thesis work, we describe the synthesis of new nanostructured Pd-based catalysts obtained by the spontaneous deposition of Pd on Ni-Zn materials. Traditional Vulcan XC-72 supported Pd catalysts were prepared for comparative purposes by electroless reduction ^{19,20,21}.

As metal phases for the transmetallation reaction, we selected skeletal or sponge nickel alloys similar to Raney nickel (such as Ni-Al and Ni-Zn) that are being used to catalyze various chemical processes (e.g. hydrogenation and hydrogenolysis) as well as electrochemical processes, such as the water ^{22,23} and aqueous ammonia ^{24,25} electrolysis. Skeletal Ni materials have the advantage of being cheap and have a high surface area. However they present some disadvantages: pyrophoricity, the great tendency to be oxidized in air with the formation of thick surface-oxide layers and the strong corrosion in acidic conditions. All of these features have prevented so far their effective use in polymer electrolyte membrane fuel cells (PEMFCs) and DMFCs ²⁶. The alkaline environment is mandatory for Ni, and the effectiveness of Ni electrocatalysts to oxidize alcohols in alkaline media either in half ^{27,28} or monoplanar cells ²⁹ have been proved. A patent of 1997 ³⁰ reported the spontaneous deposition of palladium onto a Ni-Al alloy for the oxidation of hydrogen in a fuel cell. The presence of Zn in the material for depositing palladium is not a drawback as Zn is more electropositive than Ni and therefore prone to undergo fast transmetalation by reaction with Pd^{II} or Pd^{IV} salts. The Ni-Zn phases were prepared through two procedures. The first is reported for the Ni-Zn Urushibara catalysts, which exist in two forms depending on whether the excess of Zn is

removed by using an acid or a base ³¹. The second one is referred to the Ni-Zn-P composites, developed for the protection of steel from corrosion ³². During the synthesis both of them were supported on Vulcan XC-72. To the best of our knowledge, there are no other reports describing the use of Urushibara-like or Ni-Zn-P composites as starting materials for transmetalation reactions with noble metals, eventually leading to anode electrocatalysts for DAFCs. All new materials were characterized by high resolution microscopy (HRTEM), combined with Energy-Dispersive X-ray spectroscopy (EDX) measurements, X-ray Powder Diffraction (XRPD), Inductively Coupled Plasma-Atomic Emission Spectroscopy (ICP-AES) Extended X-ray Absorption Fine Structure (EXAFS) and X-ray Absorption Near Edge Structure (XANES). The latter two techniques have provided insight into the local environment of the palladium and nickel atoms. The electrochemical measurements were carried out primarily in half-cells (cyclic voltammetry, cronopotentiometric tests, Tafel plots) in the presence of different fuel solutions (ethanol, glycerol, methanol, ethylene glycol, generally in 5-10 wt%) and in alkaline media 2M KOH. The tests in active monoplanar cells were carried out using a fuel cell control system by Scribner (USA) and in passive monoplanar cells by ARBIN potentiostat-galvanostat.

2.3 Results and discussion

2.3.1 Catalyst synthesis

The Ni-Zn Urushibara type used for the spontaneous deposition of palladium was obtained by reducing a hydrous nickel (II) salt with Zn powder in the presence of Vulcan XC-72, followed by treatment of the resulting Ni-Zn phase with an alkaline hydroxide, generally NaOH, to remove the Zn excess. The resulting material is denoted as Ni-Zn/C.

The Ni-Zn-P support was prepared by the reduction of mixtures of Ni and Zn salts with sodium hypophosphite in the presence of sodium citrate, ammonium chloride and Vulcan XC-72, followed by treatment with concentrated KOH solution to remove the excess of zinc. The resulting support product is denoted as Ni-Zn-P/C.

The spontaneous deposition of Pd was achieved by stirring an aqueous solution of K_2PdCl_4 in the presence of either materials under a nitrogen atmosphere for several hours³³.

The amount of Pd deposited onto the Ni-Zn/C or Ni-Zn-P/C materials was, in all cases, proportional to the loss of Ni and Zn from the support, which confirms the occurrence of a redox transmetalation process. Control experiments in which an aqueous solution of K_2PdCl_4 was added to a stirred dispersion of Vulcan XC-72, followed by washing with water did not show any appreciable deposition/adsorption of Pd on the carbon black.

Finally, the Pd/C catalyst was prepared by electroless reduction of an aqueous dispersion of Vulcan XC-72 impregnated with a $PdCl_2/HCl$ solution with ethylene glycol at high temperature^{19,20,21}.

2.3.2 Catalyst characterization

The distribution diagram of volume particles vs diameter for Pd-(Ni-Zn)/C showed an average diameter Pd particle of 2.3 nm (σ 0.5 nm) (Figure 1a). By an in column EDX probe, palladium was found often in aggregates of several small particles where Pd/Ni ratio was 1:2. Here, the two metals are not alloyed and show well defined truncated cuboctahedron-hexagonal geometry habit and diffraction fringes of metal Ni(110) ($d=0.249$ nm), Ni(111) ($d=0.203$ nm), Pd(110) ($d=0.275$ nm) and Pd(200) ($d=0.194$ nm) crystal planes, indicated a Ni and Pd face-centered-cubic packing (fcc) in a cubohoctaedral growth geometry.

Where the metal particles were sufficiently large and isolated to allow for a single particle EDX analysis, the composition was predominantly Pd or predominantly Ni-Zn (5:1), with the palladium particles larger than Ni particles and not alloyed (Figure 1b). Indeed, a comparison of the metal element map distribution, performed at high magnification (250000 X) for Pd and Ni, showed clearly the proximity of the particles of the two atomic species, as the distribution density was well reproduced, but the images were not superimposable, suggesting the absence of alloys or decoration effects. Most of the support grains were crystalline with well resolved diffraction fringes of the graphite planes and showed a uniform dispersion of the metal particles over the entire support surface.

Samples of Pd-(Ni-Zn)/C was investigated by EXAFS and XANES in an attempt of elucidating the local environment of the Pd and Ni atoms in the corresponding agglomerates. The Pd-(Ni-Zn)/C sample was kept all the way under a nitrogen atmosphere. The spectroscopic analysis results defined that the Ni atoms was largely present as small metal particles with an average size of 1.5 nm (Figure 2) and that the large majority of Pd was present as small metal phase with a mean size of 1 nm (Figure 3), with a little amount of Pd oxidized.

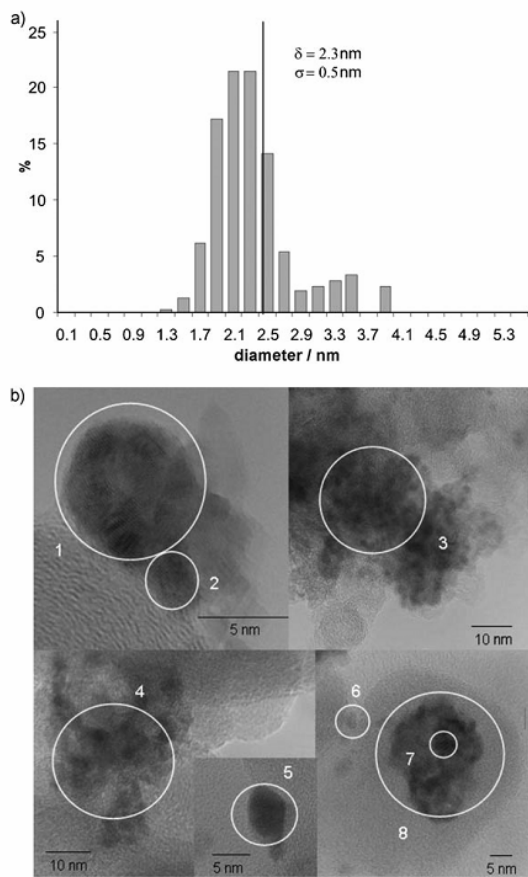


Figure 1. a) HRTEM histograms of particle volume distribution versus diameter for Pd-(Ni-Zn)/C. The average size (δ) and standard deviation (σ) are reported. b) HRTEM images of Pd-(Ni-Zn)/C at different magnifications. Spots of EDX analysis are shown in circles; Pd/Ni relative compositions as detected by EDX integrated peak areas: 1) Ni > Pd with Ni(110) plane fringes; 2) Ni(111) plane fringes; 3) Pd/Ni=1:2; 4) Pd/Ni=1:1; 5) Pd with cubooctahedron crystal facets; 6) Ni; 7) Pd(110) plane fringes; 8) Pd > Ni. There is a minor O contribution everywhere³³.

The Pd(II) particles were most probably due to a little oxide layer at the metal surface, which could not ruled out a coordination to four oxygen atoms by the isolated palladium ions. There was no evidence of the Ni-Pd alloy phase, as we found neither Ni neighbors at the Pd edge nor the contrary.

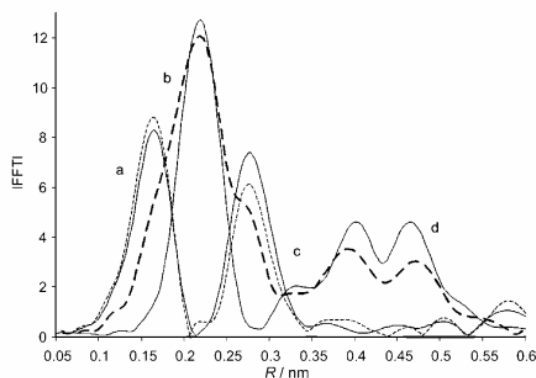


Figure 2. Ni-K edge Fourier transform EXAFS spectra (not phase-corrected): a) Pd-(Ni-Zn-P)/C (—); b) Pd-(Ni-Zn)/C (---); c) NiO (...); and d) Ni foil reference standards (—)³³.

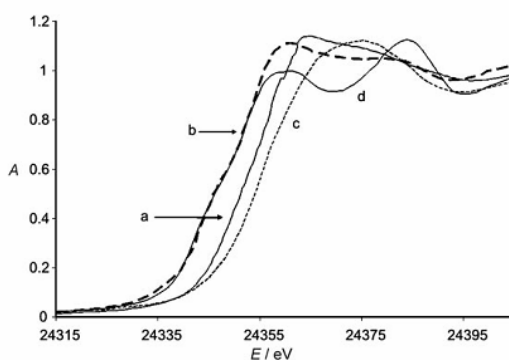


Figure 3. Pd-K edge XANES spectra: a) Pd-(Ni-Zn-P)/C (—); b) Pd-(Ni-Zn)/C (---); PdO (...); and d) Pd foil reference standards (—)³³.

The HRTEM image of Pd-(Ni-Zn-P)/C showed a broad metal particle size distribution, with a mean diameter of 3.2 nm (σ 1.3 nm) (Figure 4). In the areas where EDX analysis was possible 70% of metal particles were agglomerated with Pd:Ni composition of ca. 1:1. Ni small amorphous particles were detected together with some particles having lamellar structure. Zn and P were not detected, because their concentrations were below the instrumental resolution, while oxygen is present in moderate concentration everywhere in the sample. Few larger Pd particles were also visible (4-6 nm) that could be included in a thick amorphous oxide layer surrounding small metal cores.

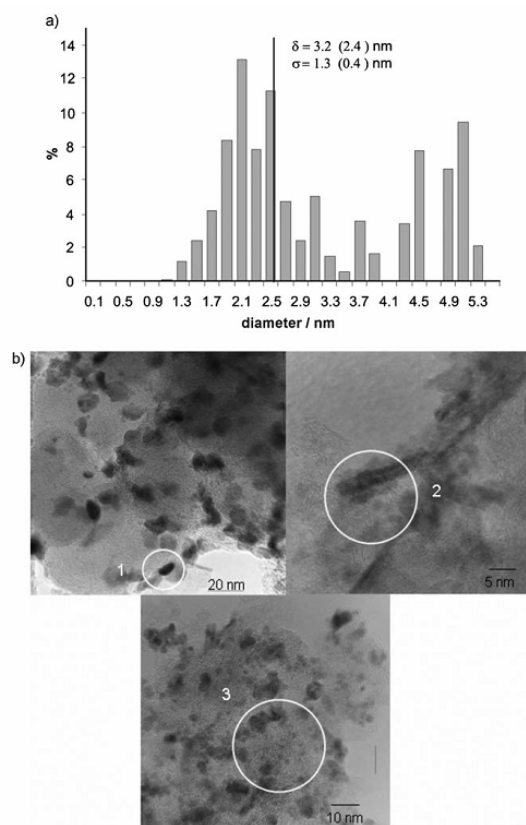


Figure 4. a) HRTEM histograms of particle volume distribution versus diameter for Pd-(Ni-Zn-P)/C. the average size (δ) and standard deviation (σ) are reported. b) HRTEM images of Pd-(Ni-Zn-P)/C at different magnifications. Spots of EDX analysis are shown in circles; Pd/Ni relative compositions as detected by EDX integrated peak areas: 1) Pd; 2) Ni; 3) Ni/Pd=1:1; There is a minor oxygen contribution everywhere³³.

The diffraction fringes of graphite support grains were present, but the metal particle distribution were inhomogeneous on the surface.

Pd-(Ni-Zn-P)/C was characterized by EXAFS and XANES experiments, after being purposefully exposed to air for 12 h before being examined. In Pd-(Ni-Zn-P)/C. Ni was present in a Ni bulk oxide phase (Figure 2), with small contributions from Zn at distance consistent with Ni-Zn and Ni-Zn-P (Table 1) in many of the possible alloy phases in which they can exist. Pd was present in metal phase to form small clusters (<0.5 nm) with an average number of 1.8 Pd-Pd metal neighbours and partly as isolated ions in a four-oxygen coordination sphere (Figure 5).

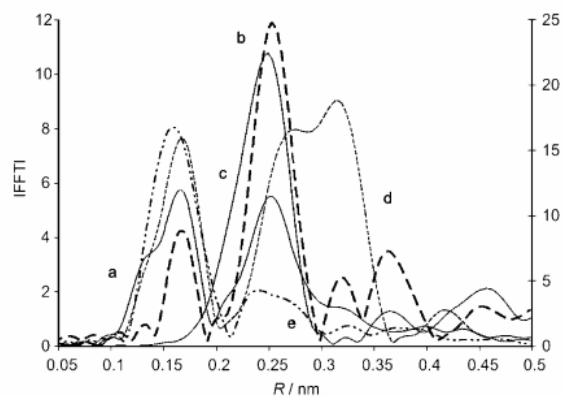


Figure 5. Pd-K edge Fourier transformed EXAFS spectra (not phase-corrected): a) Pd-(Ni-Zn-P)/C; b) Pd-(Ni-Zn)/C; reference standards: c) Pd foil (right axis); d) PdO; and e) $[\text{Pd}(\text{acac})_2]$.³³

Table 1. EXAFS best fit results at Ni and Pd K-edges and estimated average metal particle diameters (D). ^[a]					
Sample	Ni K-edge				
	shell	N	R [Å]	σ_{DW} [Å]	D [Å]
Pd-(Ni-Zn-P)/C	Ni-O	5.4(1)	2.04(2)	0.072(2)	
	Ni-Zn	1.3(2)	2.48(3)	0.097(4)	
	Ni-Ni _{ox}	8.9(1)	3.12(2)	0.098(3)	
	Ni-Zn _{NiPZn}	1.5(2)	3.08(3)	0.099(1)	
Pd-(Ni-Zn)/C	Ni-O	2.5(1)	2.02(2)	0.074(2)	15
	Ni-Ni _{ox}	3.7(3)	2.96(2)	0.081(3)	
	Ni-Ni _{met}	5.3(2)	2.46(3)	0.084(1)	
Ni foil	Ni-Ni	12	2.48(1)	0.073(1)	
NiO	Ni-O	6	2.08(2)	0.065(3)	
	Ni-Ni	12	2.94(3)	0.081(2)	
Sample	Pd K-edge				
	shell	N	R [Å]	σ_{DW} [Å]	D [Å]
Pd-(Ni-Zn-P)/C	Pd-O	4.0(2)	2.02(2)	0.077(4)	< 5
	Pd-Pd _{met}	1.8(3)	2.74(3)	0.071(2)	
	Pd-Ni _{ox}	1.9(2)	3.24(3)	0.089(4)	
Pd-(Ni-Zn)/C	Pd-O	3.5(3)	2.05(3)	0.079(2)	10
	Pd-Pd _{met}	3.3(4)	2.75(2)	0.070(4)	
	Pd-Pd _{ox}	1.7(2)	3.38(4)	0.071(2)	
Pd foil	Pd-Pd	12	2.738(1)	0.006(1)	
PdO	Pd-O	4	2.032(2)	0.056(2)	
	Pd-Pd	4	3.042(2)	0.088(3)	
$[\text{Pd}(\text{acac})_2]$ ^[b]	Pd-Pd	8	3.378(4)	0.089(2)	
	Pd-O	4	1.963(1)	0.006(2)	

[a] Error bars for the last decimal place are provided in parentheses. Subscripts: ox = oxidized, met = metal. [b] acac = acetylacetonate.

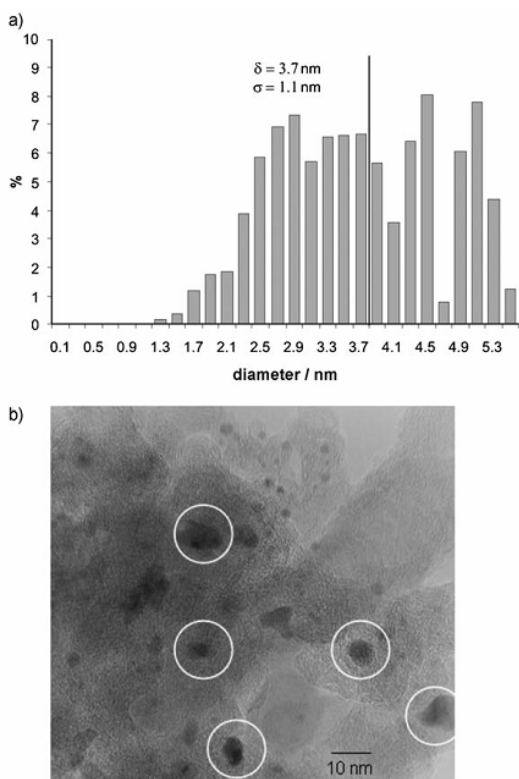


Figure 6. a) HRTEM histograms of particle volume distribution versus diameter for Pd/C. The average size (δ) and standard deviation (σ) are reported. b) HRTEM images of Pd/C. Spots of EDX analysis are shown in circles (Pd with minor O contribution)³³.

This is consistent with a spontaneous deposition process during the synthesis. The distance of 3.24 \AA from Ni and Pd was consistent with a Pd-O-Ni shell to indicate that Pd single sites are stabilized by oxygen of NiO on the Pd-(Ni-Zn-P)/C surface³⁴.

The HRTEM image of Pd/C showed quite a broad particle size distribution with mean diameter of 3.7 nm and a standard deviation (σ) of 1.1 nm. (Figure 6). The EDX analysis of the circled spots showed much larger and less crystalline Pd particles than in Pd-(Ni-Zn)/C or Pd-(Ni-Zn-P)/C.

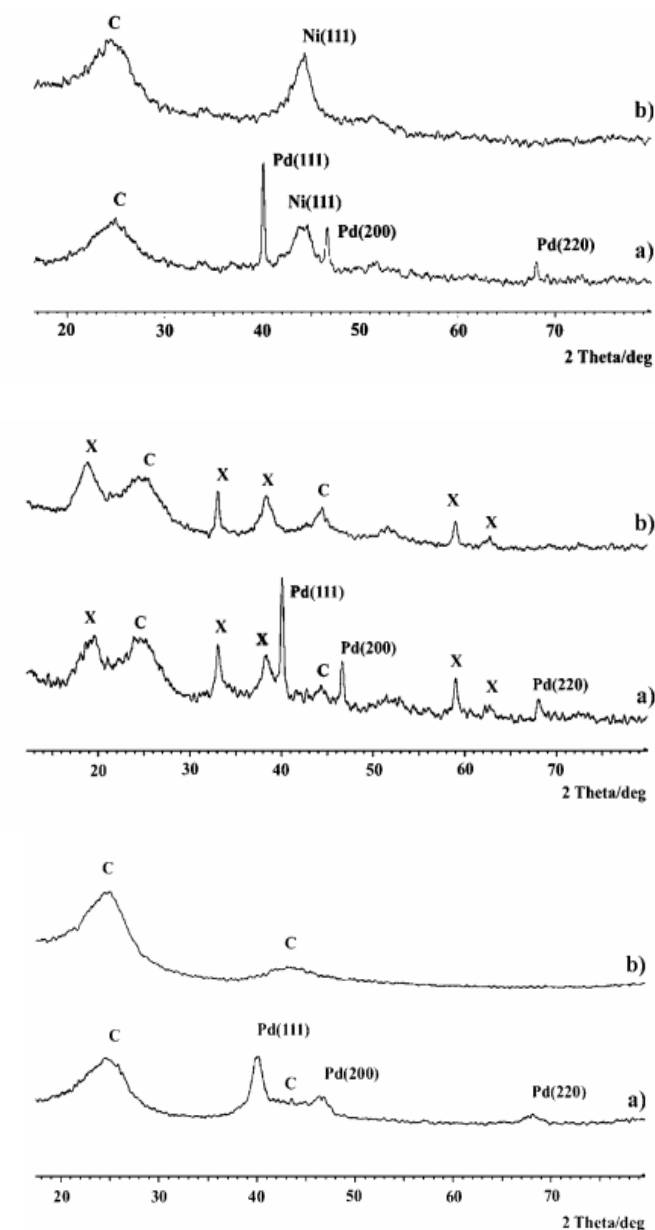


Figure 7. XRPD patterns of 1a) Pd-(Ni-Zn)/C and 1b) Ni-Zn/C; 2a) Pd-(Ni-Zn-P)/C and 2b) Ni-Zn-P/C; 3a) Pd/C and 3b) C (Vulcan XC-72) materials³³.

The XRPD spectra of Pd-(Ni-Zn)/C, Pd-(Ni-Zn-P)/C, and Pd/C, (a) together with those of the corresponding support material (b) are reported in Figure 7. All spectra revealed the presence of the typical diffraction peaks of the carbon support at around 25° and 44° and the diffraction peaks at the Bragg angles of 40.10°, 46.40°, and 68.08° for respectively (111), (200), (220) facets of fcc Pd crystals³⁵. The XRPD spectra of (Ni-Zn)/C showed a peak at 44.5° due to Ni(111)³⁵, as well as several peaks to the (Ni-Zn-P)/C

phase. A clear assignment of the peaks at 19°, 32.8°, 38.2°, 59° and 62.8° (“X” peaks) is not possible as Ni-Zn-P alloys can exist in a variety of compositions and morphologies depending on the experimental synthesis conditions (above all pH and stoichiometric ratio of the reagents)^{32,36,37,38}. Cross experiments on the supports containing the Zn-P/C and Ni-P/C phases confirmed that nickel contributes to all the peaks “X” marked in Figura 7. The Pd/C material exhibited less crystalline metal particles, still representative of fcc Pd. In accordance with the EXAFS and HRTEM results, the XRPD analysis confirm that highly crystalline Pd particles are obtained on the Ni-Zn and Ni-Zn-P phases.

2.3.3 Electrochemical characterization of the Pd-based catalysts in alkaline environment

The Ni-Zn-P/C and Ni-Zn/C materials were electrochemically characterized in the same experimental conditions used in fuel cell systems (vide infra). A preliminary cyclic voltammetry (CV) was carried out in 2M KOH. Nickel alone^{27b),c),28,29} or combined with other transition metals^{36,37,38,39,40} is known to be an active electrocatalyst for alcohol oxidation in alkaline media, through at high overpotentials, never attained in a DAFC (vide infra). In Figure 8 the Ni-Zn/C CV was reported in 2M KOH (fifth scan) at scan rate of 50 mV/s. In the forward sweep one may notice the oxidation peak of Ni(OH)₂ to NiO(OH) at 0.44 V (vs Ag/AgCl/KCl_{sat}) and the relative reduction peak in the backward scan at 0.29 V^{41,42,43,44}. The assignment of the reduction peak at -0.30 V is not straightforward. The reduction of Ni(OH)₂ to Ni⁰ usually occurs at -1 V in alkaline environment^{43,44}, but the catalyst nanostructure might contribute to a positive shift. As suggested by Henn and co-workers⁴², a metal species of the type NiO₂H_{2-x} with 0<x<0.3 can be reduced to an effective Ni(OH)₂ state at -0.30 V. The CV voltammograms did not show a clear oxidation peak due to Ni⁰ to Ni(OH)₂ (-0.70/-0.60 V in alkaline media⁴⁴) in accordance with a complex oxidation path involving α-Ni(OH)₂ formation, followed by its transformation to β-Ni(OH)₂⁴¹. As shown in the inset of Figure 8, ethanol is actually oxidized by NiO(OH) species, but the relative overpotential is not available in any DAFC^{27c),28,29}. The Ni-Zn-P/C material exhibits a similar cyclic voltammogram compared to that of Ni-Zn/C (Figure 9) with some minor differences. The Ni(OH)₂ to NiO(OH) oxidation occurs at 0.49 V (vs 0.44 V for Ni-Zn/C) and the relative reduction peak is at 0.21 V (vs 0.29 V for Ni-Zn/C). There is also a shoulder at 0.35 V and the peak at -0.30 V is shifted to -0.35 V, which are probably due to the different nickel nature in Ni-Zn-P phase^{45,46,47}. Again, the onset of ethanol oxidation occurs at the formation of NiO(OH) species.

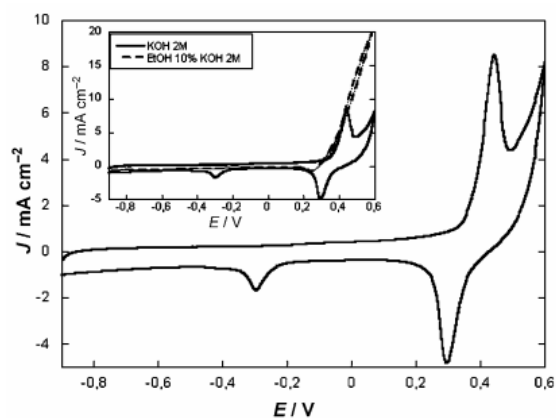


Figure 8. CV on Ni-Zn/C electrode in 2M KOH vs Ag/AgCl/KCl_{sat}. Scan rate 50 mV/s. Nickel loading 40 $\mu\text{g}/\text{cm}^2$. Inset: CV with 10 wt% EtOH in 2M KOH solution under nitrogen ³³.

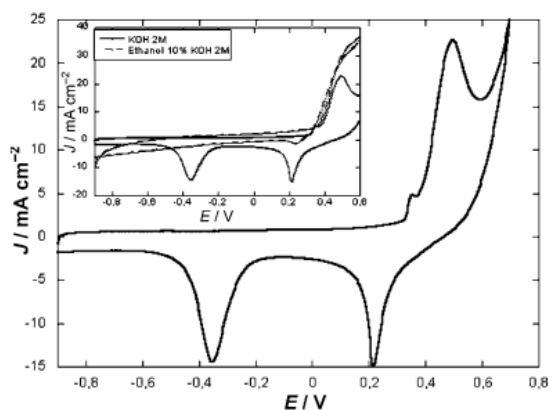


Figure 9. CV on Ni-Zn-P/C electrode in 2M KOH solution vs Ag/AgCl/KCl_{sat}. Scan rate 50 mV/s. Nickel loading 40 $\mu\text{g}/\text{cm}^2$. Inset: CV with 10 wt% EtOH in 2M KOH solution under nitrogen ³³.

Next the Pd-(Ni-Zn)/C, Pd/C, Pd-(Ni-Zn-P)/C catalysts were investigated by cyclic voltammetry in 2M KOH (Figure 10). The only difference respect to the CV of the Ni-based phases is the presence of the reduction peak of Pd^{II} species, either PdO or Pd(OH)₂, with an onset at -0.20 V and a peak at -0.47 V (the potential values are consistent with the nanostructured nature of the material). The CVs of Pd-(Ni-Zn)/C and Pd-(Ni-Zn-P)/C confirm that Pd and Ni are not alloyed in either materials. In the range of potentials investigated in the CV study, the formation of Pd^{IV} species can be ruled out safely^{48,49}.

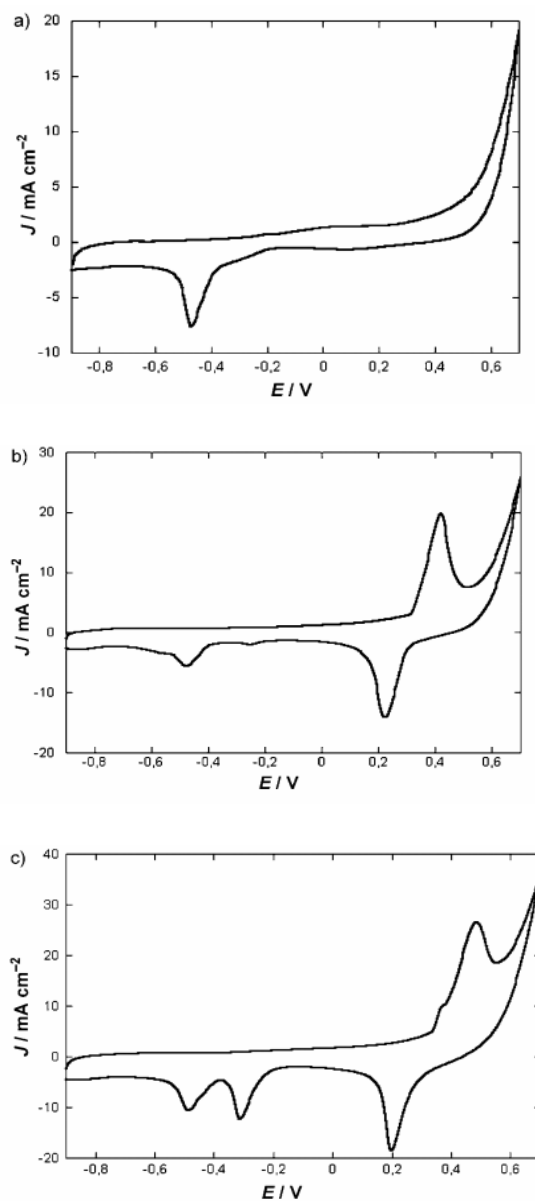


Figure 10. CVs on a) Pd/C electrode, Pd loading $23 \mu\text{g}/\text{cm}^2$; b) Pd-(Ni-Zn)/C electrode, Pd loading $24 \mu\text{g}/\text{cm}^2$; c) Pd-(Ni-Zn-P)/C electrode, Pd loading $22.1 \mu\text{g}/\text{cm}^2$ in 2M KOH solution, at scan rate of 50 mV/s vs Ag/AgCl/KCl sat under nitrogen³³.

It is not easy to explain the broad shape of Pd(0) to Pd(II) peak due to the complexity of the oxide/hydroxide palladium(II) species formed at the surface^{48,50}. The CV of Pd/C under comparable experimental conditions shows a broad oxidation peak starting at -0.2 V with a peak at 0.1 V, while a much narrower and more intense reduction Pd^{II} peak to Pd⁰ peak was observed to start at -0.20 V with a peak at -0.47 V (Figure 10).

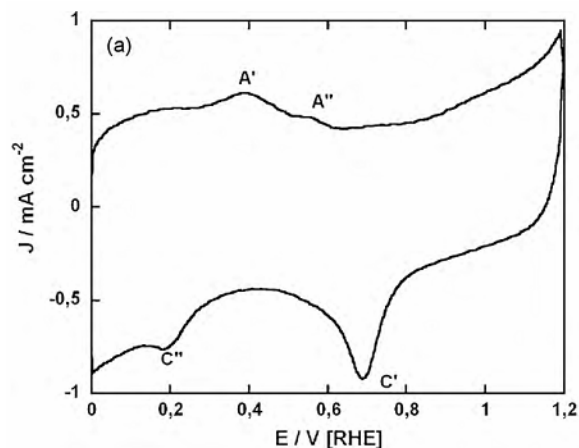
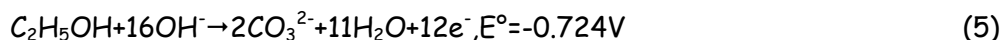
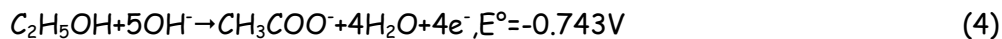


Figure 11. a) CV of a Pd/C electrode (vs RHE) in a 2M KOH solution under nitrogen. Scan rate 50 mV/s . Pd loading $23 \mu\text{g}/\text{cm}^2$ ⁵¹.

In an attempt of rationalizing the oxidation of Pd to Pd(II) in 2M KOH, a CV study was carried out on Pd/C. The results are illustrated in Figure 11. The peak A' (0.39 V vs RHE) is assigned to the oxidation of the adsorbed and absorbed hydrogen, which current depends on the hydrogen dissolved into palladium. A'' (0.53 V) is associated to oxidation of palladium to Pd(OH)⁵² and is overlapped to A'. The formation of PdO starts at 0.60 V and the formation of an oxide coverage of the surface was argued through the current increase. The cathodic peak C' at 0.69 V was associated to PdO reduction⁵³, while C'' (0.18 V) is attributed to hydrogen uptake⁵⁴.

2.3.4 Half cell studies of ethanol oxidation on the Pd-based catalysts in alkaline environment

The electrochemical activity of Pd-(Ni-Zn)/C, Pd-(Ni-Zn-P)/C and Pd/C towards ethanol oxidation was investigated by CV in 2M KOH + 10 wt% ethanol at room temperature. For all catalysts, the Pd loading varied from 20 to 25 $\mu\text{g}/\text{cm}^2$. The scan rate was kept to 50 mV/s. The KOH concentration was purposefully kept very high to maintain the pH higher than 13 during all the experiments in both half cell and monoplanar fuel cell. Indeed, an in situ FTIR study from our lab has shown that Pd behaves as a selective electrocatalyst for ethanol oxidation to acetate only for pH values higher than 13 (vedi infra)⁶⁷. Another reason to use a high OH^- concentration is the fact that ethanol oxidation in alkaline media consumes OH^- groups (Eq (4)-(5)).



The ethanol concentration was fixed to 2M (about 10 wt%, 2.17 M), although in terms of current density better results can be obtained for higher concentrations. On the other hand, the selected concentration is optimal to minimize alcohol crossover in DEFCs (direct ethanol fuel cells) as well as the loss of FC efficiency due to fuel evaporation^{55,56}. The CVs of the three catalysts investigated in the presence of 2M KOH solution containing 10 wt% ethanol are illustrated in Figure 12.

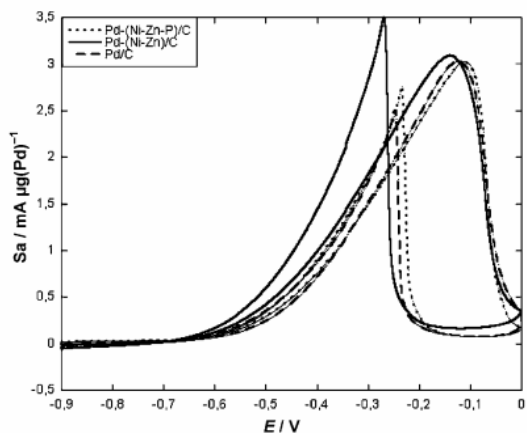


Figure 12. CVs (at the tenth cycle; E vs Ag/AgCl/KCl_{sat}) on Pd/C, Pd-(Ni-Zn)/C, and Pd-(Ni-Zn-P)/C electrodes in 2M KOH and 10 wt% EtOH solution under nitrogen. Scan rate 50 mV/s³³.

All the catalysts showed high efficiency for ethanol oxidation in terms of onset potential (-0.60 V) and specific current densities (around -0.10 V and 3.6 mA/μg Pd). Pd-(Ni-Zn)/C was the most active material. Considering that the oxidation of ethanol on the support (Ni-Zn/C or Ni-Zn-P/C) occurred at about 0.4 V, we can conclude that the nickel is not directly involved in the oxidation process. The backward scan revealed an additional anode peak. It can be associated to the oxidation of either fresh chemisorbed ethanol on newly generated Pd(0) species (vide infra) or weakly adsorbed species, most likely Pd-acetyl species⁵⁷. In Table 2 the electrochemical data for ethanol oxidation were reported for our catalysts as well as other catalysts fished out in the literature.

Shen et al. described several Pd-based electrocatalysts obtained with different procedures as well as different support materials^{2c),4,5}. In general, the Pd loading in Shen's catalysts is ten times higher than that in our electrocatalysts (300 vs 20-30 μg/cm²). The good dispersion and small size of the palladium nanoparticles obtained by the spontaneous deposition procedure as well as the presence of single Pd ions may account for the excellent performance of the Pd-(Ni-Zn-P)/C, and Pd-(Ni-Zn)/C electrocatalysts.

Table 2. Relevant electrochemical parameters for the ethanol oxidation reaction at room temperature on electrodes coated with the catalysts investigated in this work^[a] or with previously reported catalysts.

Catalyst	J_p [mA cm ⁻²]	Sa_p [mA μg(Pd) ⁻¹]	V_p [V]	Q_{sa} [C μg(Pd) ⁻¹]	Tafel slope [mV] ($\alpha=0.4$)
Pd/C	84.5	3.03	-0.12	0.0136	153 ($\alpha=0.4$)
Pd-(Ni-Zn-P)/C	108.7	3.03	-0.10	0.0135	132 ($\alpha=0.4$)
Pd-(Ni-Zn)/C	78.5	3.60	-0.14	0.0152	140 ($\alpha=0.4$)
Pd/C ^[b]	21	0.07	0.04		188 ^[c]
Pd-NiO/C ^[d]	95	0.32	-0.08		195 ^[c]
Pd/TiO ₂ C ^[e]	76	0.25	-0.19		
Pd/CPAA ^[f]	69	0.23	-0.08		

[a] Average values for at least three measurements. Peak current density (J_p), specific peak current density (Sa_p), forward anodic peak potential (V_p), integrated specific charge of the anodic peak area (Q_{sa}), Tafel slopes, and electronic transfer coefficient α . [b] Data taken from ref. [12]. [c] Data taken from ref. [10]. [d] Data taken from ref. [13]. [e] Data taken from ref. [19]. [f] Data taken from ref. [18] (CPAA = carbonized and pulverized porous anodic alumina).

Tafel plots for ethanol oxidation reaction (10 wt% EtOH +2M KOH) on Pd/C, Pd-(Ni-Zn-P)/C, and Pd-(Ni-Zn)/C electrodes were obtained at scan rate of 5 mV/s in the potential interval from -0.7 to -0.6 V vs Ag/AgCl/KCl_{sat}. The values for the Tafel slopes and of the α coefficients (Table 2) are comparable with each other as well as with those reported by Shen et al.^{2c}. The slope indicates the same reaction mechanism, while the α coefficients (0.4) are consistent with an electrochemical rate-limiting step for ethanol oxidation reaction on Pd. As for the absolute values of the Tafel slopes, the relatively high values observed are in line with porous high-surface-area electrodes with high electrocatalytic activity^{2c,50}. The catalyst stability was studied by chronopotentiometric experiments lasting 5.5h at 3 mA/cm² in EtOH 10 wt% + 2M KOH, using the same palladium loading used for the CVs experiments. As is apparent from perusal of Figure 13, the chrono-curves showed some potential oscillations only within the first 2-3 h, but the potential did not increase significantly, suggesting little electrode deterioration or poisoning^{58,59,60}. Under the present experimental conditions, the electrodes with the Pd-(Ni-Zn)/C and Pd-(Ni-Zn-P)/C catalysts are more stable than with Pd/C catalyst.

Plotting the value of anode peak current density against the square-root of the scan-rate for all the three catalysts investigated (Figure 14), a typical relationship of an electrochemical reaction under diffusion control was observed for Pd-(Ni-Zn-P) at scan rates lower than 100 mV/s. Above 100 mV/s the ethanol reaction seems to be limited by substrate diffusion, desorption of the oxidation product and low presence of catalytically active sites (due to extremely low Pd loading 22-25 μg/cm²). For Pd-(Ni-

Zn)/C the linear relationship between S_a and $v^{1/2}$ changed in slope after 50 mV/s. Below this value the ethanol reaction was under diffusion control, while for higher scan rates other factors seem to control the reaction rate. A similar behaviour has been reported for ethanol oxidation on Pt in alkaline media^{27a)} and it has been ascribed to the formation of a passive layer during the early stages of the electron transfer. Here CV and chronopotentiometric studies seem to exclude electrode passivation, because the high activity would also generate high instantaneous acetate concentration at the surface, with consequent slowing down of substrate adsorption at high scan rates. Unlike Pd-(Ni-Zn)/C and Pd-(Ni-Zn-P)/C, Pd/C exhibits a linear dependence on S_a and $v^{1/2}$ under 50 mV/s similar to those reported by Shen et al. for Pd/TiO₂C and Pd/CPAA^{10,11}. The parabolic trend has been attributed to the prevailing occurrence of activation polarization. In the little inset of Figure 13c we reported a plot obtained using a higher palladium loading (130 $\mu\text{g}/\text{cm}^2$) to demonstrate that the curve shape changes depending on the metal loading, showing that the ethanol oxidation is diffusion-controlled over the range of scan rates investigated.

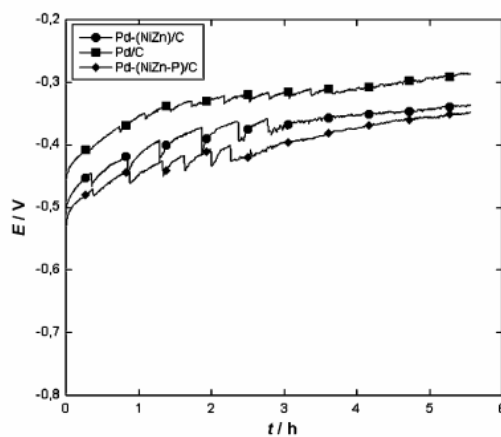


Figure 13. Chronopotentiometric traces of ethanol oxidation on Pd/C, Pd-(Ni-Zn)/C, Pd-(Ni-Zn-P)/C electrodes at 3 mA/cm² in 2M KOH + 10 wt % EtOH³³.

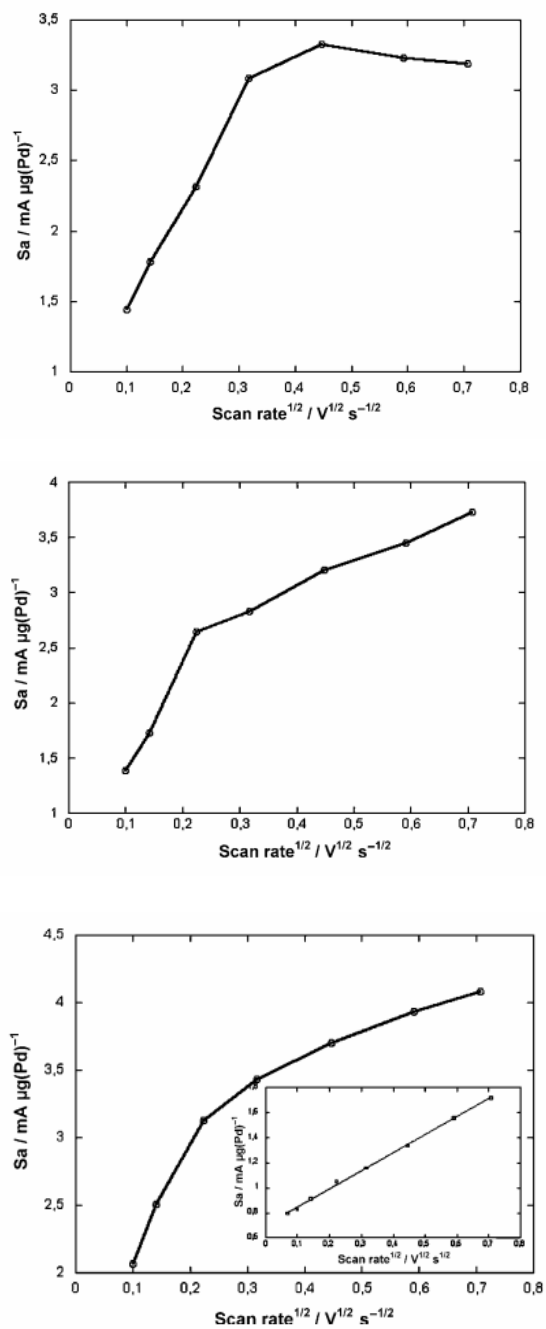


Figure 14. Plot of the anode peak current density against the square-root of the scan rate for a) the Pd-(Ni-Zn-P)/C, b) Pd-(Ni-Zn)/C, c) Pd/C electrodes ³³.

2.3.5 Direct Ethanol Fuel Cells (DEFCs) with Pd-based anode electrocatalysts

The anode electrocatalysts were primarily tested in passive (air/oxygen breathing) monoplanar fuel cell (see cell hardware in Figure 47). To this purpose, membrane-electrode assemblies (MEAs) were realized in conjunction with proprietary Fe-Co/C cathodes⁶¹ and an anion-exchange membrane from Tokuyama (A-006). The MEA was fabricated by mechanically pressing anode, membrane and cathode. The anode electrocatalysts were dispersed in distilled water and then spread onto a 5 cm² Ni-foam plate (Pd loading of 1 mg/cm²). The cathode ink was sprayed or spread onto carbon cloth (Fe:Co (1:1) loading 2-2.5 mg/cm²). The membrane was rinsed in a 1M KOH solution for a few minutes and gently dried before assembling the MEA. After filling the anode compartment with 10 mL of 10 wt% EtOH 2M KOH, the DEFC was conditioned for 1h at room temperature at the open circuit voltage (OCV). After this time, the cell polarization and power density curves were registered at room temperature. Figure 15. shows such curves for the three catalyts. Apparently, Pd-(Ni-Zn)/C exhibits the best power performance for ethanol oxidation with a power density of 58 mW/cm² at 225 mA/cm² as well as an exceptionally high OCV voltage value (0.90 V).

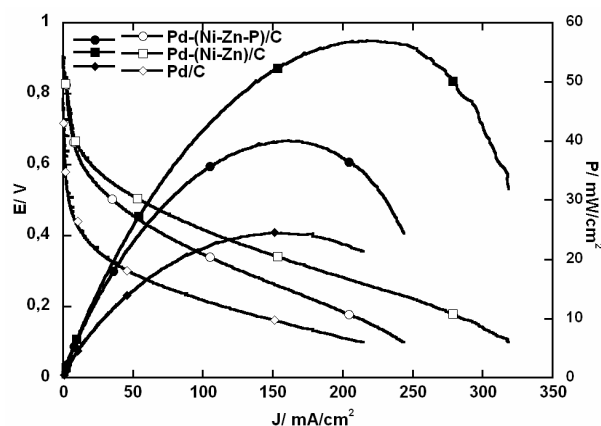


Figure 15. Polarization and power density curves provided by DEFCs filled with a 2M KOH solution of ethanol (10 wt%) air breathing system at 20-22°C. The MEAs were composed of Pd-(Ni-Zn)/C⁶², Pd-(Ni-Zn-P)/C and Pd/C anodes (on 5 cm² Ni foam) 1 mg/cm² Pd loading, Tokuyama A006 membrane and Fe-Co/C (on carbon cloth) cathodes 2-2,5 mg/cm² Fe, Co loading.

Next, the anode electrocatalysts were tested in active monoplanar fuel cell (see cell hardware in Figure 48) using the following fluxes: 200 mL min⁻¹ oxygen; 4 mL min⁻¹ 10 wt% EtOH + 2M KOH. The membrane-electrode assemblies (MEAs) were realized as previously reported. The cathode and electrolytic membrane were the same as in the passive anode ink was prepared by mixing the powdered catalysts with a 5-10 wt% aqueous dispersion of polytetrafluoroethylene (PTFE) and spread onto a 5 cm² Ni-foam plate (Pd loading 1 mg/cm²). The active DEFC was then conditioned for 1h at 25°C, 40°C, 60°C and 80°C before closing the circuit. After this time, the cell polarization and power density curves were registered at each temperatures. As shown in Figure 16. Pd-(Ni-Zn)/C⁶² exhibits the best power performance for ethanol oxidation at 80°C (170 mW/cm² at 600 mA/cm²).

The cell containing Pd-(Ni-Zn-P)/C anode electrocatalyst performs similarly to that with Pd-(Ni-Zn)/C, whereas lower power densities are obtained with Pd/C anode especially at high temperatures.

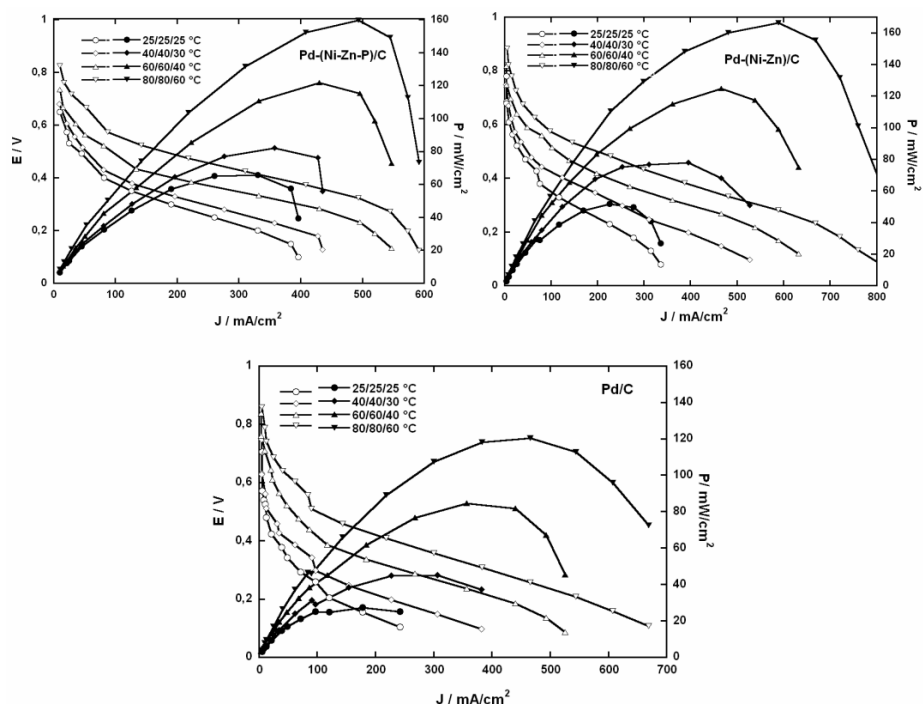


Figure 16. Polarization and power density curves provided by active DEFCs with a 2M KOH solution of 10 wt% ethanol (4 mL/min), oxygen-breathing system (200 mL/min) at 25°C, 40°C, 60 °C, 80°C. The MEAs were composed of Pd-(Ni-Zn)/C⁶², Pd-(Ni-Zn-P)/C and Pd/C anodes (on 5 cm² Ni foam plate), 1 mg/cm² Pd loading; Tokuyama A006 membrane and Fe-Co/C (on carbon cloth) cathodes, 2-2,5 mg/cm² Fe, Co loading.

A series of galvanostatic experiments were carried out at room temperature in the passive DEFCs using oxygen instead of air at cathode side just to avoid any CO₂ interference on the oxidation products (vide infra). After filling the anode compartment with 21.70 mmol of EtOH 2M KOH solution and conditioning the cell for 1h, a current of 102 mA was allowed to pass in the cell until 0V potential.

The DEFC assembled with the Pd-(Ni-Zn)/C⁶² anode lasted for 9.5 h (Figure 17) converting 9.98 mmol of acetate (isolable as potassium acetate), which correspond to 46% ethanol conversion (Figure 18). The qualitative and quantitative analysis of the DEFC exhausts were performed by ¹³C{¹H} NMR spectroscopy and ionic chromatography (IC). 1,4-Dioxane was used as internal reference for the ¹³C{¹H} NMR experiments, while sodium propionate was used as internal standard for the IC analysis. In Figure 18 is shown the NMR spectrum: the only product was acetate with no trace of carbonate (168 ppm) or acetaldehyde (206 ppm) detected at any stage of the galvanostatic experiment. The IC analysis was in agreement with fuel cells. Accordingly, the anode reaction can be summarized as in Eq (6).

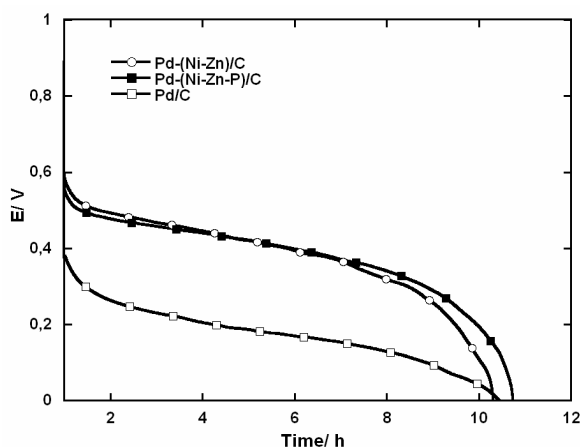
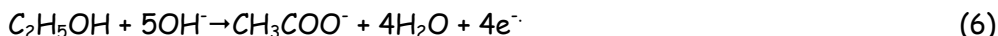


Figure 17. Galvanostatic curves registered at 102 mA until 0V in inert atmosphere provided by passive DEFCs filled with a 2M KOH solution of 21.7 mmol of ethanol, oxygen-breathing system at room temperature. The MEAs were composed of Pd-(Ni-Zn)/C⁶², Pd-(Ni-Zn-P)/C and Pd/C anodes (on Ni foam 5 cm²), 1 mg/cm² Pd loading; Tokuyama A006 membrane and Fe-Co/C (on carbon cloth) cathodes, 2-2,5 mg/cm² Fe, Co loading.



Analysis of the cell exhausts showed that our Pd-based catalysts, in the present experimental conditions, are selective for the conversion of ethanol into acetate with no appreciable formation of C-C bond cleavage products such as carbonate. Such a selectivity is never shown by Pt-based catalysts that generate mixtures of acetate and carbonate in alkaline fuel cells^{63,64,67}. NMR spectroscopy allowed us to estimate the loss of ethanol by direct or cross-over evaporation (4.2 mmol). Finally the anode compartment was freshly recharged with further 10 mL of fuel solution. The cell was fully regenerated with the same OCV voltage (about 0.90 V) and gave similar galvanostatic duration and conversion performance. The voltage decay shown in Figure 17 has been attributed to other factors than catalyst poisoning or membrane carbonation, i.e. the increasing viscosity of the solution, the pH decrease due to OH⁻ consumption, and, most importantly, the competitive substrate adsorption /product desorption and the formation of PdO layer.

Galvanostatically, Pd-(Ni-Zn-P)/C exhibited similar behaviour (9.27 mmol of acetate obtained with an ethanol loss of 4.4 mmol) as Pd-(Ni-Zn)/C (Figure 17). The passive DEFC with the Pd/C anode gave less energy efficiency and converted 8.98 mmol of acetate, leaving 9.82 mmol of unreacted ethanol.

From our experiments, one may conclude that the catalysts obtained by the spontaneous deposition procedure perform better than the catalysts obtained by

traditional electroless procedure. Besides affecting the Pd particle distribution and morphology, the Ni-Zn and Ni-Zn-P phases may also play a sort of co-catalytic effect. In particular, a bifunctional mechanism⁶⁵, where the nickel phase would increase the concentration of OH_{ads} species on the catalysts surface, promoting the acyl- $_{\text{ads}}$ - OH_{ads} coupling⁶⁶ cannot be excluded. This effect is illustrated in Scheme 2 that reports a generally accepted mechanism of ethanol oxidation to acetate on anode electrocatalysts in alkaline media⁶⁸.

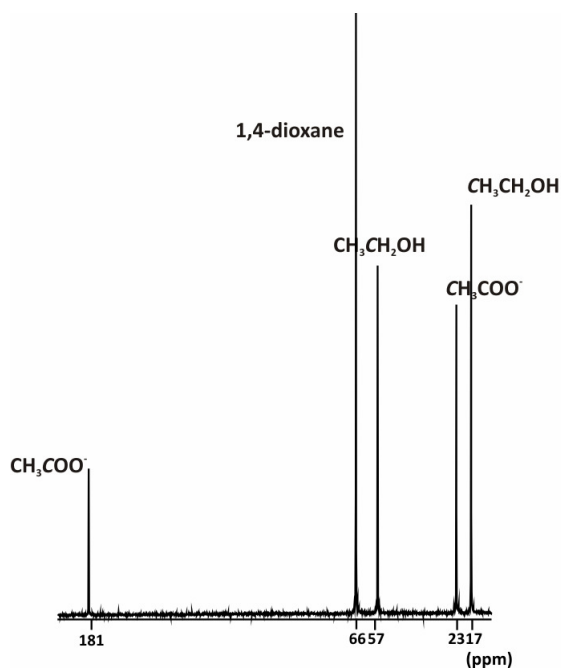
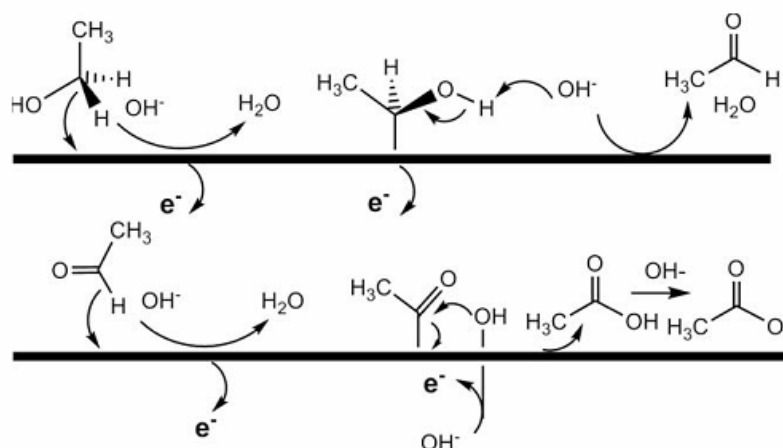


Figure 18. $^{13}\text{C}\{^1\text{H}\}$ NMR spectra of cell exhaust after 10.5h of galvanostatic experiment for passive DEFC equipped with Pd-(Ni-Zn)/C anode (0V 102 mA)⁶².



Scheme 2. Proposed mechanism for the selective conversion of ethanol into acetate on Pd-based electrocatalysts in alkaline media⁶⁸.

2.3.6 NaBH_4 : an additive that improves the DEFC performance

The polarization losses observed in the galvanostatic experiments after ca. 50% conversion of the fuel (see above) are not apparently originated from irreversible poisoning of the catalyst surface, as the cells re-start working upon filling with a fresh anolyte solution. Among the factors that may be responsible for the performance decay one may suggest the difficult desorption of the acetate groups from the catalyst surface, the competitive adsorption of ethanol, acetate, hydroxyl groups^{62,75}, and the catalyst passivation due to the formation of a PdO layer^{33,52}. In an attempt of understanding why our Pd-electrocatalysts lose activity with time, generally after 50% conversion of ethanol to acetate^{62,77,67} (Figure 17, 2.3.5), a reducing additive was added to the fuel solution.

A recent CV study of ethanol oxidation on a smooth palladium electrode⁵² has suggested that the adsorption/dehydrogenation of ethanol on Pd is a fast process ($\text{Pd}(\text{COCH}_3)_{\text{ads}}$ formation), while the coupling of the adsorbed acyl with the adsorbed hydroxyl ($\text{Pd-OH}_{\text{ads}}$) is the rate determining step. Accordingly, the formation of $\text{Pd-OH}_{\text{ads}}$ at low potential would be a crucial factor to control the activity of any Pd-based electrocatalysts towards ethanol oxidation in alkaline media, while the formation of PdO would disfavour the process.

As an additive to reduce PdO to Pd, we selected NaBH₄ as it is relatively cheap, no toxic, and capable of maintaining its reducing action in alkaline water solutions for months. It is also used as fuel in direct borohydride fuel cells (DBFCs)⁶⁸. The effect of adding NaBH₄ to the anode compartment of our DEFCs was studied in half cells by CV and in situ FTIR spectroelectrochemistry as well as in monoplanar cells with anodes containing the Pd/C anode electrocatalyst. The cathode and membrane are the same as in all fuel cells here described. The results obtained are compared to those reported in Section 2.3.5. The different analytes in 2M KOH solution investigated are reported in Table 3. The polarization and power density curves for DBFCs and DEFCs with the different analytes are shown in Figure 19. In all cases, the MEAs were assembled using a Pd/C anode (100 mg of Pd/C anode powder mixed with 100 mL of water and 100 mg of 5 wt% PTFE spread onto 5 cm² Ni foam plate, Pd loading 1 mg/cm²), a Tokuyama A006 anion-exchange membrane (rinsed in 1M KOH solution for a few minutes and gently dried) and a carbon cloth cathode onto which was spread a proprietary Fe-Co/C electrocatalyst (2-2.5 mg/cm²).

Anolyte	NaBH ₄ (wt%)	EtOH (wt%)
1	-	-
2	-	10
3	0.1	-
4	0.2	-
5	0.5	-
6	1.0	-
7	0.1	10
8	0.2	10
9	0.5	10
10	1.0	10

Table 3. Anolyte solutions in 2M KOH investigated to comprehend NaBH₄ effect in DEFCs⁵¹.

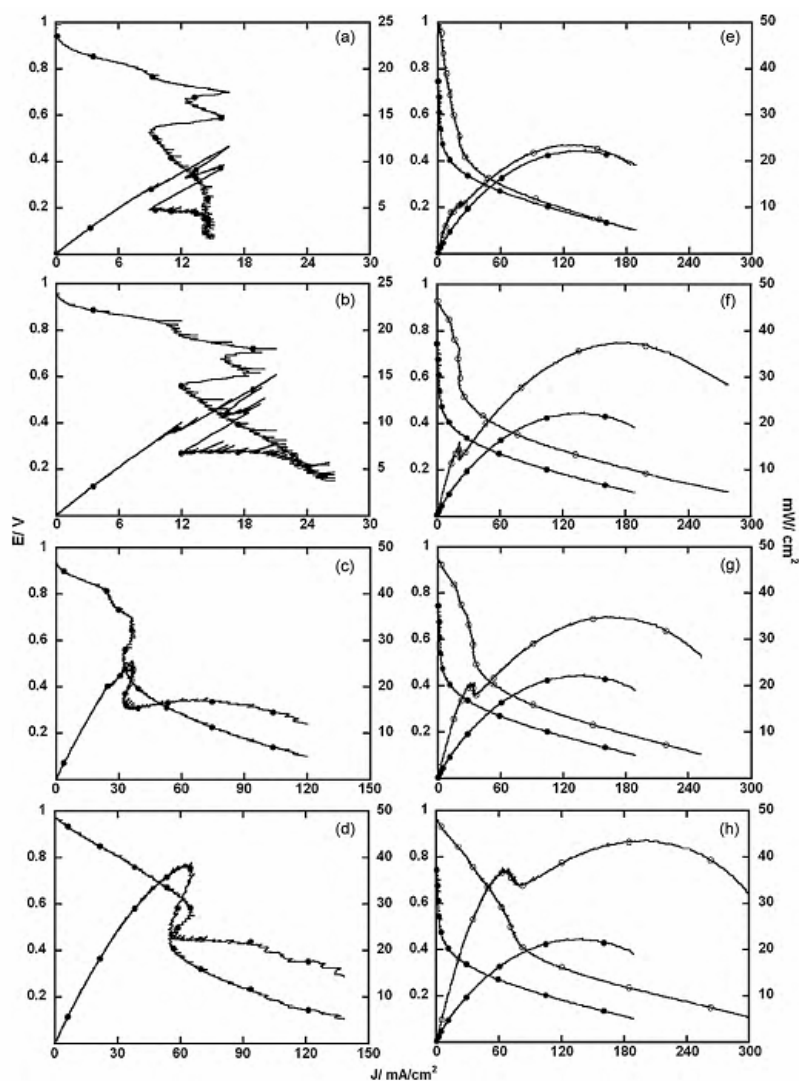


Figure 19. Polarization and power density curves provided by DAFCs filled with the following analytes: NaBH_4 (0.1 wt%) (a); NaBH_4 (0.2 wt%) (b); NaBH_4 (0.5 wt%) (c); NaBH_4 (1 wt%) (d); (○) ethanol (10 wt%) + NaBH_4 (0.1 wt%) and (●) ethanol (10 wt%) (e); (○) ethanol (10 wt%) + NaBH_4 (0.2 wt%) and (●) ethanol (10 wt%) (f); (○) ethanol (10 wt%) + NaBH_4 (0.5 wt%) and (●) ethanol (10 wt%) (g); (○) ethanol (10 wt%) + NaBH_4 (1 wt%) and (●) ethanol (10 wt%) (h)⁵¹.

As shown in Figure 19, the polarization curves for DBFCs show an irregular trend in the high potential region with peaks that are likely due to adsorbed-absorbed hydrogen on palladium⁵³. The analyte solutions containing 0.1 and 0.2 wt% NaBH_4 (Figures 19 a and b) give current densities of 14 and 24 mA cm^{-2} at 0.2 V, while at the same potential value the analyte containing only ethanol 10 wt% gives 107 mA cm^{-2} (Fig. 19 e).

The addition of NaBH_4 to EtOH 10 wt% (2M KOH) makes the Pd/C anode electrode more efficient for the oxidation of ethanol. Indeed, just by adding NaBH_4 0.1 wt% (Fig. 19 e) the current density increases to 124 mA cm^{-2} , which is slightly higher than the sum of

the current densities recorded for the single analytes (121 mA cm^{-2}). By adding NaBH_4 0.2 wt% (Fig. 19 f) the current density registered at 0.2 V increases to 188 mA cm^{-2} , a value much higher than the sum of the current densities provided by the solutions of the single fuels (131 mA cm^{-2}). A perusal of Figure 19 e-g readily shows that NaBH_4 promotes the oxidation of ethanol on the palladium electrocatalyst, when the former fuel is added in concentrations lower than 0.5 wt%. For higher concentrations, the oxidation of NaBH_4 prevails over that of ethanol behaving itself as the fuel rather than the additive. Indeed, in Figure 19 g, the current density at 0.2 V is 170 mA cm^{-2} , while the sum of the contributions of ethanol and NaBH_4 alone is 190 mA cm^{-2} . The observed decrease in power output suggests that the sluggish ethanol oxidation subtracts active sites for NaBH_4 oxidation. The enhanced ability of Pd/C to oxidize ethanol in the presence of tiny amounts of NaBH_4 , has been unequivocally proved by the quantitative analysis of the cell exhausts obtained by potentiostatic experiments at 0.2 V for 17 h. A $^{13}\text{C}\{^1\text{H}\}$ NMR analysis of the fuel exhaust of a DEFC with no NaBH_4 showed 50% of ethanol conversion into acetate (as in Figure 18, section 2.3.5), whereas the addition of 0.2 wt% NaBH_4 increased the conversion to 80%. An $^{11}\text{B}\{^1\text{H}\}$ NMR analysis of the same cell exhausts showed the selective oxidation of BH_4^- to metaborate (BO_2^-) ([Eq(7)]). For further additions of NaBH_4 , neither the ethanol conversion nor the selectivity showed substantial changes.

In an attempt of rationalizing these results, a careful CV analysis of NaBH_4 /ethanol oxidation on Pd was carried out. In Figure 11 (see section 2.3.3) we have shown the CV of a Pd/C electrode in 2M KOH solution. The effect of adding 0.1 wt% NaBH_4 is reported in Figure 20. One may readily realize that the A^I and A^{II} peaks, attributed to adsorbed and adsorbed hydrogen, grow up in intensity⁶⁹. Indeed, the two peaks are not visible in Figure 11 as they are merged into a single peak (A^I).



The A^{III} and A^V peaks are due to the direct oxidation of BH_4^- anion ([Eq(8)]).



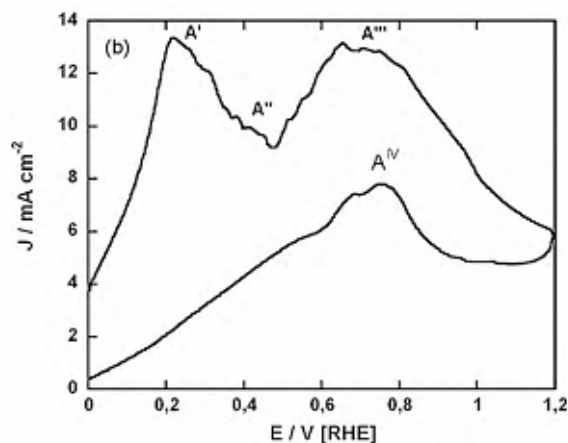


Figure 20. CV of a Pd/C electrode in a 2M KOH 0.1 wt% NaBH₄ solution under nitrogen⁵¹.

Figure 21b shows the CV of a Pd/C electrode in a solution containing 2M KOH, 0.1 wt% NaBH₄ and 10 wt% EtOH. The A^I peak is due to hydrogen oxidation at 0.30 V, while the onset (0.4 V) of a broad intense A^{II} peak is the convolution of ethanol and borohydride oxidation. A current peak is observed at 0.89 V, while at higher potentials the current density is controlled by PdO formation. In the absence of NaBH₄ (Figure 21a), the current peak is at lower potential (about 0.8 V vs RHE) than in the presence of NaBH₄ as this additive allows for an efficient ethanol oxidation at more positive potential. It is notably that the current density continued to be anode even at 1.2 V, suggesting the surface was still active for the oxidation of ethanol-borohydride mixture.

This suggests that the additive can reduce PdO to Pd. Furthermore the sum of the peak density current is higher (82 mA/cm²) than the sum of the peak current density (72 mA/cm²) supplied by the cells containing the anolytes 2M KOH + NaBH₄ 0.1 wt% and 2M KOH + NaBH₄ 0.1 wt% + EtOH 10 wt%, in accordance with DEFCs and DBFCs power densities and polarization studies.

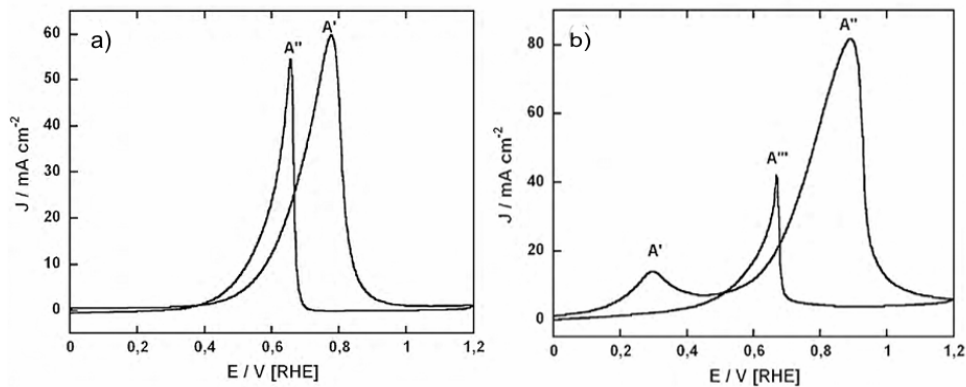


Figure 21. 21a) CV of a Pd/C electrode in a solution containing 2M KOH, 10 wt% EtOH; 21b) CV of a Pd/C electrode in a solution containing 2M KOH, 0.1 wt% NaBH₄ and 10 wt% EtOH under nitrogen⁵¹.

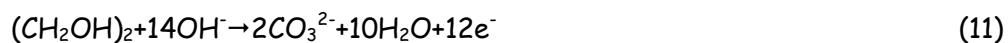
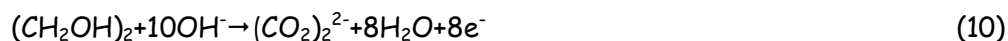
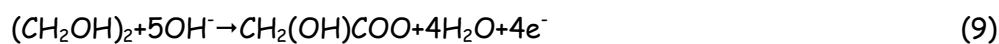
In situ FTIR⁵¹ studies in accordance with the CVs studies suggest that ethanol competes with NaBH₄ for adsorption on the Pd active sites. EtOH seems to prevail in adsorption for NaBH₄ concentrations <0.1 wt%.

In conclusion, NaBH₄ amounts of about 0.1-0.2 wt% in the anolyte result in higher power densities, increased catalyst lifetime and larger ethanol conversion to acetate.

2.3.7 Half cell studies of ethylene glycol oxidation on the Pd-based catalysts in alkaline environment

The electrooxidation of ethylene glycol (EG) on Pd-(Ni-Zn)/C, Pd-(Ni-Zn-P)/C and Pd/C electrodes has been investigated by CV⁷⁰. This diol can be an effective fuel in direct fuel cells in both alkaline [Eq(9-11)] and acidic media^{71,72}. There is great interest in the use of EG as a fuel because it may be obtained from abundant and renewable resources such as cellulose⁷³.

The cyclic voltammograms were registered at a scan rate of 50 mV/s with a Pd loading varying from 24-28 $\mu\text{g}/\text{cm}^2$ (corresponding to 18-20 mg of ink), in the presence of 5 wt % EG⁷⁴, 2M KOH solution.



The cyclic voltammograms are illustrated in Figure 22 and the relevant electrochemical parameters are reported in Table 3. The three anode catalysts investigated show high activity towards EG oxidation with an onset potential of about 0.4 V (vs RHE) and specific current densities higher than 3.2 mA/ μg Pd, comparable to those obtained for the ethanol electrooxidation (2.3.4 section). The Pd-(Ni-Zn)/C electrode gives the higher specific current densities (3.4 mA/ μg Pd). The EG oxidation starts with the formation of $\text{Pd}(\text{OH})_{\text{ads}}$ on the catalyst surface (section 2.3.3 Figure 10, 11)^{2c),4,33,76,75}.

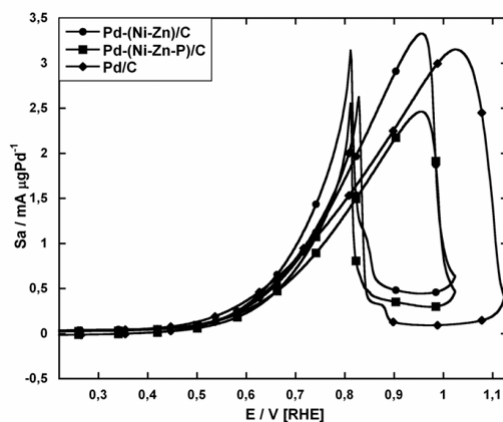
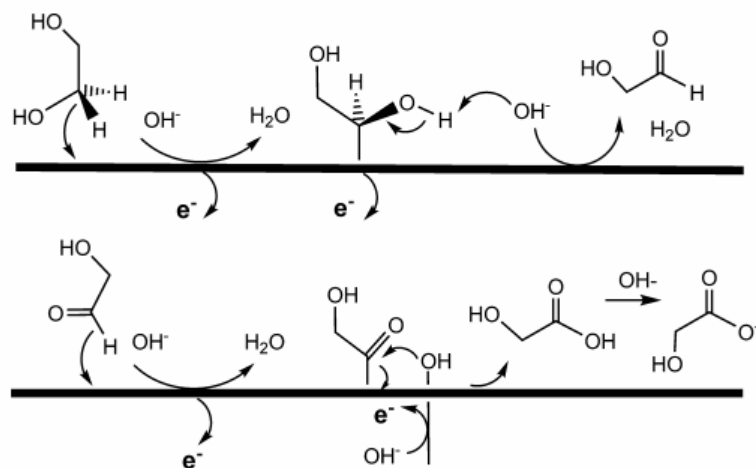


Figure 22. CVs (at the tenth cycle) on Pd/C, Pd-(Ni-Zn)/C, Pd-(Ni-Zn-P)/C electrodes in 5 wt% EG in 2M KOH solution under nitrogen. Scan rate 50 mV/s⁷⁰.

Catalyst	J_p (mA cm ⁻²)	Sa_p mA(μg Pd) ⁻¹	V_{onset} (V)	V_p (V)	Tafel slope (mV dec ⁻¹)
Pd-(Ni-Zn)/C	84.2	3.33	0.37	1.02	205 (α 0.284)
Pd-(Ni-Zn-P)/C	65.5	2.46	0.42	0.95	190 (α 0.307)
Pd/C	84.5	3.15	0.42	0.95	180 (α 0.324)

Table 4. Selected electrochemical parameters for CVs of EG oxidation in 2M KOH solution on Pd/C, Pd-(Ni-Zn)/C, Pd-(Ni-Zn-P)/C electrodes⁷⁰.

The CVs shown in Figure 22 illustrate clearly that the peaks associated to the backward scan decrease in terms of specific current densities as compared to the forward potential scan, while the peak potential moves anodically to 1.6 V (vs RHE). Besides the formation of a PdO layer can cause the current decrease originated by mass transfer phenomena as well as instantaneous shortage of OH⁻ groups at the electrode-anolyte interface. Indeed, a previous CV study of EG electrooxidation on a smooth Pd electrode has demonstrated that the current densities are independent on the substrate concentration, but proportional to the OH⁻ concentration with a reaction order of ca.1⁷⁶.



Scheme 3. Proposed mechanism of EG oxidation to glycolate ion in alkaline media ⁷⁰.

Tafel plots for the EG oxidation reaction (5 wt% fuel in 2M KOH solution) on Pd/C, Pd-(Ni-Zn)/C, Pd-(Ni-Zn-P)/C electrodes were registered at scan rate of 5 mV/s in the potential range from 0.3 V to 0.5 V (vs RHE). The values for the Tafel slopes and for the α coefficients (Table 4) are comparable with those reported in the literature for other Pd catalysts ^{33,75}, but they are higher than those for Pd smooth electrodes (120 mV/dec) ^{2c),75}.

The α values (ca.0.3) suggest an electrochemical rate limiting step of EG oxidation for all the three electrocatalysts. The Tafel slopes result similar to each other, denoting also a similar oxidation mechanism.

Plotting the peak current density value against the square root of the scan rate (Figure 23), gives a linear relationship for the Pd-(Ni-Zn)/C and Pd-(Ni-Zn-P)/C electrodes, which indicates an electrochemical diffusion control of the EG oxidation reaction. In contrast, a parabolic curve is obtained for the Pd/C electrode as the oxidation reaction would be controlled by activation polarization. As previously reported for the oxidation of ethanol on the same Pd/C electrode, this effect can be related to the very low number of catalytically active sites on the electrode.

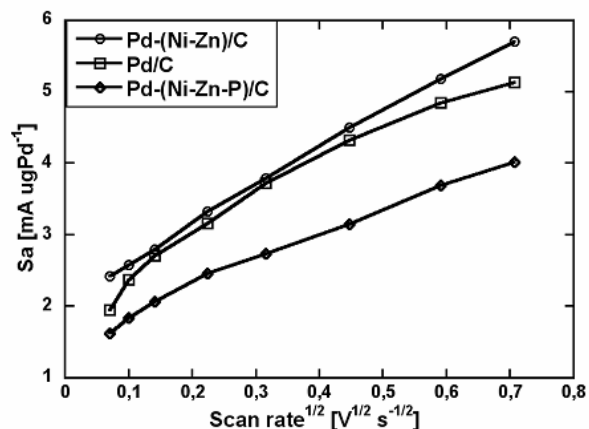


Figure 23. Plots of the anode peak current density against the square-root of the scan rate for the oxidation of 5 wt% EG in 2M KOH on Pd/C, Pd-(Ni-Zn)/C, Pd-(Ni-Zn-P)/C electrodes ⁷⁰.

Chronopotentiometric experiments have been performed at a constant current of 3 mA/cm² for 5 h (Figure 24). In general, the curves show a negligible potential oscillation for 2 h, indicative of no strongly adsorbed species on the catalyst surface.

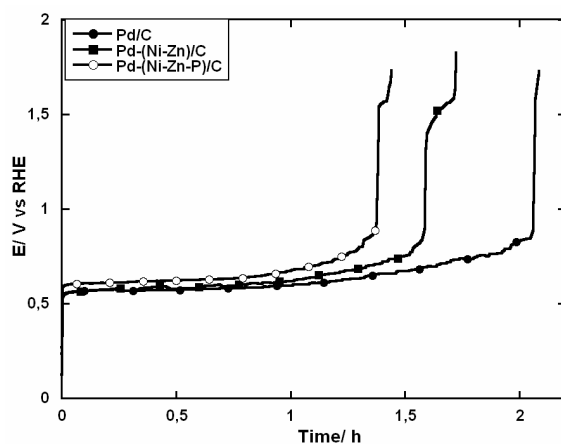


Figure 24. Chronopotentiometric experiments in 5 wt% EG + 2M KOH solution with Pd/C, Pd-(Ni-Zn)/C, Pd-(Ni-Zn-P)/C electrodes 3 mA/cm² for 5h.

Notably, analysis of the chrono-exhausts by IC/¹³C NMR show an almost selective formation of glycolate with traces of oxalate and carbonate for Pd/C. A less selective reaction is observed for the reactions catalyzed by Pd-(Ni-Zn)/C or Pd-(Ni-Zn-P)/C.

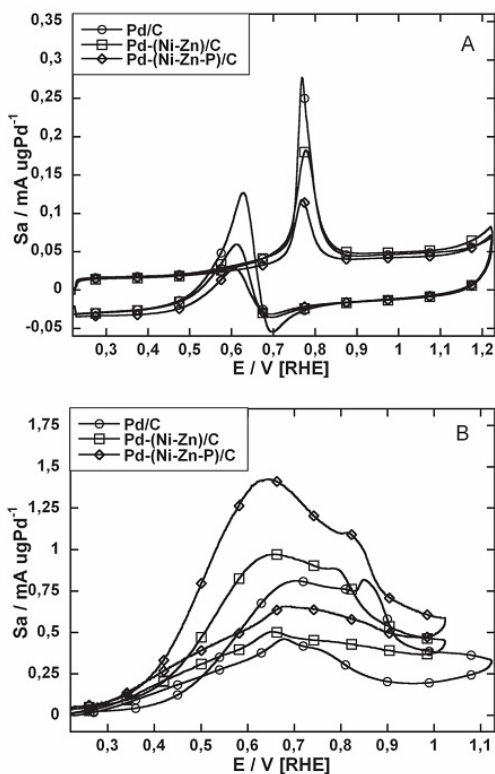
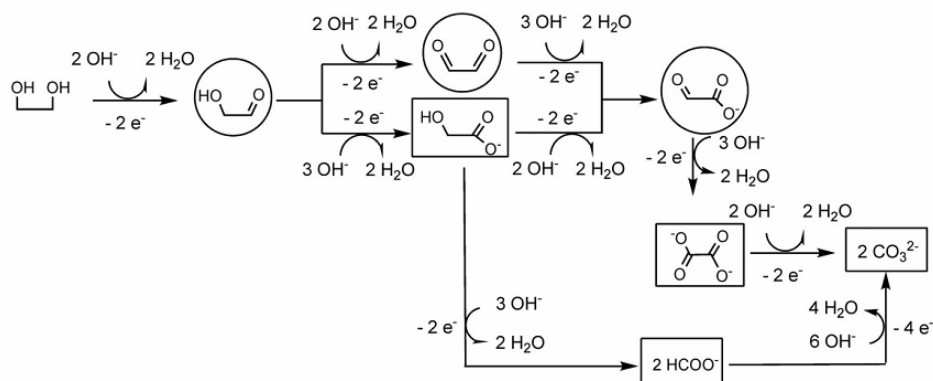


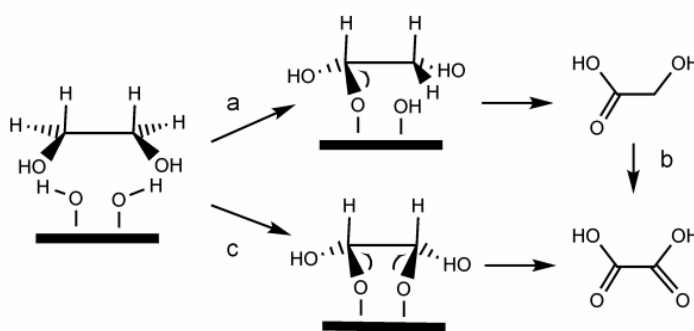
Figure 25. CVs of (A) 2 wt% glycolic acid and (B) 2 wt% glyoxylic acid in 2M KOH on Pd/C, Pd-(Ni-Zn)/C, Pd-(Ni-Zn-P)/C electrodes under nitrogen. Scan rate 50 mV/s⁷⁰.

Indeed on both electrocatalysts, EG is prevalently converted to glycolate (ca. 60%), oxalate (ca. 33%) and carbonate (ca. 7%). The different product distribution provided by the three catalysts seems to be inconsistent with a unique oxidation mechanism, as suggested by the Tafel slopes. A proposed mechanism of EG oxidation in alkaline media (Scheme 4) on the basis of relevant literature reports⁷² is in good agreement with our experimental data. To gain further insight into the EG oxidation mechanism, CV studies on the same Pd/C electrode were carried out using some EG intermediates, such as glycolic and glyoxylic acid in 2M KOH solutions. The results obtained are illustrated in Figure 25.

Glycolate is easily less oxidized (S_a 0.3 mA/ μg Pd at 0.8 V vs RHE) than glyoxylate (1.5 mA/ μg Pd at 0.6 V vs RHE). The shoulder at 0.8 V in the glyoxylate CV is assigned to the disproportionation of the glyoxylate to glycolate in alkaline environment.



Scheme 4. Overall reaction scheme of EG oxidation on metal electrocatalysts in alkaline media. Products in boxes have been isolated; products in circles have been detected spectroscopically⁷⁰.



Scheme 5. Direct and sequential routes for the electrooxidation of EG to oxalic acid⁷⁰.

The glycolate anion is not oxidized to oxalate on the Pd/C electrode; its concentration in the Pd-(Ni-Zn)/C, Pd-(Ni-Zn-P)/C chrono-exhausts suggests two parallel routes for oxalate production, with path c prevailing over paths a-b (Scheme 5).

In Figure 26 CVs of 2 wt% oxalate with 2M KOH solution and of only 2M KOH solution on Pd/C, Pd-(Ni-Zn)/C and Pd-(Ni-Zn-P)/C electrodes were shown. In the CVs with 2 wt% oxalate 2M KOH solution a significant decrease in the peak associated to PdO reduction (0.65 V vs RHE backward scan) is observed together with an oxidation peak at 0.47 V vs RHE of 0.03 mA/ μ g Pd of specific current density. In the light of our experimental evidence, one may conclude that the carbonate formed upon electrooxidation of EG on Pd-(Ni-Zn)/C and Pd-(Ni-Zn-P)/C is prevalently obtained from the glycolate oxidation rather than from the oxalate oxidation⁷⁰. In Scheme 5 is shown a possible mechanism of EG electrooxidation on Pd/C, Pd-(Ni-Zn)/C and Pd-(Ni-Zn-P)/C electrodes.

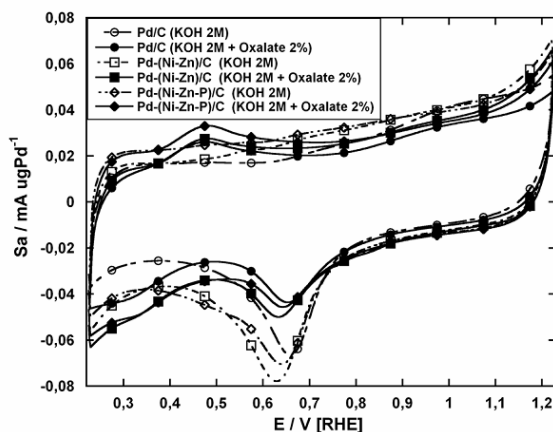


Figure 26. CVs of 2 wt% oxalic acid in 2M KOH on Pd/C, Pd-(Ni-Zn)/C, Pd-(Ni-Zn-P)/C electrodes under nitrogen. Scan rate 50 mV/s⁷⁰.

2.3.7.1 *In situ* FTIR study in alkaline environment with ethylene glycol on Pd-based catalysts

In an attempt to get insight into the oxidation mechanism of EG on the Pd-based catalyst here investigated, an in-situ spectroelectrochemical FTIR study was carried out (Figure 27). A smooth Pd electrode was used in 1M EG solution with different NaOH concentrations with the same ionic strength⁷⁰.

From a perusal of the FTIR spectra (Figure 27), one may readily conclude that palladium does not effectively catalyze the EG oxidation at pH lower than 12 (like for the ethanol)⁷⁷, while no activity at all is observed in neutral or acidic media. This evidence is in accord with previous DFT calculations indicating that the dehydrogenation of alcohols on Pd requires a high OH_{ads} coverage on the catalyst surface⁷⁷.

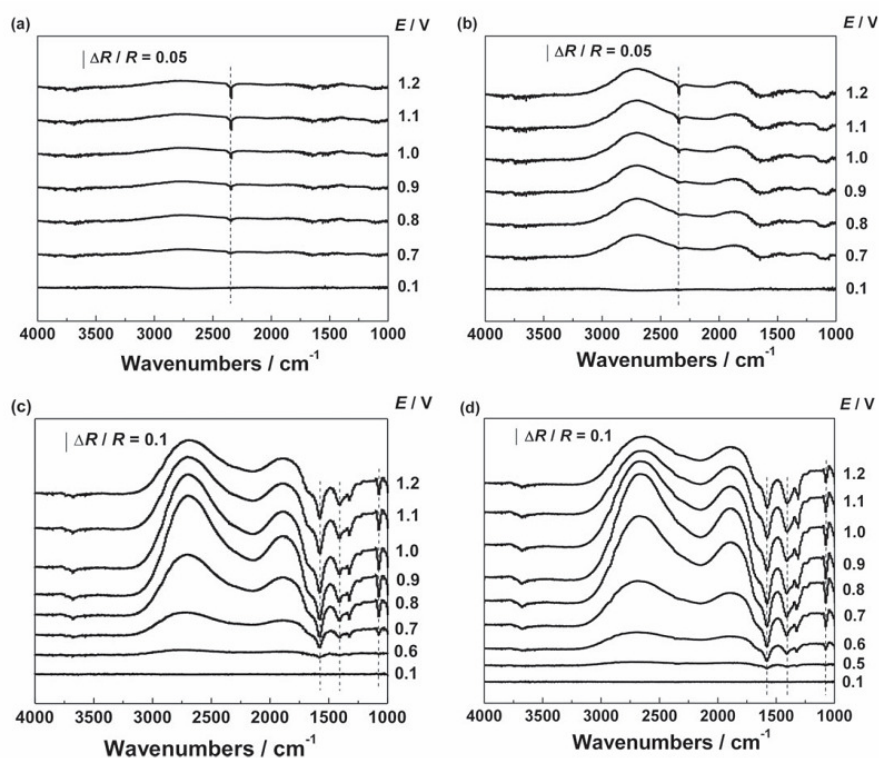


Figure 27. In situ FTIR spectra obtained under potential step polarisation of the following solutions: (a) 0.01 M NaOH + 0.99 M NaClO₄ + 1 M EG; (b) 0.1 M NaOH + 0.9 M NaClO₄ + 1 M EG; (c) 1 M NaOH + 1 M EG; (d) 2 M NaOH + 1 M EG. Scan number: 128⁷⁰.

For NaOH concentrations higher than 1M, the glycolate stretching bands were visible at 1580 cm⁻¹ (C=O) and 1070 cm⁻¹ (C-O), together with lower intensity bands due to the carbonate (1,410 cm⁻¹) and oxalate (1,310 cm⁻¹) stretching modes (Fig. 27 c), d)). An oxalate band, expected at 1600 cm⁻¹, is likely masked by the glycolate band. When NaOH was used in concentrations lower than 1M, the CO₂ band became visible at 2343 cm⁻¹ already at 0.7 V (Fig.27 a), b)).

No CO stretching band was detected at any pH or potential, although it is worth reporting that such a band is difficult to detect in alkaline media⁷⁸.

Since in situ FTIR studies of EG electrooxidation on Pd are not reported in the relevant literature, a comparison can be made only with Pt catalysts in alkaline media. According to the literature for Pt, our Pd catalysts do not diverge substantially in terms of selectivity for EG electrooxidation. Both metals lead to the production of glycolate, oxalate and carbonate at comparable potential value, with increased concentrations of oxalate and carbonate at higher potential values (ca. 0.9 V). Differently from Pd, the adsorption of EG at a Pt electrode is dissociative at any pH with formation of CO_{ads}^{79,80}. It

was suggested that glycolate and carbonate are produced from the same intermediate, e.g. [Pt-CH(OH)CH₂OH], while oxalate is obtained by oxidation of desorbed glycolate. What really seems to distinguish Pd from Pt is the higher electrochemical activity of the former metal in alkaline media towards EG electrooxidation, as demonstrated by the CVs and FTIR ⁸¹.

2.3.8 Direct Ethylene Glycol Fuel Cells (DEGFCs) with Pd-based anode electrocatalysts

The three anode electrocatalysts Pd-(Ni-Zn)/C, Pd-(Ni-Zn-P)/C and Pd/C were primarily tested in passive monoplanar fuel cell air (oxygen breathing). The cell hardware is shown in Figure 47 (see Exp. Section), while the MEAs were realized as previously described (section 2.3.5). In Figure 28 are shown the cell polarization and power density curves of a DEGFC loaded with 11 mL of 5 wt% EG in 2M KOH solution.

Pd-(Ni-Zn)/C exhibits the higher power density with 24 mW/cm^2 at 138 mA/cm^2 , while the lower power density (11 mW/cm^2 at 100 mA/cm^2) is provided by Pd/C.

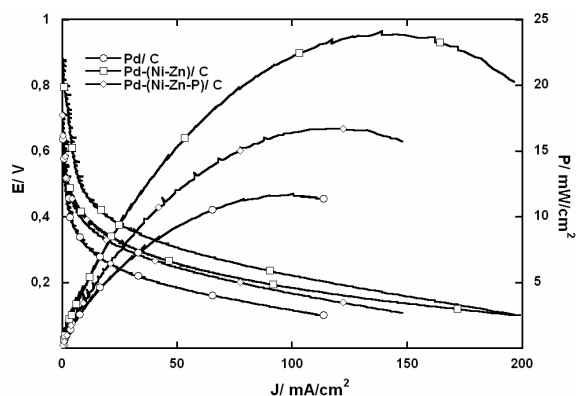


Figure 28. Polarization and power density curves provided by air-breathing DAFCs filled with 2M KOH solutions of ethylene glycol (5 wt%) at 20–22 °C. MEAs: Pd/C, Pd-(Ni-Zn)/C, Pd-(Ni-Zn-P)/C anode with Pd loading of 1 mg/cm^2 , Tokuyama A006 membrane, Fe-Co/C (1:1) 2-2.5 mg/cm^2 loading cathode.

Next, a series of galvanostatic experiments were carried out for each anode catalyst at room temperature utilizing the same MEA (Figure 29). The measurements were carried out using an oxygen atmosphere inside a bry-box. After filling the anode compartment with 8.87 mmol of EG in 2M KOH and conditioning the cell for 1h at the OCV (0.85 V for Pd-(Ni-Zn-P)/C, 0.94 V for Pd-(Ni-Zn)/C and 0.64 V for Pd/C), a current of 102 mA was discharged until 0 V.

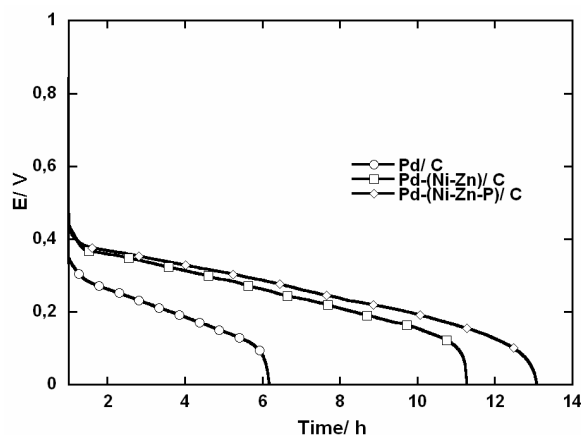


Figure 29. DEGFs galvanostatic curves with 8.87 mmol of ethylene glycol in 2M KOH (0V 102 mA) under nitrogen atmosphere, oxygen cathodic flux, at 20-22°C, on Pd/C, Pd-(Ni-Zn)/C, Pd-(Ni-Zn-P)/C electrodes.

The cell with the Pd-(Ni-Zn-P)/C anode lasted for 12 allowing the passage of an overall electric charge of 4439 C (Figure 29). From a perusal of Figure 29, one may readily realize that the present catalysts are much less efficient for EG oxidation than for ethanol oxidation. Indeed, the DEGFs with the present MEAs are not as efficient than the DEFCs (Figure 17, 2.3.5 section).

The quantitative determination of the oxidation products was performed by $^{13}\text{C}\{^1\text{H}\}$ NMR spectroscopy (Figure 30). One may notice that Pd-(Ni-Zn-P)/C converts 7.82 mmol of EG in carbonate (7.3%), glycolate (63%) and oxalate (29.7%) with no significant loss of fuel by either direct evaporation or evaporation by cross-over, likely a consequence of the high boiling point of EG (197,6°C) and larger size as compared to ethanol. The cell with the Pd-(Ni-Zn)/C anode gave carbonate (7.0%), glycolate (55.4%), oxalate (37.6%) and a trace of formate, for a total of 6.73 mmol of EG converted. Finally the Pd/C anode gave carbonate (3.9%), glycolate (89.5%) and oxalate (6.6%) for 4.84 mmol of EG converted. The chemoselectivity of EG oxidation in fuel cells is essentially identical to that observed in the chronopotentiometric experiments (2.3.7 section). In particular, it is confirmed that Pd/C is quite selective for glycolate production, while the other nickel-containing catalysts are poorly selective, with a prevalence of oxalate.

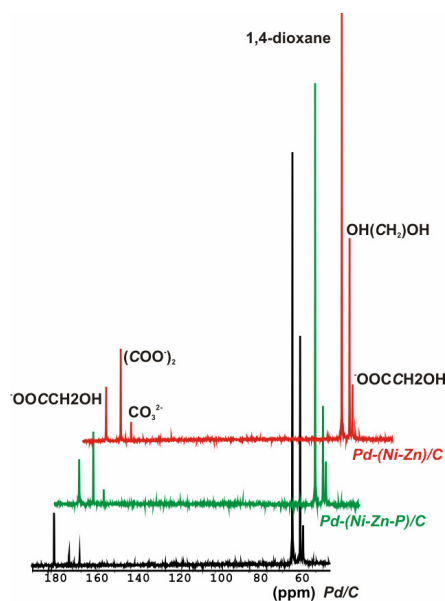


Figure 30. ^{13}C NMR spectra for Pd/C, Pd-(Ni-Zn)/C, Pd-(Ni-Zn-P)/C electrodes in passive DEGFCS after galvanostatic experiments.

In accordance with the mechanism shown in Scheme 5 (2.3.7 section), these results support the hypothesis that oxalate is a secondary oxidation product, coming from glycolate oxidation on Pd/C, yet it may be a primary oxidation product on the more oxophilic Pd-(Ni-Zn)/C and Pd-(Ni-Zn-P)/C catalysts.

The anode electrocatalysts were also tested in active monoplanar fuel cell with an oxygen flux of 200 mL/min and a fuel (5 wt% EG in 2M KOH) flux of 4 mL/min. The cell hardware is shown in Figure 48 (2.6 section). The polarization and power density curves were registered at 25, 40, 60, and 80°C (Figure 31). All the three anode catalysts show about the same power density at 25°C and 40°C, in accordance with the passive DEGFCS measurements. The Pd-(Ni-Zn)/C anode gives the highest power density at 80°C with 95 mW/cm² at 403 mA/cm².

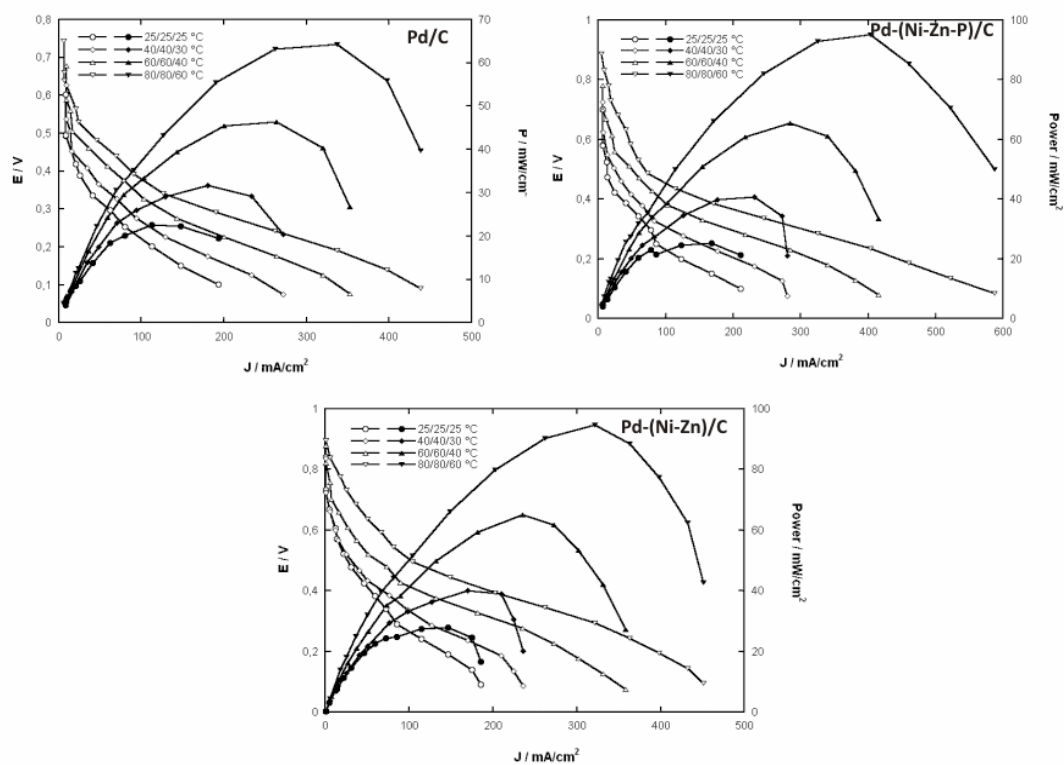
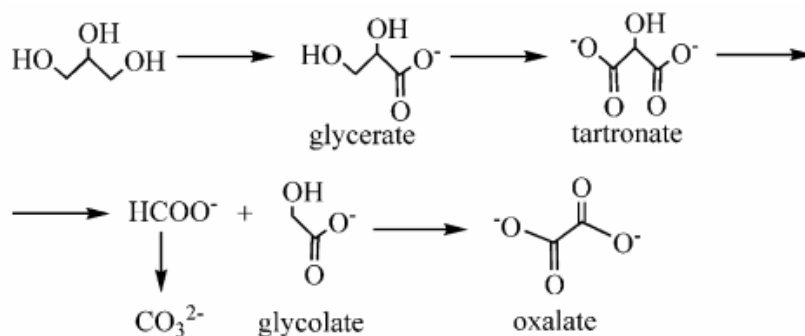


Figure 31. Polarization and power density curves provided by air-breathing active DEGFCs filled with 2M KOH solutions of ethylene glycol (5 wt%) at 25 °C, 40°C, 60°C, 80°C. Pd/C anode, Pd-(Ni-Zn-P)/C anode, Pd-(Ni-Zn)/C anode (Pd loading 1 mg/cm²) in conjunction with Tokuyama A006 membrane and Fe-Co/C (1:1) (Fe, Co loading 2-2.5 mg/cm² cathode) (MEAs).

2.3.9 Half cell studies of glycerol oxidation on the Pd-based catalysts in alkaline environment

The growing production of biodiesel by transesterification of fatty oils with methanol or ethanol is leading to a surplus production of glycerol (Gly). For this reason and the high boiling point and specific energy, there is much interest in the use of Gly as fuel in fuel cells. The presence of three hydroxyl groups makes the oxidation of Gly a more complex reaction as compared to the oxidation of methanol or ethanol (Scheme 6).

The electrochemical activity of the Pd-(Ni-Zn)/C, Pd-(Ni-Zn-P)/C and Pd/C electrodes towards Gly (5 wt%) oxidation was investigated by CV in 2M KOH solutions at room temperature with Pd loading of ca. 26-32 $\mu\text{g}/\text{cm}^2$ (corresponding to 17-19 mg of ink) and at scan rate of 50 mV/s.



Scheme 6. Proposed glycerol oxidation path.

The KOH and glycerol concentrations were fixed at 2M and 5 wt%, respectively, as these concentrations seem to be suitable for passive and active DGFCs experiments (vide infra). In Figure 32 are shown the CVs for glycerol oxidation on Pd/C, Pd-(Ni-Zn)/C, Pd-(Ni-Zn-P)/C electrodes while in Table 5 are reported the corresponding electrochemical data.

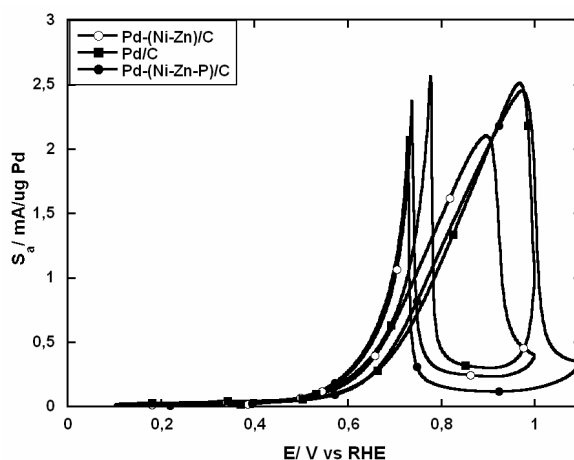


Figure 32. CVs (at the tenth cycle) on Pd/C, Pd-(Ni-Zn)/C, Pd-(Ni-Zn-P)/C electrodes in 5 wt% glycerol 2M KOH 2M under nitrogen. Scan rate 50 mV/s, at room temperature.

Catalyst	J_p (mA cm ⁻²)	S_{ap} mA(μg Pd) ⁻¹	V_{onset} (V)	V_p (V)	Tafel slope (mV dec ⁻¹)
Pd-(Ni-Zn)/C	55.5	2.10	0.41	0.87	132 (α 0.44)
Pd-(Ni-Z-P)/C	80.4	2.49	0.43	0.95	73 (α 0.80)
Pd/C	65.3	2.50	0.42	0.93	123 (α 0.47)

Table 5. Selected electrochemical parameters of 5 wt% Gly oxidation on Pd/C, Pd-(Ni-Zn)/C, Pd-(Ni-Zn-P)/C electrodes in 2M KOH.

All catalysts show good activity towards Gly oxidation with onset potentials around 0.42 V (vs RHE) and specific current densities of ca. 2.5 mA/μg Pd. In general the specific current densities are lower than that obtained for EtOH or EG electrooxidation in half-cells.

Tafel plots for Gly oxidation (Gly 5 wt% 2M KOH) on Pd/C, Pd-(Ni-Zn)/C, Pd-(Ni-Zn-P)/C electrodes were obtained at a scan rate of 5 mV/s in the potential range from 0.45 V to 0.6 V (vs RHE) (Table 5). The Tafel slope value and the α coefficient for Pd-(Ni-Zn-P)/C electrode diverge from those of the other two materials. The value for the Tafel slope is equal to 73 mV/dec and this might imply a lower glycerol oxidation overvoltage at its surface during the CV experiment. An α value of 0.8, is obtained for the Pd-(Ni-Zn-P)/C electrode, while values of 0.44 and 0.47 are calculated for Pd-(Ni-Zn)/C and Pd/C, respectively. A fractional number of α indicates generally an electrochemical rate limiting step for the electrooxidation reaction. Within this context, an α value of 0.8 might indicate faster glycerol oxidation kinetics on Pd-(Ni-Zn-P)/C electrode surface.

Plotting the value of anode peak current density against the square root of the scan rate for the three catalysts (Figure 33), a typical linear relationship referable to an electrochemical reaction under diffusion control is determined.

The catalyst stability was studied by chronopotentiometric measurements at a constant current of 3 mA/cm^2 , using the same palladium loading of the CV experiments. Experiments lasting for 1 or 2h, depending on the specific catalyst, are illustrated in Figure 34. The Pd/C, Pd-(Ni-Zn)/C, Pd-(Ni-Zn-P)/C electrodes are less stable for Gly oxidation than for ethanol oxidation. In agreement with the CV results, the Pd-(Ni-Zn-P)/C electrode exhibits the best durability performance.

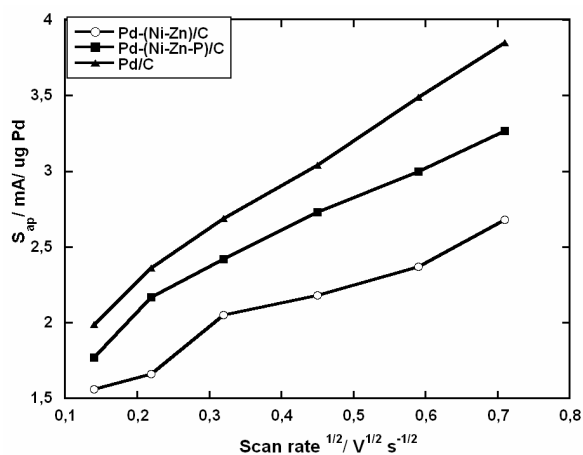


Figure 33. Plots of the anode peak current density against the square-root of the scan rate for the oxidation of 5 wt% Gly 2M KOH on Pd/C, Pd-(Ni-Zn)/C, Pd-(Ni-Zn-P)/C electrodes.

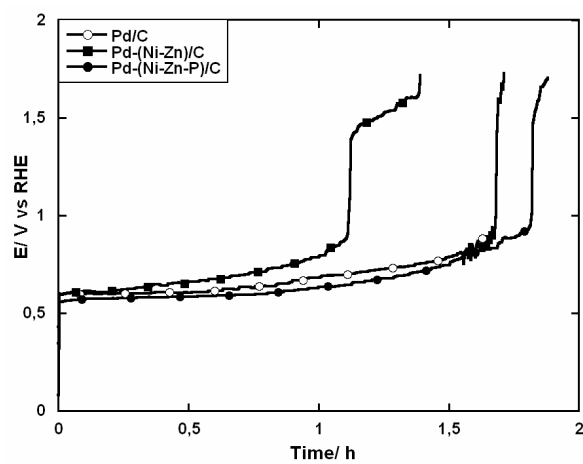


Figure 34. Chronopotentiometric experiments in the presence of Gly 5 wt% 2M KOH solutions with Pd/C, Pd-(Ni-Zn)/C, Pd-(Ni-Zn-P)/C electrodes, 3 mA/cm².

2.3.10 Direct Glycerol Fuel Cells (DGFCs) with Pd-based anode electrocatalysts

The present Pd-based anode electrocatalysts were tested in both passive and active fuel cells also for Gly oxidation. The MEAs were assembled as described in section 2.3.5, using the same experimental conditions. For the passive DGFCs, the polarization and power density curves were obtained at room temperature (Figure 35). The curves were registered, after the anode compartment was filled with 10 mL of a 5 wt% Gly in 2M KOH and a conditioning time of 1h at the OCV.

Pd-(Ni-Zn-P)/C exhibits the best performance releasing 16 mW/cm^2 at 117 mA/cm^2 , in nice accord with the CVs (2.3.9 section).

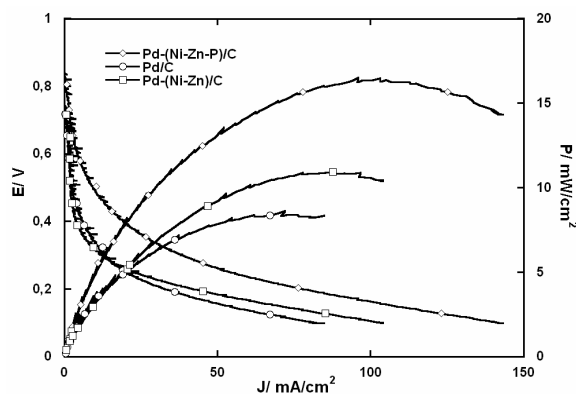


Figure 35. Polarization and power density curves provided by air-breathing DGFCs filled with 2M KOH solutions of glycerol (5 wt%) at 20–22 °C for Pd/C, Pd-(Ni-Zn)/C, Pd-(Ni-Zn-P)/C electrodes.

The galvanostatic experiments at 102 mA were carried out for each anode electrocatalyst in passive DGFCs using the same MEAs. The experimental conditions were the same of the galvanostatic DAFCs with ethanol or ethylene glycol. After charging the anode compartment with 5.43 mmol of Gly in 2M KOH solution and conditioning for 1h at the OCV, the curves were registered (Figure 36).

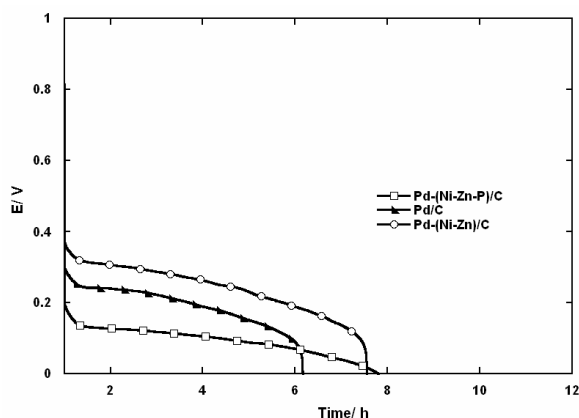


Figure 36. DGFCs (glycerol 5 wt% 2M KOH) galvanostatic curves registered at 102 mA until 0V, under nitrogen atmosphere, at 20-22°C, oxygen cathodic flux on Pd/C, Pd-(Ni-Zn)/C, Pd-(Ni-Zn-P)/C electrodes.

The cell with the Pd-(Ni-Zn)/C anode shows the highest energy efficiency and continued to work for 6.5 h. An $^{13}\text{C}\{^1\text{H}\}$ NMR analysis of the cell exhaust (Figure 37) gave the following product composition: 24.00% carbonate, 4.18% glycolate, 27.16% glycerate, 28.00% tartronate, 14.00 % oxalate and 2.50% formate. Overall, 2.14 mmol of the starting glycerol were converted without appreciable loss of fuel (Gly has a boiling point of 290°C and scarce tendency to cross-over the anion exchange membrane).

An analysis of Figure 36 shows that the Pd/C anode was the least efficient. The cell with this catalyst kept on working for 5.5 h and gave 27.17% carbonate, 11.30% glycolate, 14.40% glycerate, 27.70% tartronate, 13.00 % oxalate and 6.90% formate for a total of 2.14 mmol of Gly converted (Figure 37).

Finally, the cell containing the Pd-(Ni-Zn-P)/C anode gave 29.17% carbonate, 6.80% glycolate, 21.79 % glycerate, 23.50 % tartronate, 15.30 % oxalate and 3.45 % formate for 2.67 mmol of substrate converted.

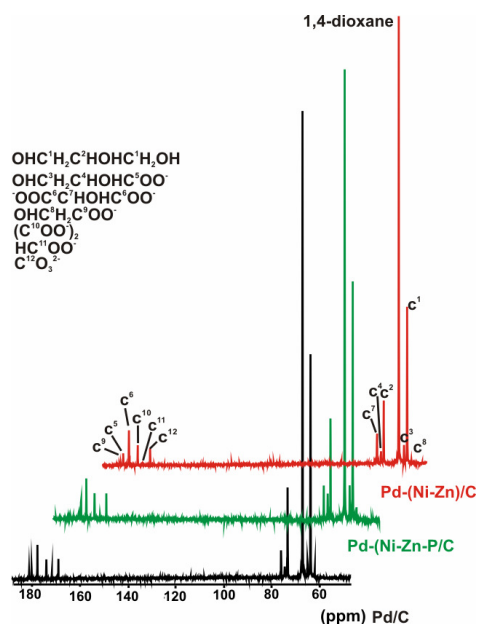


Figure 37. ^{13}C NMR spectra for Pd/C, Pd-(Ni-Zn)/C, Pd-(Ni-Zn-P)/C anodes from galvanostatic exhausts.

The variety of products obtained is a clear indication of the complex oxidation paths of Gly on Pd-based electrocatalysts. FTIR studies reported in the literature⁸² indicate that Pd/C and Pt/C electrocatalysts promote C-C bond cleavage in the Gly electrooxidation, as an appreciable amount of CO adsorbed was detected (bridging mode on Pd/C). On the basis of our experimental evidence and literature data, a mechanism of Gly oxidation on Pd/C and Pt/C is proposed in Scheme 6. In the literature the oxidation steps include: glycerol oxidation to glyceraldehyde (not experimentally detected), glycerate, tartronate and finally mesoxalate. The latter product has never been detected with our catalysts, which may be due to the fact that such a compound would rapidly evolve to formate, glycolate, or to oxalate and carbonate on our Pd-based electrocatalysts (Figure 37).

Polarization and power density curves were registered in active monoplanar fuel cells, using the apparatus described in sections 2.3.5 or 2.3.8 and identical MEAs to those employed for DEFCs and DEFCs. In Figure 38 are shown the polarization and power densities curves for the three catalysts registered at 25, 40, 60 and 80°C after 1h conditioning at the OCV. Fluxes of 4 mL/min of a 5 wt% Gly-2M KOH solution and 200 mL/min of oxygen were used at the anode and cathode side, respectively.

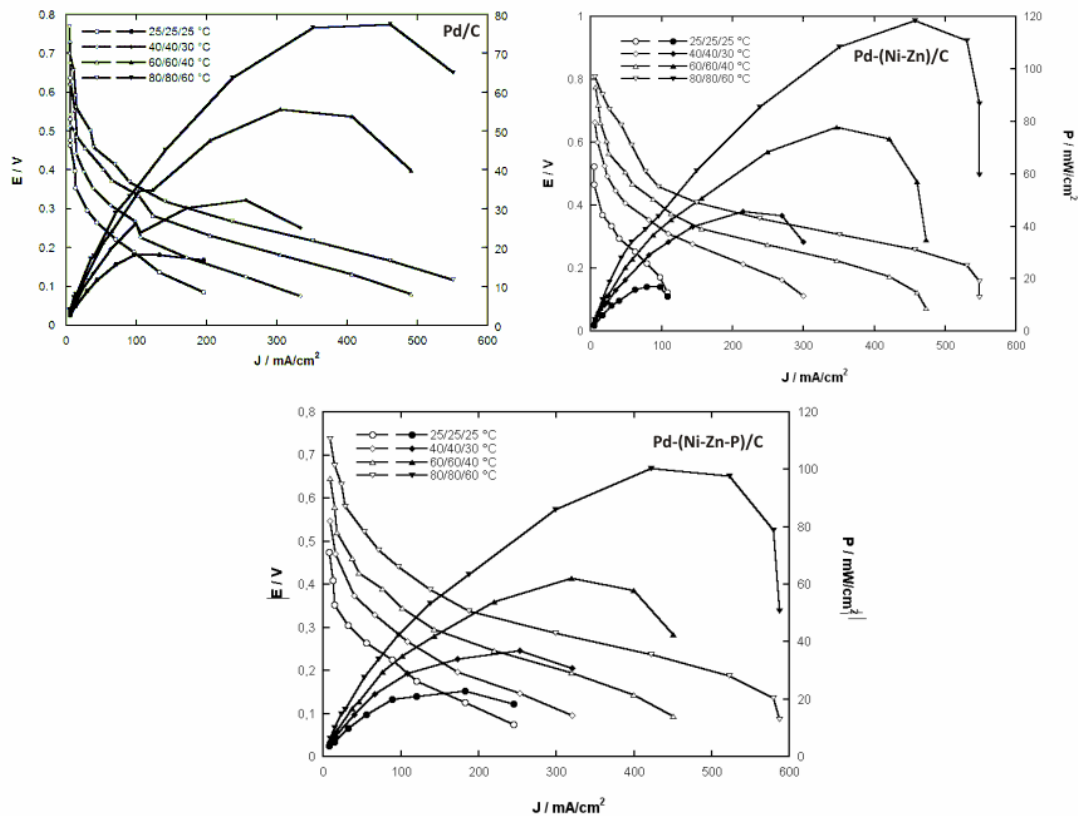


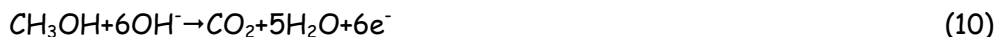
Figure 38. Polarization and power density curves provided by oxygen-breathing 200 mL/min active DGFCs. 4 mL/min of 5 wt% Gly 2M KOH solutions were pumped up at 25 °C, 40°C, 60°C, 80°C on Pd/C, Pd-(Ni-Zn-P)/C, Pd-(Ni-Zn)/C anodes.

The cell with the Pd-(Ni-Zn)/C anode was the most efficient at 80°C with 118 mW/cm^2 at 457 mA/cm^2 .

2.3.11 Half cell studies of methanol oxidation on the Pd-based catalysts in alkaline environment

Methanol is a highly attractive alcohol for fuel cell applications due to the good energy density of 6094 Wh kg⁻¹ and the relatively large abundance. The thermodynamic potential of the methanol-air fuel cell is also close to that of the hydrogen-air fuel cell (1.23 V). On the other hand, its effective energy density is only 1500-3100 Wh kg⁻¹, while its operating cell voltage is 0.4 V. In a DMFC this is mostly due to slow methanol oxidation kinetic on the anode surface, also in alkaline media [Eq(10)].

The electrochemical activity of Pd-(Ni-Zn)/C, Pd-(Ni-Zn-P)/C and Pd/C materials towards methanol oxidation was investigated by CV in 2M KOH + 10 wt% MeOH at room temperature and at a scan rate of 50 mV/s. The Pd loading varied from 24-28 μg/cm² (corresponding to 18-20 mg of ink, see 2.6 experimental section). For a reliable comparison with the other fuels investigated was used a 2M KOH concentration. This concentration is also suggested by previous studies of alcohol cross-over⁸³.



In Figure 39 are shown the CVs obtained, while the relevant electrochemical parameters are reported in Table 6. The activity towards MeOH oxidation in terms of specific current density was lower than those registered for the other substrates. Except for the Pd/C anode (2.3 mA/μg Pd), current densities of ca. 1.5 mA/μg Pd were obtained.

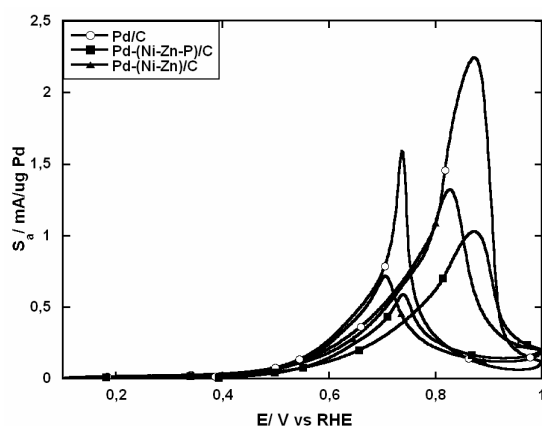


Figure 39. CVs registered on Pd/C, Pd-(Ni-Zn-P)/C, Pd-(Ni-Zn)/C electrodes in 10 wt% MeOH 2M KOH solution at room temperature and at the scan rate of 50 mV/s under nitrogen.

Catalyst	J_p (mA cm ⁻²)	S_{ap} mA(μg Pd) ⁻¹	V_{onset} (V)	V_p (V)	Tafel slope (mV dec ⁻¹)
Pd-(Ni-Zn)/C	33.49	1.3	0.44	0.83	161 (α 0.37)
Pd-(Ni-ZnP)/C	40.44	1.129	0.43	0.87	173 (α 0.34)
Pd/C	62.7	2.240	0.44	0.87	195 (α 0.30)

Table 6. Selected electrochemical parameters of MeOH oxidation on Pd/C, Pd-(Ni-Zn)/C, Pd-(Ni-Zn-P)/C electrodes in 2M KOH.

All catalysts showed methanol oxidation activity starting from 0.4 V (vs RHE). Like for the other alcohols, the oxidation begins at the potential value of Pd(OH) formation^{4,33,76,75} in alkaline environment (section 2.3.3 Figure 10, 11).

Tafel plots for the methanol oxidation reaction on the Pd/C, Pd-(Ni-Zn)/C, Pd-(Ni-Zn-P) electrodes were obtained at a scan rate of 5 mV/s in the potential range from 0.35 V to 0.6 V (vs RHE) (Table 6). A similar Tafel slope for all the three catalysts suggests the occurrence of the same reaction mechanism, while the α values are consistent with an electrochemical rate-limiting step. According to the Tafel slopes reported in Table 6, Pd/C seems to be slightly less active in terms of surface overvoltage, which contrasts with the CV study showing the highest density current peak just for Pd/C. This result might be explained looking at the scan rate of the CV experiments: at 50 mV/s the reaction is under diffusion control and methanol might approach the Pd sites more rapidly on Pd/C than on the nickel-zinc supported materials, while at 5 mV/s (Tafel experiment) a beneficial effect of the larger concentration of the OH_{ads} groups on the surface of Pd-(Ni-Zn)/C and Pd-(Ni-Zn-P)/C might prevail over diffusion effects.

For testing the catalyst stability during the methanol oxidation, chronopotentiometric measurements were performed at 3 mA/cm^2 (Figure 40). The Pd/C electrode exhibits the best stability, lasting for 3h 30'. In agreement with the J_p value obtained (Table 6), the Pd-(Ni-Zn)/C electrode gave the lowest performance.

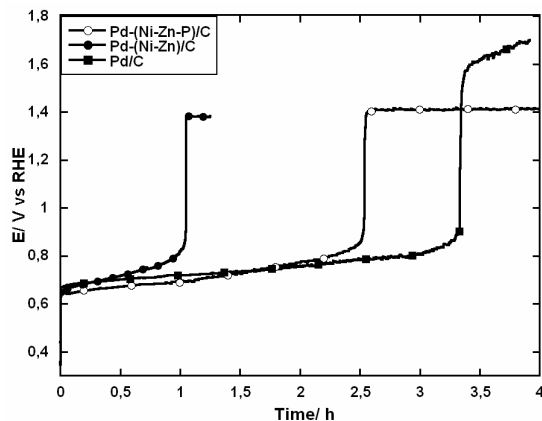


Figure 40. Chronopotentiometric experiments in 10 wt% MeOH 2M KOH with Pd/C, Pd-(Ni-Zn)/C, Pd-(Ni-Zn-P)/C electrodes, 3 mA/cm^2 .

Plotting the anode peak current density against the square-root of the scan-rate for the three catalysts investigated (Figure 41) a typical trend of an electrochemical reaction under diffusion control for Pd/C was shown until the scan rate of 100 mV/s . Above this value, the reaction is apparently controlled by other factors such as the low density of catalytic centers. From 20 mV/s to 500 mV/s , the Pd-(Ni-Zn-P)/C and Pd-(Ni-Zn)/C electrodes do not show the same progress, which suggests a different electrochemical oxidation mechanism.

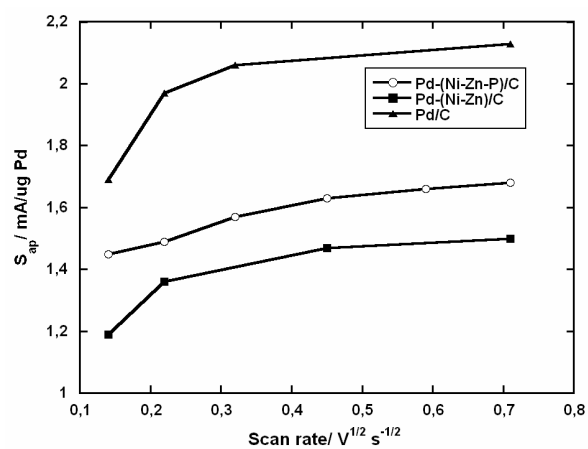


Figure 41. Plots of the anode peak current density against the square-root of the scan rate for the oxidation of 10 wt% MeOH 2M KOH on Pd/C, Pd-(Ni-Zn)/C, Pd-(Ni-Zn-P)/C electrodes.

2.3.12 Direct Methanol Fuel Cells (DMFCs) with Pd-based anode electrocatalysts

The three electrocatalysts investigated in this work have been tested in either passive or active DMFCs, using the same cell hardware and MEAs of the other DMFCs described so far. In Figure 42 are reported the polarization and power density curves for passive DMFCs (10 mL 10 wt% MeOH in 2M KOH, air breathing), while Figure 43 shows the polarization and power density curves obtained in active cells at different temperatures using a fuel flux of 4 mL/min and an oxygen flux of 200 mL/min (vide infra).

Interestingly, the Pd/C electrode showed the best performance (power density of 14 mW/cm² at 100 mA/cm²) in the passive cell with methanol than with any other fuel investigated (ethanol, glycerol and ethylene glycol). A different activity order was found in active DMFCs: the cell with the Pd-(Ni-Zn-P)/C anode gave 45 mW/cm² at 273 mA/cm² at 40°C, while the cell with the Pd-(Ni-Zn)/C anode gave 40 mW/cm² at 276 mA/cm². At 60 and 80°C, the Pd-(Ni-Zn)/C catalyst improved its power performance. In contrast to what observed in the passive cells, Pd/C was the least performing anode catalyst in terms of power density.

Galvanostatic experiments at 102 mA were carried out for each catalyst in passive fuel cell under an oxygen atmosphere at the cathode side. The anode compartment was filled with 31.25 mmol of methanol in 2M KOH and the cell was conditioned for 1h at the OCV. The galvanostatic traces are shown in Figure 43.

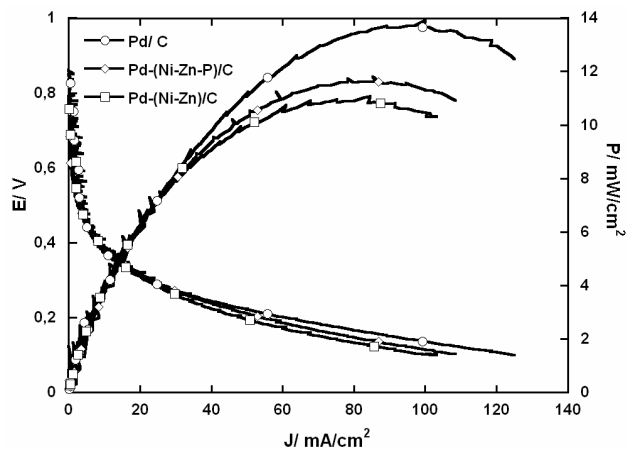


Figure 42. Polarization and power density curves provided by air-breathing DMFCs filled with 2M KOH solutions of 10 wt% MeOH at 20–22 °C on Pd/C, Pd-(Ni-Zn)/C, Pd-(Ni-Zn-P)/C anodes.

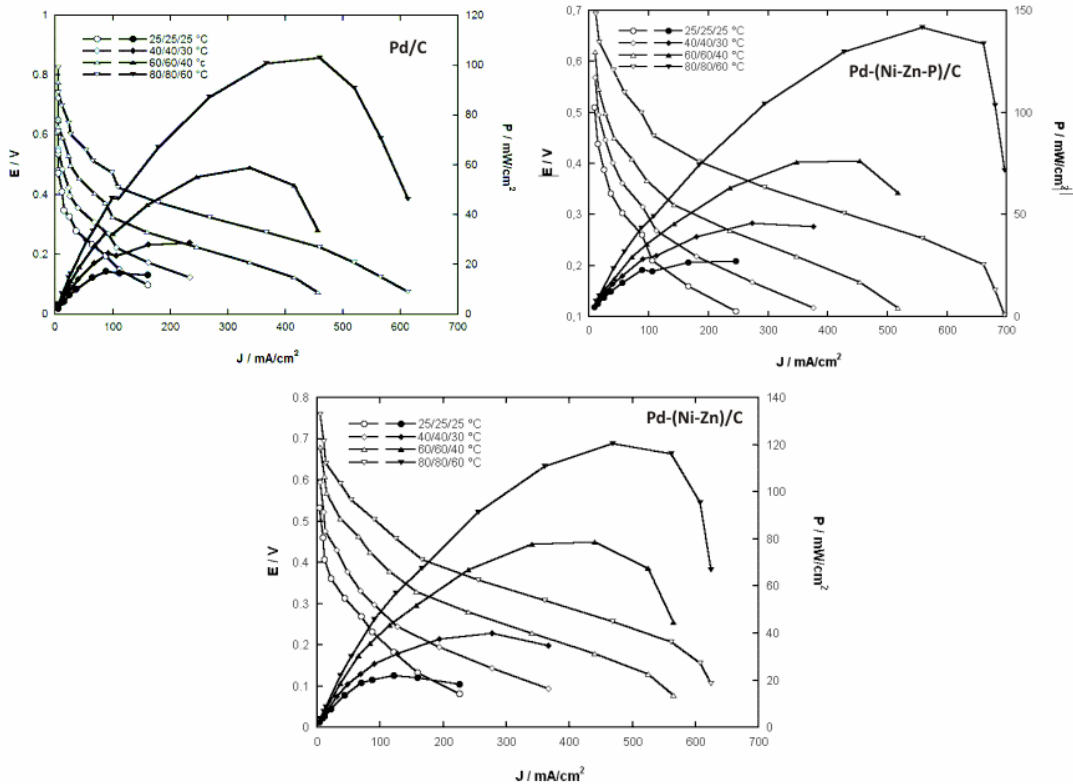


Figure 43. Polarization and power density curves provided by oxygen-breathing active DMFCs filled with 2M KOH solutions of 10 wt% MeOH at 25 °C, 40 °C, 60 °C, 80 °C on Pd/C, Pd-(Ni-Zn-P)/C, Pd-(Ni-Zn)/C anodes.

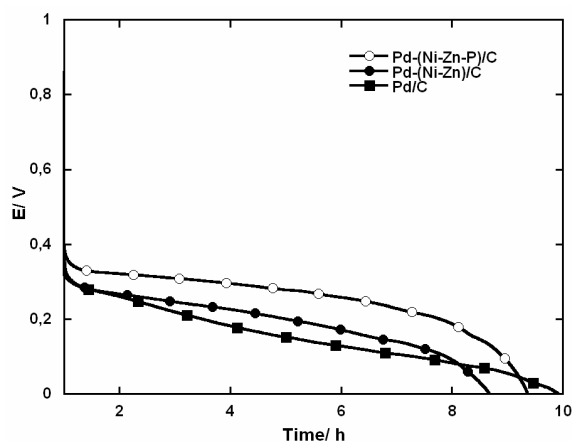


Figure 44. Galvanostatic experiments at 102 mA until 0V under nitrogen atmosphere, at 20-22°C with oxygen cathodic flux (10 mL/min) in passive DMFCs with methanol 31.25 mmol (2M KOH) on Pd/C, Pd-(Ni-Zn)/C, Pd-(Ni-Zn-P)/C anodes.

The cell with the Pd/C anode kept working for 9h, while those with the Pd-(Ni-Zn-P)/C and Pd-(Ni-Zn)/C electrodes continued to work for 8.5 and 7.5 h, respectively. ^{13}C NMR spectra of the galvanostatic exhausts showed the conversion of methanol into formate and carbonate (Figure 45). A reliable quantitative determination of the methanol conversion was precluded by the methanol cross-over and its evaporation from both the cathode and anode sides (boiling point of methanol 64.7 °C). The NMR spectra showed a 1:1 molecular ratio between carbonate (168 ppm) and formate (171 ppm) for the cell with the Pd/C anode, while carbonate prevailed over formate (2:1 molecular ratio) for the Pd-(Ni-Zn)/C and Pd-(Ni-Zn-P)/C anodes.

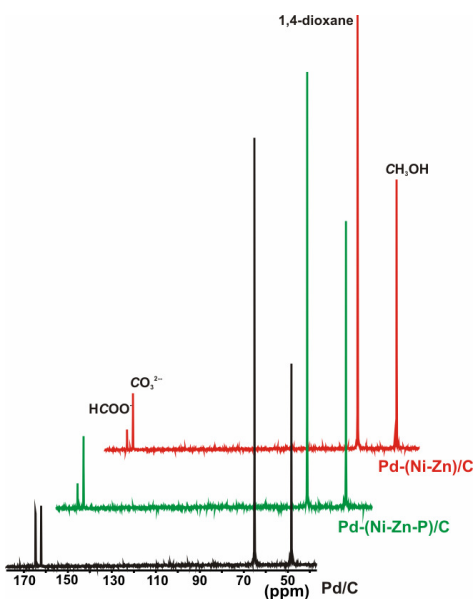


Figure 45. ^{13}C NMR spectra of DMFCs exhausts after galvanostatic experiment (0V 102 mA) for Pd/C, Pd-(Ni-Zn-P)/C, Pd-(Ni-Zn)/C anodes, starting from 31.25 mmol of methanol (2M KOH).

Most of the known DMFCs make use of Pt and Pt-Ru catalysts in acidic media where CO_2 is the largely prevailing product. On the other hand, any Pt-based catalyst suffers irreversible poisoning by CO with time^{84,85}. The Pd catalyst are less sensitive to CO poisoning, yet the power densities are significantly lower than those obtainable by Pt-based electrocatalysts.

2.4 Conclusions

In this PhD thesis work, we have described and discussed the synthesis and characterization of some nanosized Pd-based materials that exhibit excellent activity as anode electrocatalysts in direct alcohol fuel cells. In particular, we have known that Ni-Zn and Ni-Zn-P alloys supported on a conductive carbon black (Vulcan XC-72) are appropriate materials for the spontaneous deposition of palladium through redox transmetalation reaction. The materials obtained, Pd-(Ni-Zn)/C and Pd-(Ni-Zn-P)/C, have been characterized by a variety of techniques, including HRTEM, EXAFS, EDX, ICP-AES, XANES, and XRPD. The analytical and spectroscopic data allowed us to conclude that the surface of Pd-(Ni-Zn)/C and Pd-(Ni-Zn-P)/C contain very small (0.5–1 nm), highly

dispersed, and crystalline palladium clusters as well as single palladium(II) sites, likely stabilized by interaction with oxygen atoms from the surrounding Ni-O phase. The oxidation of ethanol in alkaline media on electrodes coated with the Pd-(Ni-Zn)/C and Pd-(Ni-Zn-P)/C materials, containing very low Pd loadings ($22\text{--}25\ \mu\text{g cm}^{-2}$), have been studied by cyclic voltammetry. Analogous studies have been carried out with a Pd/C catalyst prepared by a standard electroless procedure. The results obtained place Pd-(Ni-Zn)/C and Pd-(Ni-Zn-P)/C in the top band of the electrocatalysts for ethanol oxidation. Indeed, specific currents as high as $3600\ \text{A g(Pd)}^{-1}$ at room temperature can be obtained with onset potentials as low as $0.6\ \text{V}$ (vs RHE). The present Pd-based electrocatalysts have been used to fabricate anodes for DAFCs upon deposition on Ni foam plates. These electrodes have been employed to realize membrane-electrode assemblies (MEAs) in conjunction with an anion-exchange membrane from Tokuyama (Japan) and home-made Fe-Co cathodes. Both passive and active monoplanar DEFCs have been constructed and studied using either a potentiostat-galvanostat or a Scribner Associates fuel cell station. The polarization and power density curves have shown the Pd-(Ni-Zn)/C and Pd-(Ni-Zn-P)/C anodes to be much more stable and active than the Pd/C anode, especially at temperatures below 50°C . Most importantly, ethanol is selectively converted to acetate, provided when the pH is kept above 13. The chemical-physical features of the Pd-(Ni-Zn)/C and Pd-(Ni-Zn-P)/C materials may account for their excellent electrochemical performance, which, as a whole, is better than that of the Pd/C catalyst where the Pd particles are larger, less dispersed, and amorphous. In view of the CV experiments in KOH solution with electrodes coated with the Ni-Zn/C and Ni-Zn-P/C supports, prior to and after addition of ethanol, any direct role of the Ni support on the ethanol oxidation reaction at the potentials achievable in a fuel cell can be ruled out. One cannot exclude, however, the existence of a co-catalytic effect of the Ni support on the Pd-catalyzed oxidation reaction of ethanol. Indeed, it is generally agreed that the presence of Ni may have a beneficial effect on the electrooxidation of alcohols on late transition metals especially in alkaline media⁴. In particular, Shen et al. have demonstrated that the presence of NiO increases remarkably the activity and stability of carbon-supported Pd nanoparticles for the electrooxidation of ethanol in alkaline media⁵. Although no clear-cut explanation has been offered so far, it is generally believed that Ni and NiO can generate surface Ni-OH at low potentials. Increasing the amount of OH_{ads} on the catalyst surface would actually favour the formation of acetate

by coupling with adsorbed acyl groups ($\text{CO}(\text{CH}_3)_{\text{ads}}$), in turn generated by dehydrogenation of aldehyde intermediates. One may also hypothesize that the greater oxophilicity of Ni as compared to Pd and the higher binding affinity of Ni towards the acetate ion may facilitate the desorption of the acetate from the active Pd sites, thus accounting for the stability of the Pd-(Ni-Zn)/C and Pd-(Ni-Zn-P)/C catalysts even at high ethanol conversion⁶².

To elucidate mechanistic aspects involved in the oxidation of ethanol to acetate by the present catalysts, we have investigated the effect of adding small amounts of NaBH_4 into the anode compartment of DEFCs equipped with Pd/C electrocatalyst with and without 10 wt% of ethanol (2M KOH). It is apparent that NaBH_4 promotes the ethanol oxidation on palladium-based electrocatalysts. At 0.2 V 0.2 wt% NaBH_4 gives a current density of 180 mAcm^{-2} higher than the sum of the current densities (117 mAcm^{-2}) supplied by similar DEFCs fuelled with 0.2 wt% NaBH_4 + 2M KOH and with 10 wt% ethanol + 2M KOH. In the absence of NaBH_4 , 50% of ethanol is converted to acetate (17 h at 0.2 V), the fuel cell stops working. The addition of NaBH_4 , even in a low amount (0.1-0.2 wt%), increases the ethanol conversion to more than 80%. A detailed CV study of a Pd/C electrode in different solutions (NaBH_4 alone, ethanol alone, NaBH_4 ethanol mixtures) led us to conclude that NaBH_4 is able to reduce the inactive PdO phase to active Pd, thus increasing the catalyst activity at high potential as well as its lifetime.

The Pd-(Ni-Zn)/C, Pd-(Ni-Zn-P)/C and Pd/C materials have been tested as anode catalysts for the oxidation of a variety of renewable alcohols, including ethylene glycol, glycerol and methanol, in alkaline media (generally 2M KOH). Again, Pd-(Ni-Zn)/C and Pd-(Ni-Zn-P)/C showed a better performance for the EG oxidation than Pd/C, yielding specific currents as high as $3200 \text{ A g(Pd)}^{-1}$ at room temperature with onset potentials as low as 0.6 V (vs RHE). Tests in both passive and active DEFCs with the same cathodes and anion-exchange membrane as those described above confirmed that the Pd-(Ni-Zn)/C and Pd-(Ni-Zn-P)/C anodes are much more stable and active than the simple Pd/C anode. Analysis of the cell exhausts by NMR and IC showed a different product distribution for the three catalysts. Glycolate was the prevailing oxidation product on the Pd/C anode, while mixtures of glycolate (>60 %), oxalate and carbonate were obtained with the Pd-(Ni-Zn)/C and Pd-(Ni-Zn-P)/C anodes. In situ FTIR and CVs measurements were carried out on a smooth Pd electrode and on a Pd/C catalyst, respectively. Like for ethanol, CO_2 formation is observed for pH values lower than 12,

while at higher pH values glycolate, carbonate and oxalate are formed almost simultaneously at a potential of ca. 0.4 V vs RHE. Carbonate is produced by oxidation of both glycolate (major contribution) and oxalate, while the major part of oxalate seems to be produced by the direct oxidation of EG. It has been proposed that the nickel phases that support the Pd clusters and atoms favour the chelating adsorption of EG, leading to its direct oxidation to oxalate, by virtue of the oxophilic nature of Ni³³.

Analogous CV studies as well as evaluation of monoplanar cell performance in either passive or active systems were carried out for glycerol and methanol as fuels. Both alcohols gave worse results in terms of catalytic activities and overall alcohol conversion. In the half cell, the Pd-(Ni-Zn-P)/C gives specific current density of 2500 and 2200 A g(Pd)⁻¹ with glycerol and methanol, respectively. A maximum power density of 20 mW/cm² was obtained with glycerol at room temperature with little chemoselectivity. The Pd-(Ni-Zn)/C, Pd-(Ni-Zn-P)/C catalysts gave prevalently glycerate, together with appreciable amounts of tartronate, formate, glycolate, oxalate and carbonate. In contrast, the Pd/C catalyst is more selective for tartronate.

Methanol was converted into 1:1 or 2:1 mixtures of carbonate and formate on Pd/C and Pd-(Ni-Zn)/C, Pd-(Ni-Zn-P)/C, respectively. Overall, methanol is the worst fuel on Pd-based electrocatalysts in alkaline media. The formation of carbonate upon oxidation of methanol, which may lead to membrane carbonation, does not seem to account for the lower performances of the DMFCs as compared to the DEFCs, DEGFCs and DGFCs.

Finally, it is worth commenting that the partial oxidation of renewable alcohols to oxidation products might represent an obstacle to the use of the present Pd catalysts to fabricate stacks of DAFCs capable of delivering kilowatts of energy. However, especially the good response observed at room temperature, up to 60 mWcm⁻² at 0.3 V⁶², presages an effective application of the present monoplanar DAFCs to produce small generators for portable electronics and first aid devices. Likewise, an appropriate scale up of the MEAs may be exploited for the contemporaneous production of energy and selective chemicals, mainly alkali metal carboxylates from alkaline solutions of alcohols.

2.5 Experimental section

2.5.1 Catalyst Synthesis

All the synthesis were carried out in nitrogen atmosphere, except were specified. Water solution were freshly prepared with double distilled water. Vulcan XC-72 were supplied by Cabot Corp.(USA), precious metal salts were purchased by Aldrich and used without any further purification. Ultrasound treatments were performed by SBL ultrasound bath or Bandelin Sonoplus sonde.

Pd-(Ni-Zn-P)/C: NiSO₄·6H₂O (3.51 g, 13.35 mmol), ZnSO₄·7H₂O (2.03 g, 7.05 mmol), NaH₂PO₂ (3.3 g, 37.5 mmol), Na₃C₆H₈O₇·2H₂O (8.56 g, 97.3 mmol), and NH₄Cl (5.2 g, 97.3 mmol) were introduced into a 250 mL three-necked round bottomed flask, containing distilled water (90 mL). The pH of this solution was adjusted to 11 with an aqueous solution of KOH (1M), and then Vulcan XC-72 (6.2 g) was added with stirring to the resulting green-blue solution. After 20 min of ultrasound treatment, this slurry was heated to reflux temperature for 2 h and then cooled to room temperature. KOH flakes (10 g) were added, and the mixture was refluxed for 1h, then cooled to room temperature for product filtration. The collected product was washed with distilled water to neutral pH. A small portion of this product was dried by means of a stream of nitrogen and analyzed by ICP-AES (wt %) analysis: Ni 10.90, Zn 0.61.

The product was suspended in water (150 mL), and the resulting mixture was sonicated for 30 min. A solution of K₂PdCl₄ (1.0 g, 3.06 mmol) in water (250 mL) was slowly added to this suspension, and the resulting suspension was stirred for the night at room temperature. The solid product was filtered off, washed several times with distilled water, and finally dried under vacuum at 40°C until constant weight.

Yield: 6.2 g. ICP-AES (wt%):Pd 4.73, Ni 7.45, Zn 0.43. EDX analysis (wt%): Pd 4.9, Ni 7.0, Zn 0.5,

Pd-(Ni-Zn)/C: A slurry of Zn powder (2.8 g, 43 mmol) and Vulcan XC-72 (6.0 g) in H₂O (40 mL) in a 100 mL three-necked round-bottomed flask was treated by ultrasounds for 20 min. The mixture was heated to 90°C, and then a boiling 10 mL solution of NiCl₂·6H₂O

(5.06 g, 21.28 mmol) was added quickly in 1–2 min under vigorous stirring. Foaming was observed owing to gas evolution that gradually disappeared in 3–4 min. The resulting reaction mixture was stirred at room temperature for 30 min, then the solid product was filtered off and washed portionwise with hot water (50°C; 200 mL). The solid was suspended in an aqueous solution of NaOH (13 wt%; 300 mL), and the suspension was stirred for 40 min until no H₂ gas evolution was evident. The final product was separated from the reaction mixture by filtration and washed with distilled H₂O to neutral pH. A small portion of this product was dried under nitrogen atmosphere and analyzed by ICP-AES (wt%): Ni 14.4, Zn 3.4.

The Ni-Zn/C obtained was suspended in water (400 mL), and sonicated for 30 min. 250 mL of K₂PdCl₄ (1 g, 3.01 mmol) solution was added drop to drop (ca. 3 h) to this suspension under vigorous stirring, and the reaction mixture was gently stirred overnight at room temperature. The final product was filtered off, washed with water (4 X 100 mL), and dried at 40°C under vacuum to constant weight.

Yield: 6.0 g. ICP-AES (wt%): Pd 6.4, Ni 9.7, Zn 2.6.

Pd/C: Vulcan XC-72 (5.94 g) was sonicated for 20 min in a 500 mL three-necked round-bottomed flask containing ethylene glycol (250 mL). An aqueous solution (50 mL) obtained by treatment of PdCl₂ (0.6 g, 3.38 mmol) with 6 mL of HCl (37% w/w) was added dropwise to the resulting dispersion with stirring. After addition of the Pd salt was complete, a solution of NaOH (5.1 g) in water (10 mL) was introduced into the reactor, which was then heated to 140°C. After 3 h, the reaction mixture was allowed to cool to room temperature and the solid product was filtered off and washed with distilled water to neutral pH. The final product was dried at 40°C under vacuum and nitrogen atmosphere to constant weight. Yield: 5.8 g. ICP-AES (w %): Pd 5.2.

2.5.2 Physical material characterization

EXAFS and XANES measurements were carried out at the XAFS beamline of the Elettra synchrotron facility in Basovizza (Trieste), by means of a double-crystal Si (111) monochromator at the Ni K-edge and of Si (311) at the Pd K-edge (synchrotron ring

operating at 2.4 GeV). All samples were measured in transmission mode at room temperature at both metal edges. Data were analyzed with the FEFF8 software package.

HRTEM images were recorded with a JEOL Jem-2010 EX microscope. The instrument was equipped with an in-column EDX Spectrometer (probe spot 5 nm, sensitivity 0.5 %). Pictures were taken at 250000–1200000X magnifications, spanning wide regions of several support grains in order to provide a representative map of the catalyst system. The samples were ground, and the powders were dispersed in isopropyl alcohol. A drop of each suspension was deposited on the carbon grid, which, after solvent evaporation under vacuum, was inserted in the column of the microscope.

The metal content in all catalysts was determined by inductively coupled plasma atomic emission spectroscopy (ICP-AES) with an Intrepid Iris instrument (Thermo Elemental). Each sample (20–50 mg) was treated in a microwave-heated digestion bomb (Milestone, MLS-200) with concentrated HNO₃ (1.5 mL), 98% H₂SO₄ (2 mL), and a pellet (0.4 g) of a digestion aid reagent (0.1% Se in K₂SO₄). The solutions were analyzed after the carbon residue was filtered off.

EDX was employed to analyze Pd-(Ni-Zn-P)/C. The measurements were performed on untreated powder samples directly deposited on specimen stubs covered with a conductive carbon adhesive, using a FEI Quanta200 microscope operating at 20 KeV accelerating voltage in the low-vacuum mode (0.8 torr).

X-ray powder diffraction spectra (XRPD) were acquired at room temperature with a Bruker D8-Advance diffractometer, employing CuK α radiation ($\lambda=1.5418 \text{ \AA}$) in the range between 2.5 and 80° and using an acquisition step of 0.030°/s.

2.5.3 Electrochemical studies

The cell used for the cyclic voltammetry and chronopotentiometric experiments was a Keleff cylinder with an inner diameter of 7.2 mm and an outer diameter of 50 mm (Figure

46). The inner volume of the cell was about 1 mL. The working electrode, Glassy Carbon (Sigradur G; 0.867 cm²), covered by the catalyst, was put in a special cavity at the top end of the cylinder, and the counter electrode was a gold disc placed at the bottom end. The solution contained in a Pyrex flask was previously deaerated by bubbling N₂ and then flushed into the cell at a pressure as low as 0.3 bar N₂. This pressure was applied until the cell was completely filled and then stopped. The inlet and the outlet for the solutions were placed on the side walls of the cell. The inlet was inclined towards the counter electrode so as to allow the solution to gradually fill in slowly getting wet the working electrode without disturbing the catalyst layer. The electrical contact with the working electrode was secured with two stainless steel screw terminals. Leakage was avoided by pressing both the working and the counter electrode against a suitable silicone O ring. The reference electrode, a miniaturized Ag/AgCl/KCl_{sat} electrode, was placed on the outlet tubing. This location allows contamination to be avoided and at the same time is sufficiently close to the working electrode to reduce the uncompensated resistance. All CV studies were carried out using a Parstat 2277 potentiostat-galvanostat (Princeton Applied Research).

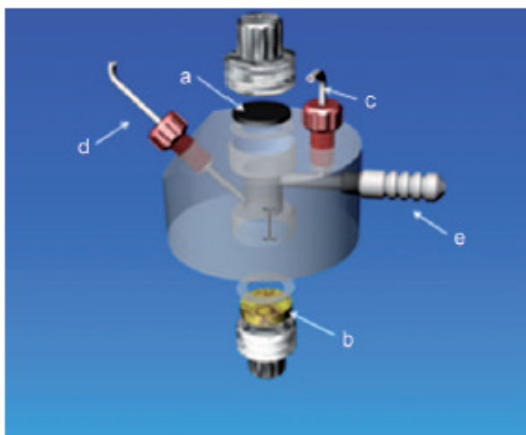


Figure 46. Electrochemical cell for CV experiments: a) working electrode, b) counter electrode, c) reference electrode, d) inlet, and e) outlet³³.

Ink preparation. A portion of 45 mg of each electrocatalyst was introduced inside a 5 mL high-density polyethylene container together with water (1.01 g), KOH (99.99%, Sigma–Aldrich, 65 mg), absolute ethanol (99.8 %, Fluka; 0.50 g), and 5% Nafion ion-exchange resin (Sigma–Aldrich; 0.37 g) in ethanol solution. The resulting suspension was sonicated for 30 min with a Branson 3200 bath. Each suspension was freshly prepared just before

carrying out the experiment scheduled. The metal loading on each electrode was determined by weighting the amount of ink (17-20 mg) deposited on the glassy carbon disk. All the solution analyzed were previously desaired for ten minutes and maintained under inert atmosphere during the measurements.

Tafel plots for all the catalysts studied were registered at 5 mV/s in the potential range from 0.3-0.35 V to 0.5-0.55 V (vs RHE). Plotting potential vs current or current density logarithm, a relationship linear curve was determined. The line slope opposite represents the anode overvoltage to oxidize the fuel (mV/dec), while α value means the electron transfer coefficient. The α value was deduced from Butler-Volmer simplifying equation, effective for kinetic control processes.

In situ FTIR spectroelectrochemical study was made inside a cell equipped with a CaF_2 window . The working electrode was a palladium electrode with a 6 mm diameter. A platinum foil and an Hg/HgO electrode were used as the counter and reference electrode, respectively. The electrochemical measurements were performed on a 263A potentialstat/galvanostat (EG&G-PARC, USA), connected to the FTIR spectrometer (Nicolet 5700 with DTGS detector, Thermo Electron Corporation, USA). The measurements were carried out at 25°C. When necessary, NaClO_4 was added to the NaOH solutions to ensure a constant ionic strength. The EG concentration was fixed at 1M and NaOH was changed to indagate the pH effect on EG electrooxidation. All solutions were purged with nitrogen prior to use. Prior to each experiment, the palladium electrode was polished with alumina powder, followed by a supersonic rinsing in pure water and a potential cycling in 0.1M HClO_4 at 0.1 V s^{-1} between 0.242 and 1.2 V versus SCE with a reductive final potential. During the in situ FTIR spectroelectrochemical experiments, the electrode was pressed against the CaF_2 window to form a thin layer solution. Each infrared spectrum was recorded from 128 interferograms at the resolution of 4 cm^{-1} . The reference spectrum (R_{ref}) was collected at 0 V versus reversible hydrogen electrode (RHE). The electrode potentials were increased by 0.1 V intervals from the reference potential up to 1.2 V. The equilibrium at each potential was achieved in 5 s before the collection of the sample spectra (R_s). Each final spectrum was reported using Eq.(12). Accordingly, the negative bands represent the

species produced and the positive bands the species consumed. All the potentials in the figures were quoted with respect to the RHE.

$$\Delta R/R = (R_s - R_{ref})/R_{ref} \quad (12)$$

2.5.4 Fuel cell assembly

The home-made, air/oxygen-breathing DAFC used to evaluate the electrochemical performance of the Pd-(Ni-Zn-P)/C, Pd-(Ni-Zn)/C and Pd/C anodes, in conjunction with the Tokuyama A-006 anion exchange membrane Tokuyama Corporation and Fe-Co/C KJ cathodes, was shown in Figure 47. The device was realized with plexiglas and the electricity collectors were plated with gold. The volume of the anode compartment was ca. 20–25 mL for an actual fuel solution of 10–13 mL. The anode was realized with a 5.13 cm² nickel foam plate onto which was deposited the appropriate amount of a dense catalytic ink (generally in order to obtain 1 mg cm⁻² of palladium loading). This was prepared by dispersing the solid catalyst in the minimum amount of water with no need of a binder. The cathode was prepared using a suspension of ketjen black (C) with iron and cobalt phthalocyanines (MPC) 1:1 stoichiometric mixture, followed by heat treatment at 800 °C under inert atmosphere, brushed on carbon cloth, prepared in our lab. The A006 membrane used was purchased from Tokuyama Corporation and used after brief basic treatment (1M KOH solution) and gently drying. The membrane-electrode assembly (MEA) was obtained by mechanically pressing anode, cathode and membrane, while silicone–rubber gaskets were employed to seal the system. For galvanostatic experiments, in order to avoid any possible contamination of the alkaline anode solution by carbonate ions formed upon reaction with atmospheric CO₂, the DAFCs were positioned inside a home-made plexiglass dry-box. Here the anode compartment was maintained all the way under a static nitrogen atmosphere, while the cathode was exposed to an oxygen constant flow of 10 mL/min. For polarization and power density experiments after assembling the MEAs, the DAFCs were tested air-oxygen breathing mode. All the cell performances were evaluated with an ARBIN BT-2000 5A-4 channels instrument.

Polarization curves were registered at 5 mV/s, after 1h conditioning time. Galvanostatic experiments were registered after 1h conditioning time at 102 mA until 0V.

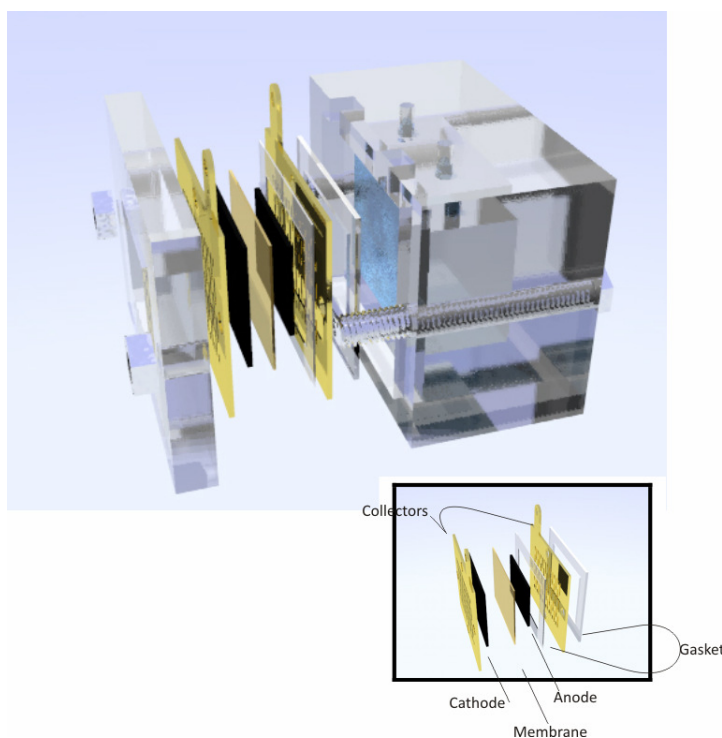


Figure 47. Lateral view of opened passive home-made direct alcohol fuel cell. In the inset the MEA was detailed.

The active DAFCs were purchased from Scribner-Associates (USA) (25 cm² fuel cell fixture). They were modified in our laboratory with gold-plated current collectors and titanium end plates to tolerate the alkaline conditions used in this work to evaluate the performance of Pd-(Ni-Zn-P)/C, Pd-(Ni-Zn)/C, and Pd/C anode. The MEA was fabricated by mechanically pressing each anode with Fe-Co/C KJ cathode (prepared in our lab) and Tokuyama A006 membrane (Figure 48). A dense anode ink was prepared by mixing the powdered catalyst with a 5-10 wt% aqueous dispersion of PTFE. As a general procedure, an identical amount of the resulting paste was spread onto two identical Ni-foam plates. One of these was used almost immediately to fabricate the MEA, the other was dried until constant weight for the quantitative determination of the Pd loading that was, in all cases, ca. 1 mg cm⁻². The effective electrode area was 5 cm². The cathode and the membrane were prepared as the same manner shown for the passive fuel cell.

The fuel (water solution containing 10 wt% methanol, 5 wt% ethylene glycol, 10 wt% ethanol or 5 wt% glycerol in 2M KOH) was delivered to the anode at 4 mL min⁻¹ by a micropump, while the oxygen flow was regulated at 200 mL min⁻¹. The entry temperatures of the fuel and of the oxygen gas were regulated at the desired temperature. Under working conditions the effective cell temperature was determined by an appropriate sensor positioned inside the end plate at the cathode side. All electrochemical measurements were carried out using an 850e Integrated PEM Fuel Cell Station by Scribner-Associates (USA). The polarization tests were completed with the same conditions used for passive fuel cells.

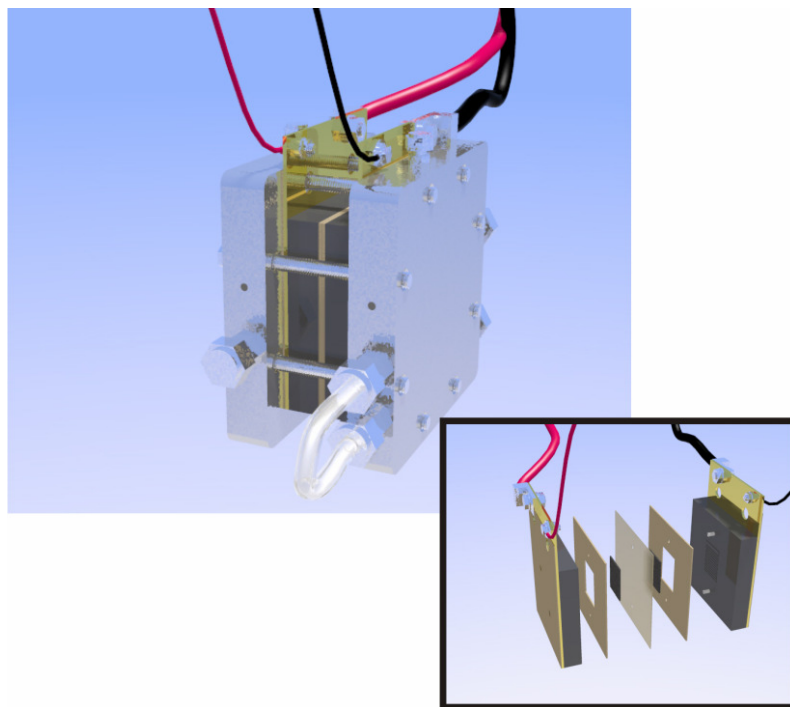


Figure 48. Lateral view of active fuel cell provided by Scribner-Associates. In the inset the MEA was opened and the same components shown for passive fuel cell were shown.

2.5.5 IC and NMR analysis

The analysis of the galvanostatic exhausts for passive fuel cells was performed by ionic chromatography and $^{13}\text{C}\{^1\text{H}\}$ NMR spectroscopy. For IC analysis was used a Metrohm 761 Compact instrument equipped with a Metrosep Organic Acids column 250 (6.1005.200) and a conductivity detector. The quantitative analysis of acetate ions were effectuated by an internal standard as sodium propionate. The chromatograms were registered after sample dilution of 0,1 factor with ultra-pure H_2O in CF_3COOH 0.1mmol/L eluent, 0.5 ml/min eluent flux, LiCl 51.5 mmol/L regenerating solution and for fixed 20 μL volume of the sample solution (loop length).

NMR analysis were effectuated by Bruker Avance DRX-400 MHz instrument. 45 μL of 1-4-dioxane internal reference was added to each galvanostatic exhaust as well as to ethanol or potassium acetate standard solutions at different concentration.

2.6 References

- ¹C.r.k. Rao, D.C. Trivedi *Coordination Chemistry Reviews*. **2005**, 249,613.
- ²a) R.Pattabiraman *Applied Catalysis A: General* **1997**, 153, 9. b) H.T. Zheng, Y. Li, S. Chen, P.K. Shen *Journal of Power Sources* **2006**, 163, 371. c) P.K. Shen, C. Xu *Electrochemistry Communications* **2006**, 8, 184.
- ³C. Coutanceau, L. Demarconnay, C. Lamy, J.-M. Léger *Journal of Power Sources* **2006**, 156, 14.
- ⁴C. Xu, Z. Tian, P. Shen, S.P. Jiang *Electrochimica Acta* **2008**, 53, 2610.
- ⁵C. Xu, P.K. Shen, Y. Liu *Journal of Power Sources* **2007**, 164, 527.
- ⁶M. Nie, H. Tang, Z. Wei, S.P. Jiang, P.K. Shen *Electrochemistry Communications*. **2007**, 9, 2375.
- ⁷C. Xu, L. Cheng, P. Shen, Y. Liu *Electrochemistry Communications* **2007**, 9, 997.
- ⁸D. Yuan, C. Xu, Y. Liu, S. Tan, X. Wang, Z. Wei, P.K. Shen *Electrochemistry Communications* **2007**, 9, 2473.
- ⁹F.P. Hu, Z. Wang, Y. Li, C. Li, X. Zhang, P.K. Shen *Journal of Power Sources* **2008**, 177, 61.
- ¹⁰Z. Wang, F. Hu, P.K. Shen *Electrochemistry Communications* **2006**, 8, 1764.
- ¹¹F. Hu, F. Ding, S. Song, P.K. Shen *Journal of Power Sources* **2006**, 163, 415.
- ¹²H.T. Zheng, Y. Li, S. Chen, P.K. Shen *Journal of Power Sources* **2006**, 163, 371.
- ¹³H. Wang, C. Xu, F. Cheng, S. Jiang *Electrochemistry Communications*. **2007**, 9, 1212.
- ¹⁴J. Zhang, M. Huang, H. Ma, F. Tian, W. Pan, S. Chen *Electrochemistry Communications* **2007**, 9, 1298.
- ¹⁵a) G.Q. Lu, A. Crown, A. Wieckowski *Journal of Physical Chemistry B* **1999**, 103, 9700. b) W.-r. Lee, M.G. Kim, J.-r. Choi, J.-L. Park, S.J. Ko, S.J. Oh, J. Cheon *Journal of American Chemical Society* **2005**, 127, 16090. c) E.V. Spinacé, A.O. Neto, M. Linardi *Journal of Power Sources* **2004**, 129, 121. d) R.S. Jayashree, J.S. Spendelow, J. Yeom, C. Rastogi, M.A. Shannon, P.J.A. Kenis *Electrochimica Acta* **2005**, 50, 4674. e) P. Waszczuk, T.M. Barnard, C. Rice, R.I. Masel, A. Wieckowski *Electrochemistry Communications* **2002**, 4, 599.

- ¹⁶a) A. Crown, C. Johnson, A. Wieckowski *Surface Science* **2002**, 506, L268. b) S.R. Brankovic, J.X. Wang, R.R. Adzic *Surface Science* **2001**, 474, L173. c) S.R. Brankovic, J.X. Wang, R.R. Adzic *Electrochemical and Solid-State Letters* **2001**, 4, A217. d) S.R. Brankovic, J. McBreen, R.R. Adzic *Journal of Electroanalytical Chemistry* **2001**, 503, 99. e) K. Sasaki, Y. Mo, J.X. Wang, M. Balasubramanian, F. Uribe, J. McBreen, R.R. Adzic *Electrochimica Acta* **2003**, 48, 3841.
- ¹⁷Z. Shi, S. Wu, J.A. Szpunar *Chemical Physics Letters* **2006**, 422, 147.
- ¹⁸T. Nakashima, S. Nohara, H. Hiroshi, C. Iwakura *Reserch on Chemical Intermediates* **2006**, 32, 561.
- ¹⁹C. Bock, C. Paquet, M. Couillard, G.A. Botton, B.R. MacDougall *Journal of American Chemical Society* **2004**, 126, 8028.
- ²⁰Z. Zhou, S. Wang, W. Zhou, G. Wang, L. Jiang, W. Li, S. Song, J. Liu, G. Sun, Q. Xin *Chemistry Communications* **2003**, 394.
- ²¹C. Luo, Y. Zhang, Y. Wang *Journal of Molecular Catalysis A: Chemical* **2005**, 229, 7.
- ²²K.Lohrgerg, P. Kohl *Electrochimica Acta* **1984**, 29, 1557.
- ²³G. Sheela, M. Pushpavanam, S. Pushpavanam *International Journal of Hydrogen Energy*, **2002**, 27, 627.
- ²⁴F.Vitse, M.Cooper, G.Botte *Journal of Power Sources* **2005**, 142, 18.
- ²⁵Botte, F.Vitse, M.Cooper, US0211569A1, **2005**.
- ²⁶J. Larminie, A. Dicks in *Fuel Cell Systems Explained*, Wiley, West Sussex, **2003**, 135.
- ²⁷a) S.-M. Park, N.C. Chen, N. Doddapaneni *Journal of Electrochemical Society* **1995**, 142, 40. b) A. Kowal, S.N. Port, R.J. Nichols *Catal.Today* **1997**, 38, 483. c) A. Kowal, C. Gutierrez *Journal of Electroanalytical Chemistry* **1995**, 395, 243.
- ²⁸M.A. Abdel Rahim, R.M.A. Hameed, M.W. Khalil *Journal of Power Sources* **2004**, 134, 160.
- ²⁹T. Kobayashi, J. Otomo, C.-j Wen, H. Takahashi *Journal of Power Sources* **2003**, 124, 34.
- ³⁰E. Sommerfeld, DE1254132, **1997**.
- ³¹K. Hata, *New Hydrogenation Catalysts*, Hastel, New York, **1971**.
- ³²B. Veeraraghavan, H.Kim, B.Popov *Electrochimica Acta* **2004**, 49, 3143.

- ³³Bambagioni, C. Bianchini, J. Filippi, W. Oberhauser, A. Marchionni, F. Vizza, R. Psaro, L. Sordelli, M.L. Foresti, M. Innocenti *ChemSusChem* **2009**, *2*, 99.
- ³⁴J. M. Basset, J.P. Candy, C. Copéret, F. Lefebvre, E.A. Quadrelli *Nanotechnology in Catalysis* **2004**, *2*, (Eds. : B. Zhou, S. Hermans, G. Somorjai), Springer Berlin, 447.
- ³⁵XRD data were extracted from PDF-2 containing ICDD (International Centre for Diffraction Data experimental powder data collection://www.icdd.com.
- ³⁶M. R. Tarasevich, Z. R. Karichev, V. A. Bogdanovskaya, E. N. Lubnin, A. V. Kapustin *Electrochemistry Communications* **2005**, *7*, 141.
- ³⁷ M. A. Abdel Rahim, R. M. A. Hameed, M. W. Khalil *Journal of Power Sources* **2004**,*135*, 42.
- ³⁸J. Bagchi, S. K. Bhattacharya *Journal of Power Sources* **2007**, *163*, 661.
- ³⁹ Z. B. Wang, G. P. Yin, J. Zhang, Y. C. Sun, P. F. Shi *Electrochimica Acta* **2006**, *51*, 5691.
- ⁴⁰S. Sen Gupta, J. Datta *Journal of Power Sources* **2004**, *145*, 124.
- ⁴¹F.-g. Luo, Q.-j. Chen, Z.-l. Yin *Transactions of Nonferrous Metals Society of China* **2007**, *17*, 654.
- ⁴²S. Deabate, F. Fourgeot, F. Henn *Electrochimica Acta* **2006**, *51*, 5430.
- ⁴³S. L. Medway, C. A. Lucas, A. Kowal, R. J. Nichols, D. Johnson *Journal of Electroanalytical Chemistry* **2006**, *587*, 172.
- ⁴⁴A. Roessler, D. Crettenand, O. Dossenbach, W. Marte, P. Rys *Electrochimica Acta* **2002**, *47*, 1989–1995.
- ⁴⁵A. Petrauskas, L. Grinceviciene, A. Ėėđūienė, R. Juđkėnas *Electrochimica Acta* **2005**, *50*, 1189–1196.
- ⁴⁶R. Wang, W. Ye, C. Ma, C. Wang *Mater Character* **2008**, *59*, 108.
- ⁴⁷M. Bouanani, F. Cherkaoui, R. Fratesi, R. Roventi, G. Barucca *Journal of Applied Electrochemistry* **1999**, *29*, 637.
- ⁴⁸C.-C. Hu, T.-C. Wen *Electrochimica Acta* **1996**, *41*, 1505.
- ⁴⁹C.-C. Hu, T.-C. Wen *Electrochimica Acta* **1995**, *40*, 495.
- ⁵⁰A.E.Bolzán, A.J.Arvia *Journal of Electroanalytical Chemistry* **1992**, *157*, 247.
- ⁵¹L. Wang, V. Bambagioni, M. Bevilacqua, C. Bianchini, J. Filippi, A. Lavacchi, A. Marchionni, F. Vizza, X. Fang, P. K. Shen *Journal of Power Sources* **2010**, *195*, 8036.

-
- ⁵²Z. X. Liang, T.S. Zhao, J.B. Xu, L.D. Zhu *Electrochimica Acta* **2009**, *54*, 2203.
- ⁵³M. Grden, M. Lukaszewski, G. Jerkiewicz, A. Czerwinski *Electrochimica Acta* **2008**, *53*, 7583.
- ⁵⁴G. Denualt, C. Milhano, D. Pletcher *Physical Chemistry Chemical Physics* **2005**, *7*, 3545.
- ⁵⁵V.M. Barragán, A. Heinzl *Journal of Power Sources* **2002**, *104*, 66.
- ⁵⁶K. Scott, E. Yu, G. Vlachogiannopoulos, M. Shivare, N. Duteanu *Journal of Power Sources* **2008**, *175*, 452.
- ⁵⁷J. Huang, Z. Liu, C. He, L.M. Gan *Journal of Physical Chemistry B* **2005**, *109*, 16644.
- ⁵⁸C. Lamy, A. Lima, V. LeRhun, F. Delime, C. Coutanceau, J.-M. Léger *Journal of Power Sources* **2002**, *105*, 283.
- ⁵⁹F. Vigier, S. Rousseau, C. Coutanceau, J.-M. Léger, C. Lamy *Topics in Catalysis* **2006**, *40*, 111.
- ⁶⁰H. Igarashi, T. Fujino, Y. Zhu, H. Uchida, M. Watanabe *Physical Chemistry Chemical Physics* **2001**, *3*, 306.
- ⁶¹V. Bambagioni, C. Bianchini, J. Filippi, A. Lavacchi, W. Oberhauser, A. Marchionni, S. Moneti, F. Vizza, R. Psaro, V. Dal Santo, A. Gallo, S. Recchia, L. Sordelli *Journal of Power Sources* in press **2010**.
- ⁶²C. Bianchini, V. Bambagioni, J. Filippi, A. Marchionni, F. Vizza, P. Bert, A. Tampucci *Electrochemistry Communications* **2009**, *11*, 1077.
- ⁶³S. Rousseau, C. Contenceau, C. Lamy, J. M. Léger *Journal of Power Sources* **2006**, *158*, 18.
- ⁶⁴C. Lamy, S. Rousseau, E.M. Belgsir, C. Contenceau, J.-M. Léger *Electrochimica Acta* **2004**, *49*, 3901.
- ⁶⁵T. Yajima, N. Wakabayashi, H. Uchida, M. Watanabe *Chemistry Communications* **2003**, 828.
- ⁶⁶F. Viguer, S. Rousseau, C. Contenceau, J.-M. Léger, C. Lamy *Topics in Catalysis* **2006**, *40*, 111.
- ⁶⁷X. Fang, L. Wang, P.K. Shen, G. Cui, C. Bianchini *Journal of Power Sources* **2009**, *195*, 1375.

- ⁶⁸J. Ma, A. Nurul, Y. Choudhury, Sahai *Renewable Sustainable Energy Review* **2010**, *14*, 183.
- ⁶⁹M. H. Martin, A. Lasia *Electrochimica Acta* **2008**, *53*, 6317.
- ⁷⁰V. Bambagioni, M. Bevilacqua, C. Bianchini, J. Filippi, A. Marchionni, F. Vizza, L.Q. Wang, P.K. Shen *Fuel Cells*, **2010**, *10*, 4, 582.
- ⁷¹K. Matsuoka, Y. Iriyama, T. Abe, M. Matsuoka, Z. Ogumi *Journal of Power Sources* **2005**, *150*, 27.
- ⁷²V. Livshits, M. Philosoph, E. Peled *Journal of Power Sources* **2008**, *178*, 687.
- ⁷³N. Ji, T. Zhang, M. Zheng, A. Wang, H. Wang, X. Wang, J. G. Chen *Angewandte Chemie International Edition in English* **2008**, *47*, 8510.
- ⁷⁴L. An, T.S. Zhao, S.Y. Shen, Q.X. Wu, R. Chen *International journal of hydrogen energy* **2010**, *35*, 4329.
- ⁷⁵V. Bambagioni, C. Bianchini, A. Marchionni, J. Filippi, F. Vizza, J. Teddy, P. Serp, M. Zhiani *Journal of Power Sources* **2009**, *190*, 241.
- ⁷⁶N. Dalbay, F. Kardigan *Journal of Electroanalytical Chemistry* **1990**, *296*, 559.
- ⁷⁷G. F. Cui, S. Q. Song, P. K. Shen, A. Kowal, C. Bianchini *Journal of Physical Chemistry* **2009**, *113*, 15639.
- ⁷⁸E. Morallón, A. Rodes, J. L. Vázquez, J. M. Pérez *Journal of Electroanalytical Chemistry* **1995**, *391*, 149.
- ⁷⁹F. Hahn, B. Beden, F. Kardigan, C. Lamy *Journal of Electroanalytical Chemistry* **1987**, *216*, 169.
- ⁸⁰P. A. Christensen, A. Hamnett *Journal of Electroanalytical Chemistry* **1989**, *260*, 347.
- ⁸¹L. Demarconnay, S. Brimaud, C. Coutanceau, J.-M. Léger *Journal of Electroanalytical Chemistry* **2007**, *601*, 169.
- ⁸²M. Simões, S. Baranton, C. Coutanceau *Applied Catalysis B: Environmental* **2010**, *93*, 354.
- ⁸³K. Scott, E. Yu, G. Vlachogiannopoulos, M. Shivare, N. Duteanu *Journal of Power Sources* **2008**, *175*, 452.
- ⁸⁴G.T. Burstein, C. J. Barnett, A.R. Kucernak, K.R. Williams *Catalysis Today* **1997**, *38*, 425.
- ⁸⁵A. Hamnet *Catalysis Today* **1997**, *38*, 445.

Chapter 3. Modified palladium electrocatalysts

3.1 Overview

This chapter reports the synthesis and performance of three new electrocatalysts based on palladium. The aim of this study was to prepare, if possible, Pd-based catalysts with improved performance with respect to the excellent materials Pd-(Ni-Zn)/C and Pd-(Ni-Zn-P)/C described in Chapter 2. In an attempt of achieving this goal, we have considered alternative supporting metal oxides for Pd, other metals to combine with Pd as well as a different morphology of the Pd particles.

All new catalysts have been characterized by TEM, XRPD, ICP-AES techniques and their electrochemical performance has been investigated both in half and monoplanar cells using ethanol as fuel.

3.2 Introduction

Several reports in the literature prove that metal oxides may have a promoting effect on palladium electrocatalysts in alkaline media, especially as regards the oxidation of alcohols¹. Among the metal oxides, rare earth materials such as ceria have been successfully tested by some authors¹. CeO₂ is actually one of the most interesting oxides, as its oxygen vacancy defects can be rapidly formed and eliminated, resulting in a high “Oxygen Storage Capacity” (OSC)^{2,3,4,57}[Eq(1)].



Generally, the oxidation of CeO_{2-x} occurs at room temperature, while the reduction of CeO₂ starts at 200°C. The OSC property declines for particles sintered at 850°C⁵⁷. For these reasons, ceria is used in the catalysts for the treatment of automotive exhausts. It is also employed for enhancing the performance of transition metal catalysts in a variety of other reaction including water gas-shift, steam reforming of oxygenates and PROX (PReferential OXYdation of CO)^{5,6,7,8,9}. Ceria is also a component of electrodes for solid oxide fuel cells^{10,57}. In addition, the reactive catalytic sites or vacancies in ceria can interact simultaneously with substrates and adsorbates, assisting their dissociation^{11,12}, and preventing metal nanoparticles sintering^{13,14,15}.

As for low temperature fuel cells, CeO₂ is used, in conjunction with carbon blacks, to support platinum in anode electrodes of DMFCs as well as to reduce the Ru content in Pt-based electrocatalysts¹⁶. Mixing Pt/C with CeO₂/C in anode electrocatalysts has led to the realization of DAFCs (methanol, ethanol, ethylene glycol and glycerol) with improved electrochemical performances in alkaline media^{17,18}.

Ceria can be prepared by solid to solid reactions (ceramic method and mechanical milling¹⁹), liquid to solid reactions and gas to solid reactions²⁰. Liquid to solid reactions are commonly used to prepare ceria-based electrocatalysts. The method consists in decomposing a cerium salt at high temperature for some hours²¹ or in irradiating a cerium salt with microwaves^{18,22}. Hydrothermal methods are also used to obtain dispersed suspensions of cerium oxide nanoparticles²³. The co-precipitation with

ammonium carbonate^{24,25} and the co-precipitation-gelation method^{26,27} with urea, which slowly decomposes to yield ammonia by heating at 343-353 K, or sol gel techniques²⁸ are often applied as well as surfactant-assisted methods^{29,30,31}. In emulsion and micro-emulsion methods, a surfactant³² as EHPNA (2-ethylhexylphosphonic acid mono-2-ethylhexyl ester) is used as an extractant³³.

CeO₂ synthesis can also be performed by electrochemical methods^{57,34}. In redox change methods (anode side), a cerium salt is oxidized at the electrode surface and its electro-generated species is hydrolyzed to oxide. At the cathode side, a base is generated at the electrode surface³⁵.

For the preparation of our Pd-based electrocatalysts, ceria has been obtained by an hydrothermal method, after precipitation of a cerium (III) precursor in alkaline condition on Vulcan XC-72 and a calcination at high temperature¹⁶. Then, a Pd precursor salt solution was reduced on the CeO₂/C material suspended in water.

As a second approach to design more efficient Pd-based catalysts, we have considered to combine Ni with chromium.

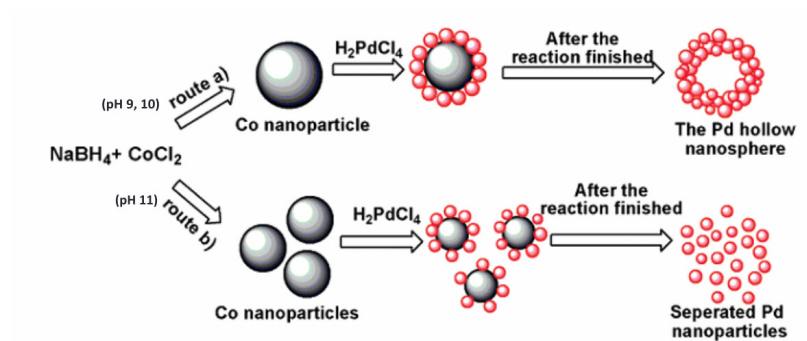
The use of Cr in APEFC (Alkaline Polymer Electrolyte Fuel Cells) has been reported in the literature³⁶: Lu et al. have realized anode electrocatalysts based on nickel and chromium (or chromium oxide) for hydrogen oxidation reaction. DFT calculations have shown that doping with a transition metal oxide such as chromium oxide a nickel surface, the Ni-O band structure might be energetically modulated. In particular, the presence of Cr seems to favour a weakening of the Ni-O bond and to promote Ni-H interactions³⁶. Cr oxide catalyzes a lot of oxidative dehydrogenation reactions^{37,38}, which is an interesting feature for alcohol electrooxidation in DAFCs.

Chromium has a potential standard reduction of -0.76V (Cr(III)/Cr(0)) and is therefore able to reduce Ni(II) to Ni(0) (-0.23V) on carbon and can be oxidized in alkaline media, creating defects for the spontaneous deposition of palladium (vide infra).

Finally, we have considered to change the morphology of the Pd nanoparticles through the realization of hollow nanospheres. In the literature there are many examples of metals prepared as hollow nanospheres for different applications (sensors, electrocatalysis ...). Pt hollow nanospheres have been synthesized on cobalt nanoparticles as template to give materials with improved activity towards methanol oxidation in DMFC³⁹. Traditional ways to synthesize hollow nanospheres involve the use of different sacrificial templates, including polystyrene spheres⁴⁰, silica spheres⁴¹, resin

spheres⁴², vesicles⁴³, liquid droplets⁴⁴, and microemulsion droplets⁴⁵. Also galvanic replacements can be used for getting hollow metal particles in water phase⁴⁶.

Our Pd hollow nanospheres (Scheme 1)^{47,48} supported on Vulcan XC-72 have been prepared through a redox reaction [Eq(2)] between Co(0) nanoparticles and Pd(II) ions in water solution (Co²⁺/Co(0) -0.277 V, Pd²⁺/Pd(0) 0.915 V vs SHE).



Scheme 1. Formation mechanisms of Pd hollow nanospheres and nanoparticles: a) Pd hollow nanospheres; b) separated Pd nanoparticles in adjusted conditions⁴⁷.

3.3 Results and discussion

3.3.1 Catalysts synthesis

As described in section 3.2 , the palladium ceria-carbon catalyst Pd-(CeO₂/C) was synthesized through the precipitation of cerium (III) hydroxide on a slurry of Vulcan XC-72 in water, followed by separation and drying overnight and then by calcination at 250°C for 2h. The CeO₂/C material obtained was suspended in water under a nitrogen atmosphere. Into this suspension was added dropwise a solution of PdCl₂. To this mixture was added ethanol, at a suitable temperature and pH, and then the resulting mixture was refluxed for 30'. The product obtained, after separation, is described here as Pd-(CeO₂/C).

For the preparation of the Pd-(Ni-Cr/C) electrocatalyst the following procedure was used: nickel(II) and chromium(III) salts were dispersed with Vulcan XC-72 in water under nitrogen: the resulting mixture was cooled down to 0°C and then reduced at 10°C with sodium borohydride in excess. The Ni-Cr/C material obtained was washed to remove the impurities (chloride and boron) ³⁶. Next, the spontaneous deposition of palladium was obtained by stirring an aqueous solution of K₂PdCl₄ in the presence of Ni-Cr/C under nitrogen atmosphere for several hours ⁴⁹. The Pd-(Ni-Cr/C) product was finally separated by filtration and dried.

Finally, the palladium hollow nanospheres, together with Pd nanoparticles, were prepared following the sacrificial cobalt(0) procedure ^{47,48}. A colloidal suspension of cobalt metal nanoparticles, obtained at suitable pH value, was mixed with Vulcan XC-72. The redox replacement of the cobalt metal nanoparticles by Pd was achieved by addition of a Pd(IV) salt. The final catalyst is denoted here as Pd/C hn_s (hollow nanospheres).

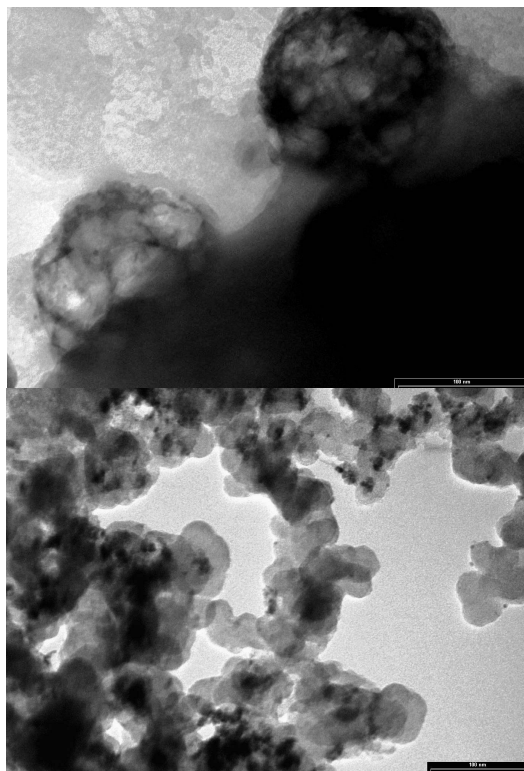


Figure 1. TEM images of Pd-(CeO₂/C) material (100 nm scale).

3.3.2 Catalysts Characterization

TEM images of the Pd-(CeO₂/C) catalyst are reported in Figure 1 (100 nm scale). Moving to different areas of the sample, one may notice different features. Indeed, in the upper inset the material shows spherical agglomerates, probably due to carbon, with little darker spots signaling the presence of heavy elements, as ceria, palladium or both of them. In the lower inset, the foamy background is likely due to carbon, while the darker spots are due to CeO₂, Pd or Pd-CeO₂. In an attempt to estimate the dimensions and composition of the darker spots, HRTEM study are in progress. In Figure 2 is shown the TEM image (100 nm scale) of Pd-(Ni-Cr/C) catalyst. A series of sample zones presents similar homogeneity. Looking at the image is quite easy to distinguish between the Vulcan and the heavy particles. On the other hand, in these experimental conditions and for the instrumental sensitivity limit it is not possible to distinguish between palladium and nickel-chromium support.

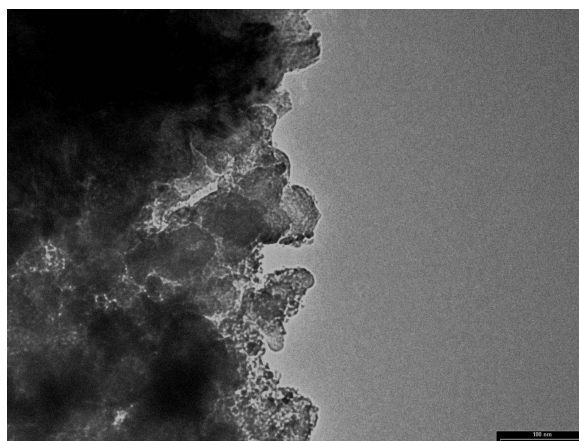


Figure 2. TEM image of Pd-(Ni-Cr/C) material (100 nm scale).

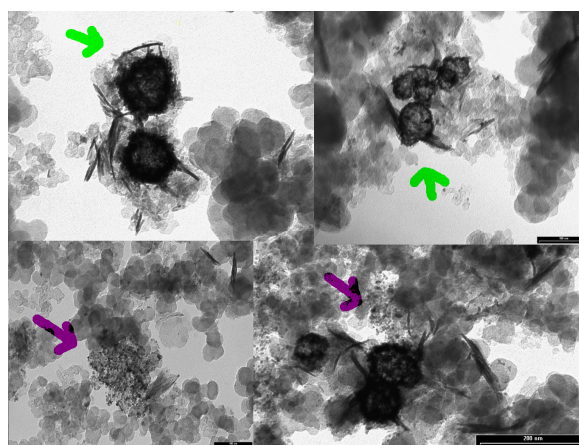


Figure 3. TEM images of Pd/C hn_s material (200 and 100 nm scale).

In Figure 3 are shown Pd/C hn_s images (200 nm scale). Green arrows indicate the hollow nanospheres smaller than 100 nm and close to each other. Violet arrows indicate the Pd nanoparticle regions.

The XRPD spectra of Pd-(CeO₂/C) and (CeO₂/C) are shown in Figure 4. All spectra reveal the presence of the typical diffraction peak of the carbon support at 25°, while the other one at 44° is masked by the CeO₂ (220) peak. Diffraction peaks at the Bragg angles of 40.10°, 46.40°, and 68.08° are typical of the (111), (200), (220) facets of fcc Pd⁵⁰ (-). The peaks at 27°, 33°, 47°, 56°, 76°, typical of the (111), (200), (220), (311), (331) facets of cubic fluorite type of CeO₂²² are present in both spectra (-)(-). According to the material stoichiometry, the palladium diffraction peaks are lower in intensity than the ceria peaks.

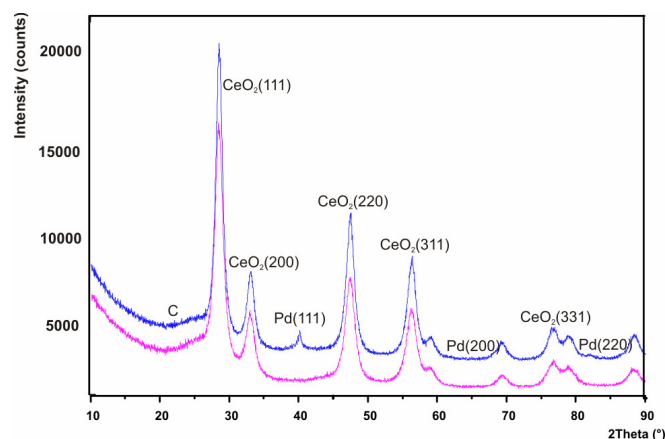


Figure 4. XRPD spectra of CeO_2/C support (—) and of Pd-(CeO_2/C) catalyst (—).

The XRPD spectra of Pd-(Ni-Cr/C) and (Ni-Cr/C) are illustrated in Figure 5. In the Ni-Cr/C spectrum (—) are clearly present the diffraction peaks at the Bragg angles of 25° for carbon and 44° for the Ni (111) facet. The diffraction peaks at 40.10° , 46.40° , and 68.08° are assigned to the (111), (200), (220) facets of fcc Pd crystals⁵⁰ in Pd-(Ni-Cr/C). Some diffraction peaks have not been clearly identified in the spectrum of Pd-(Ni-Cr)/C spectra. Tentatively, one may consider some crystal facets of chromium or nickel-chromium phases.

Figure 6 compares the XRPD spectrum of Pd/C h_n s to that of the Pd/C catalyst (see chapter 2, 2.3.1 section). The diffraction peaks assigned to the carbon back and the palladium (111), (200), (220) facets are the same reported above for Pd-(Ni-Cr)/C or Pd-(CeO_2/C). The spectrum (—) of Pd/C h_n s contains a peak at the Bragg angle of 20° and broad palladium peaks, which is consistent with the presence of two different kind of palladium materials (hollow nanospheres and nanoparticles) (see the TEM analysis, Figure 3).

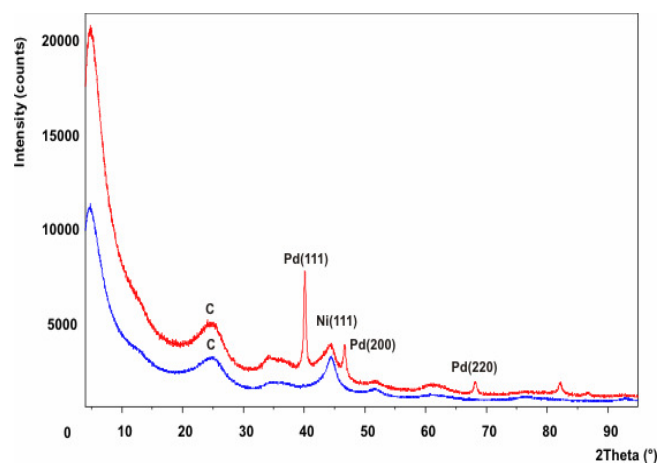


Figure 5. XRPD spectra of Ni-Cr/C support (–) and of Pd-(Ni-Cr/C) catalyst (–).

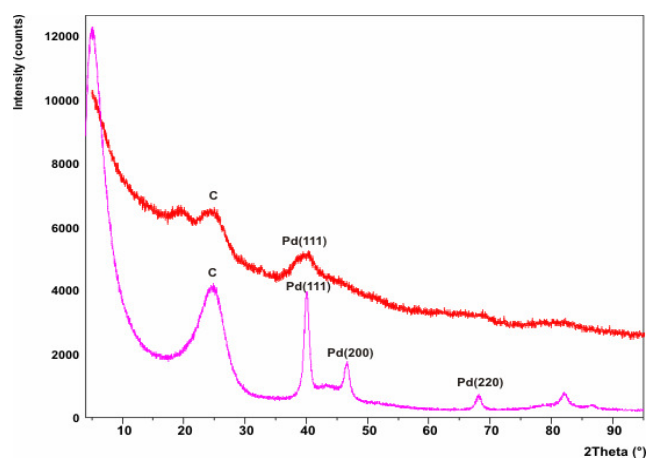


Figure 6. XRPD spectra of Pd/C (–) and of Pd/C hns catalysts (–).

3.3.3 Electrochemical characterization of the Pd-based catalysts in alkaline environment

The Pd-(CeO₂/C), Pd/C and Pd-(Ni-Cr/C) materials were electrochemically characterized in the same experimental conditions of the previously described Pd-based electrocatalysts (*vide infra*). The new catalysts were tested with ethanol as fuel.

A preliminary CV study of the CeO₂/C and Ni-Cr/C materials was carried out in 2M KOH and illustrated in Figure 7. In the upper inset of Figure 7, one may notice at 0.3 V (vs RHE) in the forward sweep a broad oxidation peak probably due to complex oxidation mechanisms of ceria, which contains Ce(III)/Ce(IV) ions in accordance with a fluorite type crystal structure. The corresponding reduction peak is at around 0.2 V. In the lower inset of Figure 7 is reported the CV of a Ni-Cr/C electrode in 2M KOH. In the forward potential scan Ni(OH)₂ is oxidized to NiO(OH) at 0.44 V (vs Ag/AgCl/KCl_{sat}) and in the backward scan the NiO(OH) species is reduced at 0.29 V^{51,52,53,54}. The reduction peak at -0.30 V is not straightforwardly assigned. The reduction of Ni(OH)₂ to Ni(0) usually occurs at -1 V in alkaline environment^{53,54}, but the catalyst nanostructure might contribute to a positive shift. As suggested by Henn and co-workers⁵², a metal species of the type NiO₂H_{2-x} with 0 < x < 0.3 can be reduced to an effective Ni(OH)₂ state at -0.30 V. The CV shows also other two oxidation peaks at -0.05 V and 0.25 V (vs Ag/AgCl/KCl_{sat}) and another reduction peak at around -0.9V (vs Ag/AgCl/KCl_{sat}). All of them are not clearly assigned, but one may suppose that the latter peaks are due to the presence of reduced or oxidized chromium species.

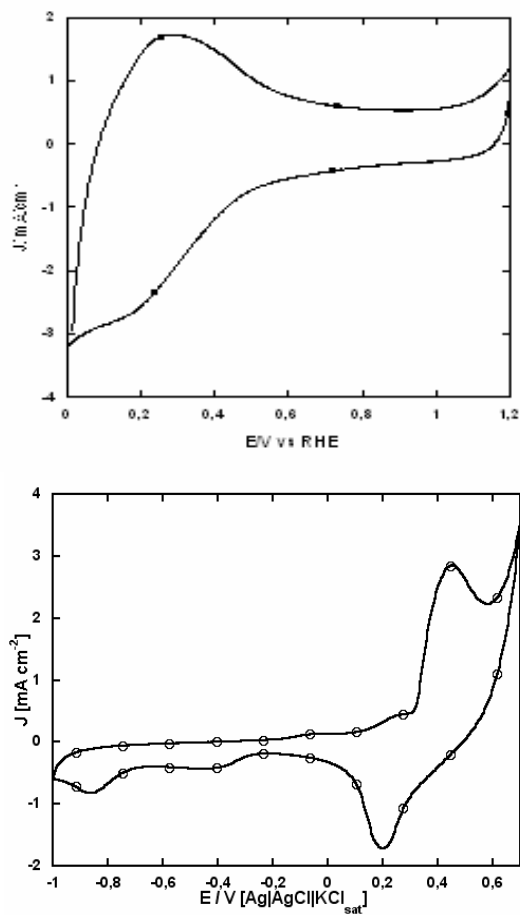


Figure 7. CVs of CeO₂/C (●) and Ni-Cr/C (○) materials in 2M KOH at 50 mV/s scan rate under nitrogen.

The CV on Ni-Cr/C electrode in 10 wt% EtOH 2M KOH solution at scan rate of 50 mV/s was reported in Figure 8. Ethanol is actually oxidized by NiO(OH) species, but the relative overpotential is not available in any DAFC. CeO₂/C material was also studied with a 10 wt% EtOH 2M KOH solution, giving the same CV reported in Figure 7 as it does not oxidize EtOH at any potential here investigated.

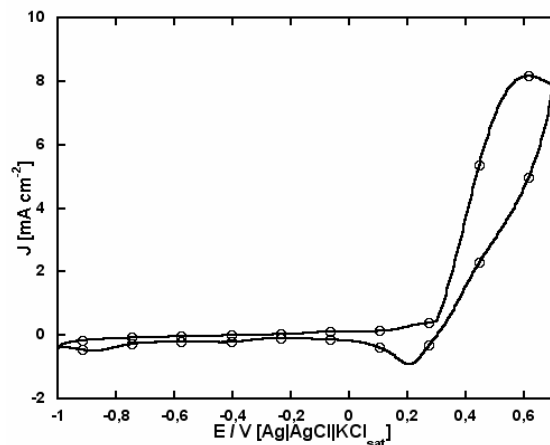


Figure 8. CV on Ni-Cr/C electrode in 10 wt% EtOH 2M KOH solution at scan rate of 50 mV/s under nitrogen.

Next, the Pd-(Ni-Cr/C) and Pd-(CeO₂/C) catalysts were characterized by cyclic voltammetry in 2M KOH (Figure 9). The only difference respect to the Ni-Cr/C CV in 2M KOH is the presence of the reduction peak of Pd(II) species, either PdO or Pd(OH)₂, with an onset at -0.20 V and a peak at -0.47 V vs Ag/AgCl/KCl_{sat} (the potential values are consistent with the nanostructured nature of the material). The CV of Pd-(Ni-Cr/C) confirms that Pd and Ni are not alloyed. On the other hand, in Figure 9 for Pd-(CeO₂/C) the reduction peak of Pd(II) species appears at around -0.25 V (vs Ag/AgCl/KCl_{sat}), while in the forward potential scan the adsorbed/absorbed hydrogen oxidation peak on palladium appears at around -0.85 V (vs Ag/AgCl/ KCl_{sat}).

In the range of the investigated potentials, the formation of Pd(IV) species can be ruled out safely^{55,56}.

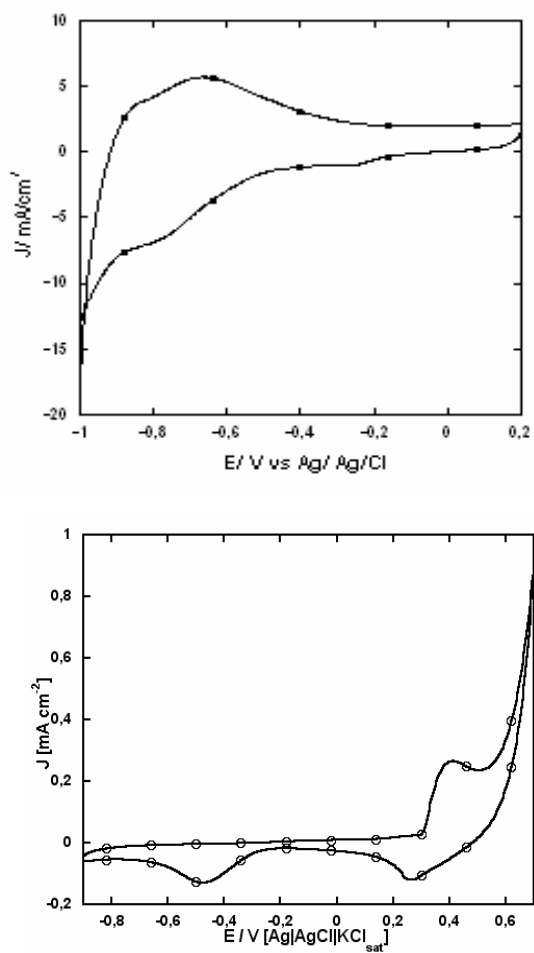


Figure 9. CVs on Pd-(CeO₂/C) (●) and Pd-(Ni-Cr/C) (○) electrodes in 10 wt% EtOH 2M KOH solution at scan rate of 50 mV/s under nitrogen.

3.3.4 Half cell studies of ethanol oxidation on the Pd-based catalysts in alkaline environment

The electrochemical activity of Pd-(Ni-Cr/C), Pd-(CeO₂/C) and Pd/C towards ethanol oxidation was investigated by CV in 2M KOH + 10 wt% ethanol at room temperature. For all catalysts, the Pd loading varied from 23 to 28 μg/cm². The scan rate was kept to 50 mV/s. The KOH concentration was purposefully kept to 2M value as well as the ethanol concentration was kept to 10 wt% value for comparative purposes with the electrochemical experiments done for Pd-(Ni-Zn)/C and Pd-(Ni-Zn-P)/C in Chapter 2. The CVs of the three catalysts investigated in the presence of 2M KOH solution containing 10 wt% ethanol are illustrated in Figure 10.

The Pd-(CeO₂/C) electrode oxidizes ethanol providing a current density of 85.50 mA/cm² at 0.81 V (vs RHE, or at around -0.2 V vs Ag/AgCl/KCl_{sat}) with an onset potential of 0.25 V (vs RHE, or -0.75 V vs Ag/AgCl/KCl_{sat}). Interestingly, the current density of ethanol oxidation on Pd-(CeO₂/C) electrode does not go to zero at 1.2 V (vs RHE), but it remains constantly at around 17 mA/cm². Apparently, some palladium sites are still active at 1.2 V (vs RHE). On the other hand, the oxidation peak of freshly chemisorbed ethanol gives in the backward potential scan the same current density as that obtained for the forward potential scan. Shen et al.¹ have studied a Pd-(CeO₂/C) catalyst, which is different from our material for the oxide preparation procedure (microwave irradiation) and for loading of palladium (ten times higher). Furthermore it was studied in different half-cell experimental conditions (1M EtOH, 1M KOH). Consequently, in Table 1 electrochemical data of the CV activity of own Pd-(CeO₂/C) with Shen's Pd-(CeO₂/C) are reported working in the same experimental conditions, for comparative purposes. Looking at the Table 1, one may notice that our catalyst shows a higher specific current density.

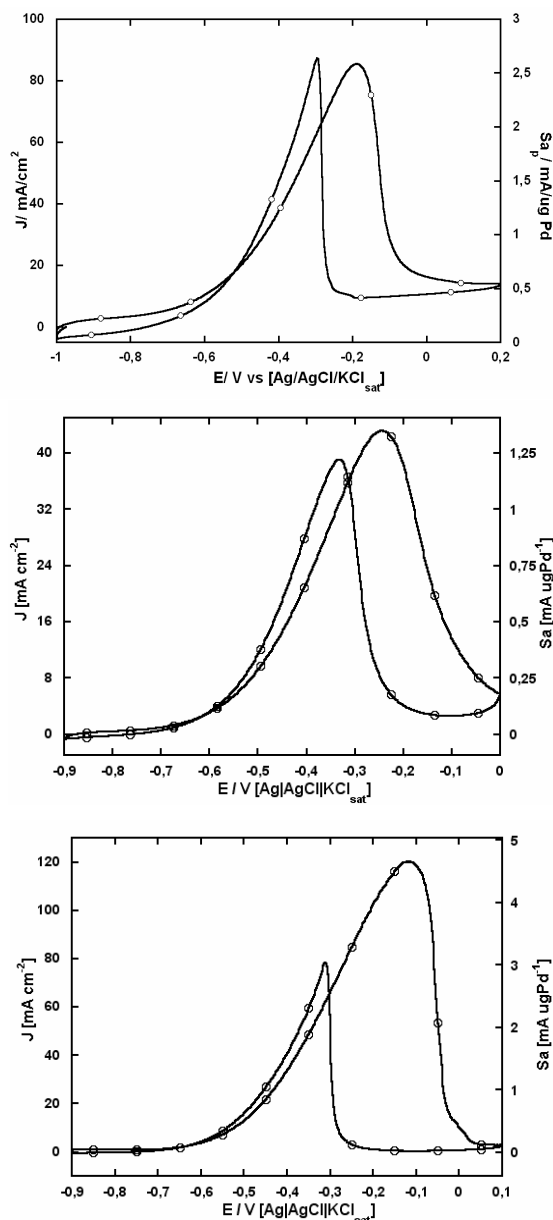


Figure 10. CVs of Pd-(CeO₂/C), Pd-(Ni-Cr/C), Pd/C h_ns electrodes in 10 wt % EtOH 2M KOH at scan rate of 50 mV/s under nitrogen, respectively.

In an attempt to explain the high Pd-(CeO₂/C) activity towards ethanol electrooxidation in CV study, Trovarelli has suggested that oxygen vacancies at the catalyst surface could allow superoxide and peroxide species acting as electron donors or acceptors at the metal-ceria interface⁵⁷. This phenomenon might explain the CV results obtained for our Pd-(CeO₂/C) catalyst in the presence of ethanol in terms of a high anode current density. Like for the Ni-Zn and Ni-Zn-P phases (Chapter 2), CeO₂/C phase may also play a sort of

co-catalytic effect. In particular, a bifunctional mechanism⁵⁸, where the ceria-carbon phase would increase the concentration of OH_{ads} species on the catalysts surface, promoting the acyl- OH_{ads} coupling⁵⁹ cannot be excluded.

Catalyst	J_p [mA/cm ²]	S_{ap} [mA $\mu\text{g}(\text{Pd})^{-1}$]	V_{onset} [V] vs RHE	V_p [V] vs RHE
Shen's Pd-(CeO ₂ /C)	40.00	0.13	0.42	0.80
Pd-(CeO ₂ /C)	32.50	1.51	0.38	0.81

Experimental conditions:

50mV/s; 303K; 1M EtOH + 1M KOH; Pd-(CeO₂/C): Pd loading of 23 $\mu\text{g}/\text{cm}^2$;

Shen's Pd-(CeO₂/C): Pd loading of 300 $\mu\text{g}/\text{cm}^2$.

Table 1. Electrochemical data from CV experiments on Pd-(CeO₂/C) and Shen's Pd-(CeO₂/C)¹ electrodes in 1M EtOH +1M KOH.

In Figure 10 the Pd-(Ni-Cr/C) CV shows a specific current density of 1.27 mA/ $\mu\text{g}(\text{Pd})^{-1}$ at -0.23 V (vs Ag/AgCl/KCl_{sat}) with an oxidation potential onset around -0.78V (vs Ag/AgCl/KCl_{sat}). As shown for nickel phase materials (Chapter 2), the ethanol oxidation is surely due to the palladium active sites, while the nickel phase might have a co-catalytic effect on the alcohol oxidation. The potential onset anticipation presented here is a direct consequence of a co-catalytic effect of nickel-chromium phase on the ethanol oxidation.

Finally, the CV of the Pd/C hns electrode in ethanol gives a specific current density of 5.2 mA/ $\mu\text{g}(\text{Pd})^{-1}$ at around -0.1 V (vs Ag/AgCl/KCl_{sat}) with an onset potential of -0.6 V (vs Ag/AgCl/KCl_{sat}). Apparently, this catalyst gives an excellent activity towards the ethanol oxidation, but the oxidation peak is shifted to anode potential and is also very broad. This might be due to the two different kinds of palladium species that characterize the material (see the TEM images in Figure 3). Indeed, it is not ruled out that Pd nanoparticles and Pd hollow nanospheres oxidize ethanol at hardly different potentials, giving a very broad oxidation peak.

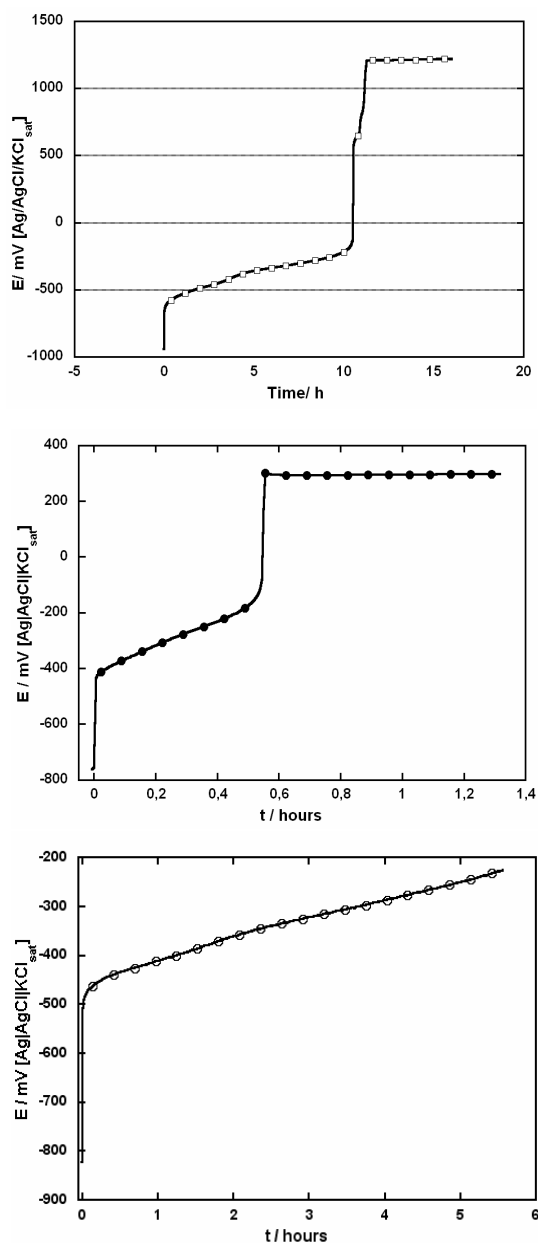


Figure 11. Chrono-curves at 3 mA/cm^2 for Pd-(CeO₂/C) (□), Pd-(Ni-Cr/C) (●) and Pd/C hn_s (○) electrodes in 10 wt% EtOH 2M KOH under nitrogen.

Concluding the Pd-(CeO₂/C) catalyst shows the best overall performance in CV measurement with 10 wt% EtOH 2M KOH solution.

The Pd-(Ni-Cr/C), Pd-(CeO₂/C) and Pd/C hn_s catalysts were also tested in terms of stability by means of chronopotentiometric measurements. The potential (V) vs time (h) curves were registered at 3 mA/cm^2 (Figure 11). In nice accord with the CV results, the

Pd-(CeO₂/C) electrode remains stable up to 10 hours. On the contrary, the Pd/C hns catalyst was stable for 5,5 h, while the Pd-(Ni-Cr/C) electrode loses activity just after 30'.

3.3.5 Direct Ethanol Fuel Cells (DEFCs) with Pd-based anode electrocatalysts

The anode electrocatalysts were tested in passive monoplanar fuel cell (air/oxygen breathing) (see cell hardware in Figure 47 of 2.5 experimental section of Chapter 2). To this purpose, membrane-electrode assemblies (MEAs) were realized in conjunction with proprietary Fe-Co/C cathodes⁶⁰ and an anion-exchange membrane from Tokuyama (A-006). The MEA was fabricated by mechanically pressing anode, membrane and cathode. The anode electrocatalysts were dispersed in distilled water and then spread onto a 5 cm² Ni-foam plate (Pd loading of 1 mg/cm²). The cathode ink was sprayed or spread onto carbon cloth (Fe:Co (1:1) loading 2-2.5 mg/cm²). The membrane was rinsed in a 1M KOH solution for a few minutes and gently dried before assembling the MEA. After filling the anode compartment with 10 mL of 10 wt% EtOH 2M KOH, the DEFC was conditioned for 1h at room temperature at the open circuit voltage (OCV) air breathing. After this time, the cell polarization and power density curves were registered at room temperature (Figure 12).

Accordingly to the CV results, the DEFC containing Pd-(CeO₂/C) as anode exhibits the best power performance for ethanol oxidation with a power density of 64 mW/cm² at 225 mA/cm² as well as an exceptionally high OCV voltage value (0.90 V). In the presence of Pd-(Ni-Cr/C) anode, the DEFC gives 33 mW/cm² at 160 mA/cm², while with Pd/C hns as anode 15 mW/cm² at 62 mA/cm².

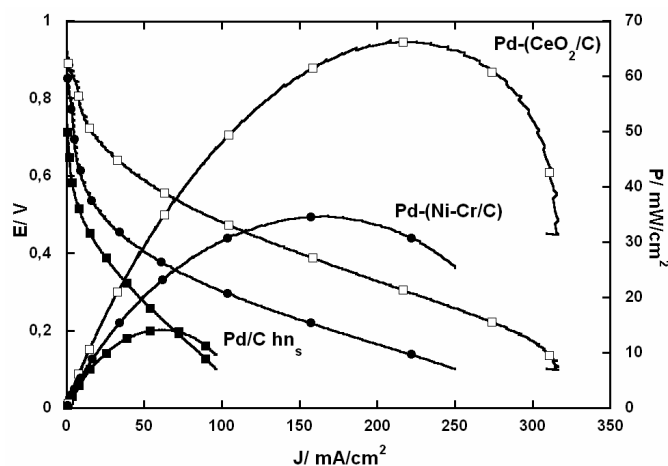
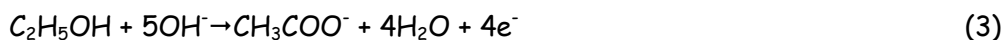


Figure 12. Polarization and power density curves for air breathing DEFCs at room temperature, registered after 1h of conditioning time at the OCV with 10 mL of a 10 wt% EtOH 2M KOH solution. The MEAs: Pd-(CeO₂/C), Pd-(Ni-Cr/C), Pd/C hn_s anodes (Pd loading 1 mg/cm²), Tokuyama A006 membrane, cathode FeCo/C (1:1) (Fe, Co loading 2-2.5 mg/cm²).

A series of galvanostatic experiments were carried out at room temperature in the same passive DEFCs used for the previous experiments, but flowing oxygen at the cathode side just to avoid any CO₂ interference on the oxidation products (vide infra). After filling the anode compartment with 21.70 mmol of EtOH 2M KOH solution and conditioning the cell for 1h, a current of 102 mA was allowed to pass in the cell until 0V potential.

The DEFC assembled with the Pd-(CeO₂/C) anode lasts for 8.5 h (Figure 13) converting 8 mmol of acetate (isolable as potassium acetate), which correspond to 37% ethanol conversion with no trace of carbonate (168 ppm) or acetaldehyde (206 ppm) detected at any stage of the galvanostatic experiment, as determined by NMR ¹³C{¹H} and IC analysis. On the other hand, fuel loss by cross-over or direct evaporation is estimated around 18-20% of starting ethanol by NMR technique. Looking at the Figure 13, the DEFCs containing Pd-(Ni-Cr/C) and Pd/C hn_s anodes last for about 9.5 h and 10 h, converting 41% and 43% of ethanol in acetate, respectively. Both of these DEFCs lose around 10-12% of starting ethanol as shown in NMR analysis. In Figure 13, one may notice that the Pd-(CeO₂/C) DEFC gives the higher energetic efficiency all over the time. Accordingly to exhaust NMR and IC analysis, the anode reaction can be summarized as in [Eq (3)] and it establishes that in the present experimental conditions our Pd-based catalysts are selective for the conversion of ethanol into acetate with no appreciable formation of C-C bond cleavage products such as carbonate.



Finally, the anode compartment of the Pd-(CeO₂/C) DEFC was freshly recharged with further 10 mL of fuel solution. The cell is fully regenerated with the same OCV voltage (about 0.90 V) and gives similar galvanostatic duration and conversion performance. The voltage decay shown in Figure 13 has been attributed to other factors than catalyst poisoning or membrane carbonation, i.e. the increasing viscosity of the solution, the pH decrease due to OH⁻ consumption, and, most importantly, the competitive substrate adsorption /product desorption and the formation of PdO layer.

Comparing with Pd-(Ni-Zn)/C and Pd-(Ni-Zn-P)/C galvanostatic curves (2.3.5 section of Chapter 2), the present anode materials do not improve the DEFC performance in terms of voltage decay and ethanol conversion.

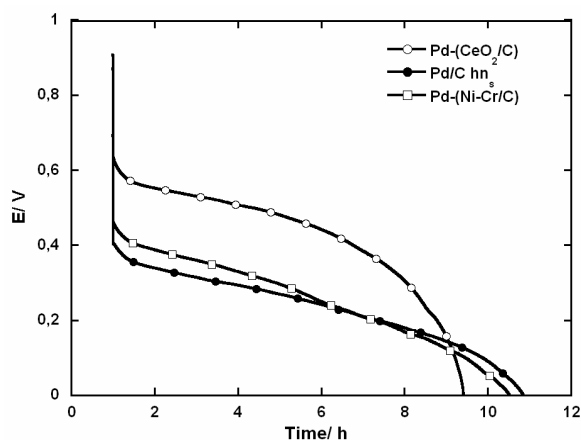


Figure 13. Galvanostatic curves for passive DEFCs oxygen breathing at room temperature, registered after 1h of conditioning time with 21.70 mmol of EtOH 2M KOH solution at 0V 102 mA. The MEAs: Pd-(CeO₂/C), Pd-(Ni-Cr/C), Pd/C hn₃ anodes (Pd loading 1 mg/cm²), Tokuyama A006 membrane, cathode FeCo/C (1:1) (Fe, Co loading 2-2.5 mg/cm²).

3.4 Conclusions

In this Chapter we have presented three different Pd-based electrocatalysts using CeO₂ as promoting metal oxide for Pd, chromium as promoting metal and a different morphology of the Pd particles: the resulting catalyst are denoted as Pd-(CeO₂/C), Pd-(Ni-Cr)/C and Pd/C hns.

All new materials have been satisfactorily characterized and their electrochemical activity have been studied for ethanol oxidation in half-cells by CV and monoplanar passive DEFCs.

The Pd-(CeO₂/C), Pd-(Ni-Cr)/C and Pd/C hns anode materials exhibit a lower oxidation ability to oxidize ethanol in half cells than Pd-(Ni-Zn)/C and Pd-(Ni-Zn-P)/C (2.3.4 section of Chapter 2). In contrast, the Pd-(CeO₂/C) electrode has been found to maintain an elevated current even at potentials as high as 1.2 V (vs RHE) and also exhibits a negatively shifted onset potential for ethanol oxidation (-0.75 V vs Ag/AgCl/KCl_{sat}) as compared to Pd-(Ni-Cr)/C, Pd/C hns, Pd-(Ni-Zn)/C, Pd-(Ni-Zn-P)/C and Pd/C (2.3.4 section of Chapter 2). Moreover, the Pd-(CeO₂/C) anode releases an excellent power density (64 mW/cm²) in a passive monoplanar DEFC (10 wt% EtOH 2M KOH), higher than those provided by the Pd-(Ni-Zn)/C, Pd-(Ni-Zn-P)/C electrocatalysts in the same experimental conditions.

3.5 Experimental section

3.5.1 Catalysts Synthesis

All the synthesis were carried out in nitrogen atmosphere, except were specified. Water solution were freshly prepared with double distilled water. Vulcan XC-72 were supplied by Cabot Corp.(USA), precious metal salts were purchased by Aldrich and used without any further purification. Ultrasound treatments were performed by SBL ultrasound bath or Bandelin Sonoplus sonde. Every transfer was done in bry-box.

Pd-(CeO₂/C): After adding Ce(NO₃)₃·6H₂O (9.94g, 22.75 mmol) at a Vulcan XC-72 (4 g) suspension in H₂O (250 mL), the suspension was maintained ten minutes in ultrasound bath and other 2h 15' under mechanical stirring in not controlled atmosphere. 100 mL of 1.5 M KOH solution were put into the reaction until pH 12 and the reaction was stirred for one hour. The solid was washed several times with water until pH 7 and filtered. The product was then dried over night at 60°C until constant weight.

After physical milling the powder was calcinated at 250°C for 2h. 4.85 g obtained were suspended in H₂O (500 mL) and ultrasound treated for ten minutes. Under mechanical stirring and nitrogen atmosphere 100 mL of K₂PdCl₄ solution (0.7g, 2.93 mmol) were added slowly, then 14.5 mL of KOH 1M solution and finally 100 mL of EtOH. The suspension was heated until 90°C to reflux for 30'.

The suspension was let cooling down and then washed several times with water until pH 7, filtered and dried at 40°C until constant weight under vacuum. (ICP-AES Pd 6 wt%).

Pd-(Ni-Cr/C): Vulcan XC-72 (3.11 g) in 100 mL of ethanol was ultrasound treated for 20' and then it was mechanically stirred (250 rpm). Drop to drop (in 10') 200 mL of NiCl₂ (2.82 g, 21.76 mmol) and CrCl₃·6H₂O (156 mg, 0.59 mmol) solution was added to Vulcan slurry. The resulting suspension was ultrasound treated for 30' and then cooled down between 0-3°C. When the temperature grew up to 10°C, 40 mL of 2.5 g NaBH₄ water solution was carefully added at the suspension in 30'. The product was washed several times (3x1L H₂O) until Cl⁻ elimination and dried at 100°C for 4h. The material was heated in a quartz oven at 120°C for 30' and then at 350°C for 30' under nitrogen flux to

fully drive out boron from the catalyst. After cooling to room temperature, the support was dispersed in 200 mL of water and ultrasound treated for 15'. Then 250 mL of water solution of K_2PdCl_4 was added drop to drop and let deposited spontaneously all over the night under mechanical stirring (200 rpm). The finished material was washed several times with water until pH 7, filtered and dried at 40°C until constant weight under vacuum. (ICP-AES Pd 5.5 wt%).

Pd/C hn_2 : Vulcan XC-72 (1.09 g) was mixed in water (100 mL) and treated in ultrasound bath for 10'. 50 mL of water solution of citric acid (337.80 mg, 1.76 mmol) was first added to Vulcan suspension and then 50 mL 5 wt% NaOH solution, 50 mL of $CoCl_2$ (228.80 mg, 1.76 mmol) water solution and 50 mL of $NaBH_4$ (102.2 mg, 2.70 mmol) water solution previously degassed for 30'. The reaction was stirred for 1h at 40°C, bubbling nitrogen inside the solution. After cooling, 100 mL of $PdCl_2/37$ wt% HCl (115.6 mg, 0.65 mmol/ 1.5 mL) solution was added drop to drop and the reaction got along for 24 h. The product was washed several times with water until pH 7, filtered and dried at 40°C until constant weight under vacuum. (ICP-AES Pd 5.3 wt%).

3.5.2 Physical material characterization

TEM (Transmission Electron Microscopy) images were registered by a JEOL JEM 1011 microscope at 100 KV. 40 mg of a powder sample was suspended in 1 mL of water in a vial and ultrasound treated for 10'. A drop of the latter suspension was deposited onto a copper grid with a FORMVAR (polyvinyl formal) supported film.

The metal content in all catalysts was determined by inductively coupled plasma atomic emission spectroscopy (ICP-AES) with an Intrepid Iris instrument (Thermo Elemental). Each sample (20–50 mg) was treated in a microwave-heated digestion bomb (Milestone, MLS-200) with concentrated HNO_3 (1.5 mL), 98% H_2SO_4 (2 mL), and a pellet (0.4 g) of a digestion aid reagent (0.1% Se in K_2SO_4). The solutions were analyzed after the carbon residue was filtered off.

X-ray powder diffraction spectra (XRPD) were acquired at room temperature with a Bruker D8-Advance diffractometer, employing CuK α radiation ($\lambda=1.5418 \text{ \AA}$) in the range between 2.5 and 80° and using an acquisition step of 0.030°/s.

3.5.3 Electrochemical studies

The cell used for the cyclic voltammetry and chronopotentiometric experiments was a Kelel cylinder with an inner diameter of 7.2 mm and an outer diameter of 50 mm (see Figure 46 in 2.5.3 section of Chapter 2). The inner volume of the cell was about 1 mL. The working electrode, Glassy Carbon (Sigradur G; 0.867 cm²), covered by the catalyst, was put in a special cavity at the top end of the cylinder, and the counter electrode was a gold disc placed at the bottom end. The solution contained in a Pyrex flask was previously bubbled by N₂ and then flushed into the cell at a pressure as low as 0.3 bar N₂. This pressure was applied until the cell was completely filled and then stopped. The inlet and the outlet for the solutions were placed on the side walls of the cell. The inlet was inclined towards the counter electrode so as to allow the solution to gradually fill in slowly getting wet the working electrode without disturbing the catalyst layer. The electrical contact with the working electrode was secured with two stainless steel screw terminals. Leakage was avoided by pressing both the working and the counter electrode against a suitable silicone O ring. The reference electrode, a miniaturized Ag/AgCl/KCl_{sat} electrode, was placed on the outlet tubing. This location allows contamination to be avoided and at the same time is sufficiently close to the working electrode to reduce the uncompensated resistance. All CV studies were carried out using a Parstat 2277 potentiostat-galvanostat (Princeton Applied Research).

Ink preparation. A portion of 45 mg of Pd-(Ni-Cr/C) and Pd/C h_ns catalysts was introduced inside a 5 mL high-density polyethylene container together with water (1.01 g), KOH (99.99%, Sigma–Aldrich, 65 mg), absolute ethanol (99.8 %, Fluka; 0.50 g), and 5% Nafion ion-exchange resin (Sigma–Aldrich; 0.37 g) in ethanol solution. The resulting suspension was sonicated for 30 min with a Branson 3200 bath. Each suspension was freshly prepared just before carrying out the experiment scheduled. The metal loading

on each electrode was determined by weighting the amount of ink (17-20 mg) deposited on the glassy carbon disk. All the solution analyzed were previously purged from air for ten minutes and kept under inert atmosphere during the measurements.

Ink preparation of Pd-(CeO₂/C) and CeO₂/C materials. A portion of 45 mg of each material was introduced inside a 5 mL high-density polyethylene container together with water (1.2 g) and 2-propanol alcohol (0.70 mg). The resulting suspension was sonicated for 30 min with a Branson 3200 bath. After the deposition and drying of about 20 mg of ink on the working electrode surface, 2.5 μ L of 2 wt% Tokuyama ionomer solution in alcohols was put on and dried. Each suspension was freshly prepared just before carrying out the experiment scheduled. The metal loading on each electrode was determined by weighting the amount of ink deposited on the glassy carbon disk. All the solution analyzed were previously purged from air for ten minutes and kept under inert atmosphere during the measurements.

3.5.4 Fuel cell assembly

The home-made, air/oxygen-breathing DAFC used to evaluate the electrochemical performance of the Pd-(CeO₂/C), Pd-(Ni-Cr/C) and Pd/C anodes, in conjunction with the Tokuyama A-006 anion exchange membrane (Tokuyama Corporation) and Fe-Co/C cathodes⁶⁰, was shown in Figure 47 of the 2.5.4 section of the Chapter 2. The device was realized with plexiglas and the electricity collectors were plated with gold. The volume of the anode compartment was ca. 20–25 mL for an actual fuel solution of 10–13 mL. The anode was realized with a 5.13 cm² nickel foam plate onto which was deposited the appropriate amount of a dense catalytic ink (generally in order to obtain 1 mg cm⁻² of palladium loading). This was prepared by dispersing the solid catalyst in the minimum amount of water with no need of a binder. The cathode was prepared using a suspension of ketjen black (C) with iron and cobalt phthalocyanines (MPc) 1:1 stoichiometric mixture, followed by heat treatment at 800 °C under inert atmosphere, brushed on carbon cloth, prepared in our lab⁶⁰. The A006 membrane used was purchased from Tokuyama Corporation and used after brief basic treatment (1M KOH

solution) and gently drying. The membrane-electrode assembly (MEA) was obtained by mechanically pressing anode, cathode and membrane, while silicone–rubber gaskets were employed to seal the system. For galvanostatic experiments, in order to avoid any possible contamination of the alkaline anode solution by carbonate ions formed upon reaction with atmospheric CO₂, the DAFCs were positioned inside a home-made plexiglass dry-box. Here the anode compartment was maintained all the way under a static nitrogen atmosphere, while the cathode was exposed to an oxygen constant flow of 10 mL/min. For polarization and power density experiments after assembling the MEAs, the DAFCs were tested in air-breathing mode. All the cell performances were evaluated with an ARBIN BT-2000 5A-4 channels instrument.

Polarization curves were registered at 5 mV/s, after 1h of conditioning time. Galvanostatic experiments were registered after 1h of conditioning time at 102 mA until 0V.

3.5.5 IC and NMR analysis

The analysis of the galvanostatic exhausts for passive fuel cells was performed by ionic chromatography and ¹³C{¹H} NMR spectroscopy. For IC analysis was used a Metrohm 761 Compact instrument equipped with a Metrosep Organic Acids column 250 (6.1005.200) and a conductivity detector. The quantitative analysis of acetate ions were effectuated by an internal standard as sodium propionate. The chromatograms were registered after sample dilution of 0,1 factor with ultra-pure H₂O in CF₃COOH 0.1mmol/L eluent, 0.5 ml/min eluent flux, LiCl 51.5 mmol/L regenerating solution and for fixed 20 μL volume of the sample solution (loop length).

NMR analysis were effectuated by Bruker Avance DRX-400 MHz instrument. 45 μL of 1-4-dioxane internal reference was added to each galvanostatic exhaust as well as to ethanol or potassium acetate standard solutions at different concentration.

3.6 References

- ¹P.K. Shen, C. Xu *Electrochemistry Communications* **2006**, *8*, 184.
- ²C.T. Campbell, C.H.F. Peden *Science* **2009**, *309*, 10.1126/science.1116710.
- ³H.X. Mai, L.-D. Sun, Ya-W. Zhang, R. Si, W. Feng, H.-P. Zhang, H.-C. Liu, C.-H. Yan *Journal of Physical Chemistry B* **2005**, *109*, 24380.
- ⁴H.C. Yao, Y.F. Yu Yao *Journal of Catalysis* **1984**, *86*, 254.
- ⁵R. Farrauto et al. *Annual Reviews of Materials Research*, **2003**, *33*, 1.
- ⁶C. Wheeler et al. *Journal of Catalysis* **2004**, *223*, 191.
- ⁷Q. Fu, H. Saltsburg, M. Flytzani-Stephanopoulos *Science* **2003**, *301*, 935.
- ⁸T. Bunluesin, R. J. Gorte, G.W. Graham *Applied Catalysis B: Environment* **1998**, *15*, 107.
- ⁹G.A. Deluga, J.R. Salge, L.D. Schmidt, X.E. Verykios *Science* **2004**, *303*, 993.
- ¹⁰H. Yokokawa, T. Horita, N. Sakai, K. Yamaji, M.E. Brito, Y.-P. Xiong, H. Kishimoto *Solid State Ionics* **2004**, *174*, 205.
- ¹¹G. Lu, A. Linsebigler, J. T. Yates, Jr. *Journal of Physical Chemistry* **1995**, *99*, 7626.
- ¹²M.A. Henderson, W.S. Epling, C.L. Perkins, C.H.F. Peden *Journal of Physical Chemistry B* **1999**, *103*, 5328.
- ¹³Y.D. Kim, J. Stultz, T. Wei, D.W. Goodman *Journal of Physical Chemistry B* **2002**, *106*, num. 27, 6827.
- ¹⁴Y.D. Kim, J. Stultz, T. Wei, D.W. Goodman *Physical Reviews B* **2001**, *64*, 075417.
- ¹⁵S. Damyanova, B. Pawelec, K. Arishtirova, M.V. Martinez Huerta, J.L.G. Fierro *Applied Catalysis A: General* **2008**, *337*, 86.
- ¹⁶M.A. Scibioh, S.-K. Kim, E.A. Cho, T.-H. Lim, S.-A. Hong, H.Y. Ha *Applied Catalysis B: Environmental* **2008**, *84*, 773.
- ¹⁷C.W. Xu, P.K. Shen *Chemistry Communications* **2004**, 2238.
- ¹⁸C.W. Xu, P.K. Shen *Journal of Power Sources* **2005**, *142*, 27.
- ¹⁹Y.X. Li, X.Z. Zhou, Y. Wang, X.Z. You *Materials Letters* **2003**, *58*, 245.
- ²⁰A. Tschöpe, J.Y. Ying, H.L. Tuller *Sensors and Actuators B* **1996**, *31*, 111.
- ²¹J.Z. Shyu, W.H. Weber, H.S. Gandhi *Journal of Physical Chemistry* **1988**, *92*, 4964.
- ²²C. Xu, P.K. Shen, Y. Liu *Journal of Power Sources* **2007**, *164*, 527.
- ²³S.L. Swartz, M.M. Seabaugh, C.T. Holt, W.J. Dawson *Fuel Cell Bulletins* **2001**, *30*, 7.

- ²⁴Lj. Kundakovic, Ph.D. Thesis, Department of Chemical Engineering, Tufts University, **1998**.
- ²⁵Lj. Kundakovic, M. Flytzani-Stephanopoulos *Journal of Catalysis* **1998**, *179*, 203.
- ²⁶Y. Amenomiya, A. Emesh, K. Oliver, G. Pleizer, in: M. Philips, M. Ternan (Eds.), *Proceedings of the Ninth International Congress Catal.*, Chemical Institute of Canada, Ottawa, Canada, **1988**, 634.
- ²⁷Y. Li, Q. Fu, M. Flytzani-Stephanopoulos *Applied Catalysis B: Environmental* **2000**, *27*, 179.
- ²⁸F. Imoto, T. Nanataki, S. Kaneko *Ceramic Transactions* **1988**, *1*, 204.
- ²⁹D. Terribile, A. Trovarelli, C. de Leitenburg, G. Dolcetti *Chemistry of Materials* **1997**, *9*, 2676.
- ³⁰D. Terribile, A. Trovarelli, J. Llorca, C. de Leitenburg, G. Dolcetti *Catalysis Today* **1998**, *43*, 79.
- ³¹H. Xu, X. Hou *International Journal of Hydrogen Energy* **2007**, *32*, 4397.
- ³²A. Bumajda, J. Eastoe, A. Mathew *Advances in Colloid and Interface Science* **2009**, *147-148*, 56.
- ³³T. Hirai, N. Okamoto, I. Komasa *Langmuir* **1998**, *14*, 6648.
- ³⁴V. Lair, A. Ringuedé, P. Vermaut, S. Griveau *Physica Status Solidi (c)* **2008**, *5*, No. 11, 3492.
- ³⁵C.L. Campos, C. Roldán, M. Aponte, Y. Ishikawa, C.R. Cabrera *Journal of Electroanalytical Chemistry* **2005**, *581*, 206.
- ³⁶S. Lu, J. Pan, A. Huang, L. Zhuang, J. Lu *PNAS (Proceedings of the National Academy of Sciences of United States of America)* **2008**, *105*, No. 52, 20611.
- ³⁷B.Y. Jibrila, N.O. Elbashir, S.M. Al-Zahrani, A.E. Abasaeed *Chemical Engineering and Processing* **2005**, *44*, 835.
- ³⁸O. F. Gorris, L. E. Cadús *Applied Catalysis A: General* **1999**, *180*, 247.
- ³⁹H.-P. Liang, H.-M. Zhang, J.-S. Hu *Angewandte Chemie International Edition* **2004**, *43*, 1540.
- ⁴⁰a) F. Caruso, R. A. Caruso, H. M. K. Hwald *Science* **1998**, *282*, 1111; b) F. Caruso, X. Shi, R. A. Caruso, A. Susha *Advanced Materials* **2001**, *13*, 740; c) Z. Yang, Z. Niu, Y. Lu, Z. Hu, C. C. Han *Angewandte Chemie* **2003**, *115*, 1987; *Angewandte Chemie International Edition* **2003**, *42*, 1943.

- ⁴¹a) Z. Dai, L. DLhne, H. MKhwald, B. Tiersch *Angewandte Chemie* **2002**, *114*, 4191; *Angewandte Chemie International Edition* **2002**, *41*, 4019; b) K. P. Velikov, A. van Blaaderen *Langmuir* **2001**, *17*, 4779.
- ⁴²A. B. Bourlinos, M. A. Karakassides, D. Petridis *Chemistry Communications* **2001**, 1518.
- ⁴³H. T. Schmidt, A. E. Ostafin *Advanced Materials*. **2002**, *14*, 532.
- ⁴⁴a) T. Nakashima, N. Kimizuka *Journal of American Chemical Society*. **2003**, *125*, 6386; b) C. E. Fowler, D. Khushalani, S. Mann *Chemistry Communications* **2001**, 2028; c) X. Gao, J. Zhang, L. Zhang *Advanced Materials* **2002**, *14*, 290.
- ⁴⁵a) S. Schacht, Q. Huo, I. G. Voigt-Martin, G. D. Stucky, F. Schuth *Science* **1996**, *273*, 768; b) D. Walsh, B. Lebeau, S. Mann *Advanced Materials* **1999**, *11*, 324; c) J. Jang, K. Lee *Chemistry Communications* **2002**, 1098.
- ⁴⁶Y. G. Sun, B. Mayers, Y.N. Xia *Advanced Materials* **2003**, *15*, 641.
- ⁴⁷J. Ge, W. Xing, X. Xue, C. Liu, T. Lu, J. Liao *Journal of Physical Chemistry C* **2007**, *111*, 17305.
- ⁴⁸H.-P. Liang, H.-M. Zhang, J.-S. Hu, Y.-G. Guo, L.-J. Wan, C.-L. Bai *Angewandte Chemie International Edition* **2004**, *43*, 1540.
- ⁴⁹Bambagioni, C. Bianchini, J. Filippi, W. Oberhauser, A. Marchionni, F. Vizza, R. Psaro, L. Sordelli, M.L. Foresti, M. Innocenti *ChemSusChem* **2009**, *2*, 99.
- ⁵⁰XRD data were extracted from PDF-2 containing ICDD (International Centre for Diffraction Data experimental powder data collection://www.icdd.com.
- ⁵¹F.-g. Luo, Q.-j. Chen, Z.-l. Yin *Transactions of Nonferrous Metals Society of China* **2007**, *17*, 654.
- ⁵²S. Deabate, F. Fourgeot, F. Henn *Electrochimica Acta* **2006**, *51*, 5430.
- ⁵³S. L. Medway, C. A. Lucas, A. Kowal, R. J. Nichols, D. Johnson *Journal of Electroanalytical Chemistry* **2006**, *587*, 172.
- ⁵⁴A. Roessler, D. Crettenand, O. Dossenbach, W. Marte, P. Rys *Electrochimica Acta* **2002**, *47*, 1989–1995.
- ⁵⁵C.-C. Hu, T.-C. Wen *Electrochimica Acta* **1996**, *41*, 1505.
- ⁵⁶C.-C. Hu, T.-C. Wen *Electrochimica Acta* **1995**, *40*, 495.
- ⁵⁷A. Trovarelli *Catalysis by Ceria and Related Materials* **2002** Catalytic Science Series Vol 2, Series editors: Graham J. Hutchings, Imperial College Press.

⁵⁸T. Yajima, N. Wakabayashi, H. Uchida, M. Watanabe *Chemistry Communications* **2003**, 828.

⁵⁹F. Viguer, S. Rousseau, C. Contenceau, J.-M. Léger, C. Lamy *Topics in Catalysis* **2006**, *40*, 111.

⁶⁰V. Bambagioni, C. Bianchini, J. Filippi, A. Lavacchi, W. Oberhauser, A. Marchionni, S. Moneti, F. Vizza, R. Psaro, V. Dal Santo, A. Gallo, S. Recchia, L. Sordelli *Journal of Power Sources* in press **2010**.

Chapter 4. Technological Applications

4.1 Overview

This short and leaflet chapter shows some power generators for portable electronics developed using the monoplanar DAFCs described in this PhD thesis work.

4.2 Technological applications of a DAFC

The aim of this PhD thesis was the design and development of Pd-based anode electrocatalysts and their use to manufacture MEAs for Direct Alcohol Fuel Cells (DAFCs) in alkaline environment.

The good response observed at room temperature in passive monoplanar cells with ethanol, up to 60 mWcm^{-2} at 0.3 V^1 (vs $\text{Ag/AgCl/KCl}_{\text{sat}}$), makes the present monoplanar cells suitable to fabricate small power generators for portable electronics and first-aid devices (Figure 1). In Figure 1 are shown two technological applications. On the left hand side is shown a device to charge the battery of portable phones constituted by six monoplanar cells each of which releases 0.4 W (0.3 V) for an overall power density of 2.4 W . A single monoplanar cell is sufficient to power three LEDs (left hand side).

Promising results are being obtained by using CeO_2 as promoting metal oxide for Pd, especially in terms of catalyst stability at low current density by virtue of the CeO_2 ability to favour the formation of Pd-OH species at low overpotential. DEFC containing Pd- (CeO_2/C) anodes can reach power densities as high as 64 mWcm^{-2} at 0.2 V (vs $\text{Ag/AgCl/KCl}_{\text{sat}}$)².

As for the use of DAFCs as chemical reactors for the conversion of renewable alcohols into carboxylates, it is worth highlighting the excellent selectivity achieved with ethylene glycol, converted to glycolate³ in DEGFCs with Pd-Ni anodes.



Figure 1. Stack of six DEFCs for recharging a mobile with Pd-(Ni-Zn)/C anode and portable torch DEFC with Pd-(CeO₂/C) anode assembled in our labs (ICCOM-CNR, Florence).

4.3 References

¹C. Bianchini, V. Bambagioni, J. Filippi, A. Marchionni, F. Vizza, P. Bert, A. Tampucci
Electrochemistry Communications **2009**, *11*, 1077.

²Unpublished results.

³V. Bambagioni, M. Bevilacqua, J. Filippi, A. Marchionni, S. Moneti, F. Vizza, C. Bianchini
Chemistry Today **2010**, *28*, 10.

Ringraziamenti

Intendo ringraziare il mio Tutor Dott. Claudio Bianchini e il Dott. Francesco Vizza per l'opportunità che mi hanno dato di svolgere il Dottorato di Ricerca in Scienze Chimiche presso ICCOM-CNR, per la pazienza e la fiducia. Il gruppo di elettrochimica del Prof. Massimo Innocenti e della Prof. Maria Luisa Foresti dell'Università degli Studi di Firenze con cui abbiamo collaborato durante e oltre il presente lavoro. Un caloroso grazie anche ai contributi della Dott. Simonetta Moneti, del Dott. Alessandro Lavacchi e del Dott. Werner Oberhauser.

E passiamo ai ringraziamenti meno formali....GRAZIE agli juniores (spero per poco ancora..) del mio gruppo di lavoro: Andrea, Jonathan, Manuela, Loredana e Yan-Xin. Mi avete sopportata a lungo e solo per questo meritereste un premio!!! Io di voi mi porto i bei ricordi, i congressi, le risate e i balli in lab, la festa di addio al celibato di Andrea, il matrimonio di Manuela, la zuppa gulasch con Jo a Vienna e....per ultima cosa, ma non da meno...la passeggiata sotto la neve sesto-campo marte il 17 dicembre 2010! In verità spero di avere imparato da ogni vostra dote: l'eccellenza di Andrea, la comprensione di Manuela, la serenità di Jonathan e la professionalità di Loredana. Un grazie ai ragazzi non appartenenti al gruppo a partire dai miei "dirimpettai" d'ufficio facendo il giro del piano fino alla stanza dei ragazzi al piano di sotto e a tutti coloro che ho visto passare! Un abbraccio a tutta la segreteria e al portiere...aò! Grazie a Gianna, because she is a very open-minded scientist and woman! Al mio livornese preferito Aldo!

Grazie poi a chi non era con me fisicamente presente al CNR, ma che mi sosteneva da Milano, da Genova o da Grosseto (vedi Jumbo!). Alla mia famiglia acquisita, a NONNA e a mia Cugina, cavallo vincente della scuderia!!! A Laura e anche a chi verrà...a Silvia e tutta la sua emotività...per tutte le cene e lo shiatsu (che non sarà mai abbastanza)! E grazie al CNR, dove ho potuto trovare dei cari amici, persone con cui ho condiviso e condividerò spero ancora per molti anni.....quindi cari Vincenzo (detto il bello-antipatico), Francesco (detto impreveduto), Stefania (lacrima gentile), Carmen (detta allegria) non finisce qui! A Barbara e Antonella un ringraziamento speciale pieno di tutti i momenti di gioia e non trascorsi, delle serate, i week end, lo studio e anche carico di tutti quelli che verranno....Infine grazie all'amore per la chimica che mi ha condotto fino

alla persona con la quale vivo ogni istante della mia vita: a te ogni sforzo per giungere a questo traguardo, per il sostegno impagabile che con generosità mi hai offerto.

E grazie a chi in qualche modo l'amore per la chimica me lo ha scritto nel corredo genetico...e anche economicamente sostenuto....: a Rina e Ivo. In bocca al lupo a tutti voi!!!!

*“La grandezza dell'uomo si misura in base a quel che cerca e all'insistenza con cui egli
resta alla ricerca”*

Heidegger

Valentina Bambagioni curriculum vitae

Personal informations

Bambagioni Valentina

08-09-1982, Italian

Via Platania 4, 58100 Grosseto (Italy)

+39 3493165419

bambagioni_v@yahoo.it

Work experiences

01-01-2008/ 31-12-2010: XXIII cycle of PhD in Chemical Sciences with the projet title “Design and development of Pd-based electrocatalysts for direct alcohol fuel cells: the conversion of renewables into energy and chemicals”. Tutor: Dr. Claudio Bianchini, via Madonna del Piano 10 ICCOM-CNR Sesto Fiorentino (Florence, Italy).

01-09-2007/ 31-12-2007: Grant research around the Tuscany project “EBH2: Elettrobiodrogeno” . Under the scientific responsibility of Dr. Claudio Bianchini, via Madonna del Piano 10 ICCOM-CNR Sesto Fiorentino (Florence, Italy).

01-03-2007/ 31-08-2007: Grant research around the project “Firenze Hydrolab” on “Synthesis of new electrocatalysts for hydrocarbon reforming”. Under the scientific responsibility of Dr. Claudio Bianchini, via Madonna del Piano 10 ICCOM-CNR Sesto Fiorentino (Florence, Italy).

Education and training

15-06-2007: Florence. Qualification of chemist

4-12-2006: Chemistry degree with a valuation of 110/110 cum laude with a title "Synthesis and characterization of transition metal complexes with polyamino-polycarboxylic ligands as NO scavengers". Tutor: Prof. Andrea Bencini, University of Florence.

25-10-2004: Chemistry degree with a valuation of 110/110 with a title " Mono and dinuclear Zinc (II) complexes as hydrolytic agents for dinucleotides" . Tutor: Prof. Andrea Bencini, University of Florence.

June 2001: Degree of scientific High School, Guglielmo Marconi Grosseto (Italy).

Personal skills and competences

Main scientific activities and responsibilities: Synthesis of nano-structured inorganic materials. TEM and SEM characterizations. NMR, IC analysis. electrochemical measurements of fuel cell systems and of electrodes in half-cell. producing of Membrane Electrode Assembling (MEA) for Fuel Cell using.

Mother tongue language: Italian

Other languages:

English -European level B1 (spoken, written, listened)

Computer skills and competences: Office, ChemOffice, Coreldraw, Origin, Kaleidagraph:

Driving licence: B driving licence

Additional informations

22-09-2008: Practical lesson "Tutorial on DAFC assembly". Brixen XIV Scuola Nazionale Scienza dei Materiali.

“6-11”-07-2008: Organizing committee member of the “16th International Symposium on Homogeneous Catalysis ISHC - XVI” congress, Florence.

08-07-2008: ECDL (European Computer Driving Licence) from AICA (Associazione Italiana per l’Informatica ed il Calcolo Automatico).

30-09-2008: THRESHOLD-B1 CERTIFICATE (BRITISH SCHOOL FLORENCE S.r.l.).

2008: Prin project of Prof. Maria Luisa Foresti University of Florence.

25-06-2009: Training course about TEM use CeME-CNR, Florence.

17-02-2010: “Selective processes by homogeneous supported catalysts”. Nano-host ICCOM-CNR, Sesto Fiorentino.

12 e 13-04- 2010: Training course about "Safety in the workplace of the Research" (art. 36 e 37 del Dlgs. 81/08). Sesto Fiorentino.

“20-24-07-2010” : Organizing committee member of the “ISCC-IX” congress, Florence.

December 2010 Training course about SEM use CeME-CNR, Florence.

Annex-Articles

V. Bambagioni, C. Bianchini, J. Filippi, A. Lavacchi, W. Oberhauser, A. Marchionni, S. Moneti, F. Vizza, R. Psaro, V. Dal Santo, A. Gallo, S. Recchia, L. Sordelli “ Single-Site and Nanosized Fe-Co Electrocatalysts for Oxygen Reduction: Synthesis, Characterization and Catalytic Performance”
doi:10.1016/j.jpowsour.2010.11.030.

V. Bambagioni, C. Bianchini, J. Filippi, W. Oberhauser, A. Marchionni, F. Vizza, R. Psaro, L. Sordelli, M.L. Foresti, M. Innocenti. “Ethanol Oxidation on Electrocatalysts Obtained by

Spontaneous Deposition of Palladium onto Nickel-Zinc Materials". *ChemSusChem* 2009, 2, 99 – 112.

V. Bambagioni, C. Bianchini, A. Marchionni, J. Filippi, F. Vizza, J. Teddy, P. Serp, M. Zhiani. "Pd and Pt–Ru anode electrocatalysts supported on multi-walled carbon nanotubes and their use in passive and active direct alcohol fuel cells with an anion-exchange membrane (alcohol = methanol, ethanol, glycerol)". *Journal of Power Sources* 190 (2009) 241–251.

C. Bianchini, V. Bambagioni, J. Filippi, A. Marchionni, F. Vizza, P. Bert, A. Tampucci. "Selective oxidation of ethanol to acetic acid in highly efficient polymer electrolyte membrane-direct ethanol fuel cells ". *Electrochemistry Communications* 11 (2009) 1077–1080.

V. Bambagioni, M. Bevilacqua, C. Bianchini, J. Filippi, A. Marchionni, F. Vizza, L. Q. Wang, P. K. Shen. "Ethylene Glycol Electrooxidation on Smooth and Nanostructured Pd Electrodes in Alkaline Media ". *Fuel Cells* 2010, 4, 582-590.

V. Bambagioni, M. Bevilacqua, J. Filippi, A. Marchionni, S. Moneti, F. Vizza, C. Bianchini. "Direct alcohol fuel cell as chemical reactors for the sustainable production of energy and chemicals". *Chemistry Today* 2010, 28 (3), 7-10.

V. Bambagioni, M. Bevilacqua, C. Bianchini, J. Filippi, A. Lavacchi, A. Marchionni, F. Vizza and P.K. Shen. "Self-sustainable production of hydrogen, chemicals and energy from renewable alcohols by electrocatalysis" *ChemSusChem* 2010, 3, 851-855.

S.P. Annen, V. Bambagioni, M. Bevilacqua, J. Filippi, A. Marchionni, W. Oberhauser, H. Schönberg, F. Vizza, C. Bianchini and H. Grützmacher. "A biologically inspired Organometallic Fuel Cell (OMFC) that converts renewable alcohols into energy and chemicals". *Angewandte Chemie International Edition* 2010, 49, 7229 –7233.

V. Bambagioni, D. Bani, A. Bencini, T. Biver, M. Cantore, R. Chelli, L. Cinci, P. Failli, L. Ghezzi, C. Giorni, S. Pappini, F. Secco, M. Tinè, B. Valtancoli, M. Venturini "Polyamine-

Polycarboxylate Metal Complexes with Different Biological Effectiveness as Nitric Oxide Scavengers. Clues for Drug Design".

J.Med.Chem. 2008, 51, 3250–3260.

L. Wang, V. Bambagioni, M. Bevilacqua, C. Bianchini, J. Filippi, A. Lavacchi, A. Marchionni, F. Vizza, X. Fang, P.K. Shen. "Sodium borohydride as an additive to enhance the performance of direct ethanol fuel cells". Journal of Power Sources 2010, 195, 8036–8043.

Congresses

Vizza F., Bambagioni V., Bianchini C., Marchionni A., Filippi J. "Celle a combustibile stato dell'arte e prospettive" Convegno: Idrogeno quale futuro?" Energetica 2008, Genova 6 March 2008.

Vizza F., Bianchini C., Marchionni A., Bambagioni V., Moneti S. Giambastiani G., Filippi J., A., Psaro R., Dal Santo V., Sordelli L., "Celle a combustibile PEMFCs alimentate con idrogeno prodotto da batteri termofili" 3° Salone dell'Energia rinnovabile e Sostenibile - Energetica 2008, Genova, 6-8 May, 2008.

Valentina Bambagioni, Claudio Bianchini, Jonathan Filippi, Andrea Marchionni, Simonetta Moneti, Francesco Vizza, Vladimiro Dal Santo, Rinaldo Psaro, Laura Sordelli "Energy & chemicals from renewables by electrocatalysis" 16th International Symposium on Homogeneous Catalysis, 6-11 July, Florence 2008.

F. Vizza, C. Bianchini, V. Bambagioni, C. Boscagli, F. Carlà, J. Filippi, M. Innocenti, A. Marchionni, M. L. Foresti "DAFC, Direct Alcohol Fuel Cells, catalizzatori a base di Pd in presenza di ossidi di metalli" SCI Congresso Nazionale Elettrochimica Genova 15-20 June 2008.

Vizza F., Bambagioni V., Bianchini C., Marchionni A., Filippi J. "Prototipo di celle elettrolitiche e celle a combustibile" Festival della Creatività 23-26 October Florence.

Vizza F., Bianchini C., Marchionni A., Bambagioni V., Filippi J., Oberhauser W., A., Psaro R., Sordelli L. "Characterization of Electrocatalysts Obtained by Spontaneous Deposition of Palladium onto Nickel-Zinc Materials for Ethanol Oxidation" Workshop AIDC Federchimica 3 December 2008 Milan.

6th European Workshop on Phosphorous Chemistry (EWPC-6), 26-27 March 2009 Florence.

V. Bambagioni, C. Bianchini, J. Filippi, W. Oberhauser, A. Marchionni, F. Vizza, R. Psaro, L. Sordelli "Characterization of Electrocatalysts Obtained by Spontaneous Deposition of Palladium onto Nickel-Zinc Materials for Ethanol Oxidation" poster at 216th ECS Meeting, Euro CVD 17 and CVD 17, and the 11th International Symposium on Solid Oxide Fuel Cells (SOFC-XI) 4-9 October 2009 Vienna.

V. Bambagioni, C. Bianchini, J. Filippi, P. K. Shen, L. Wang, A. Marchionni, F. Vizza, "An in-depth study of ethylene glycol electrooxidation on Pd-based catalysts in alkaline media: half-cells and passive and active direct ethylene glycol fuel cells" poster at 216th ECS Meeting, Euro CVD 17 and CVD 17, and the 11th International Symposium on Solid Oxide Fuel Cells (SOFC-XI) 4-9 October 2009 Vienna.

V. Bambagioni, C. Bianchini, J. Filippi, W. Oberhauser, A. Marchionni, F. Vizza, R. Psaro, L. Sordelli, M.L. Foresti, S. Moneti, M. Innocenti "Energy and chemicals from renewables by electrocatalysis" poster at 216th ECS Meeting, Euro CVD 17 and CVD 17, and the 11th International Symposium on Solid Oxide Fuel Cells (SOFC-XI) 4-9 October 2009 Vienna.

C. Bianchini, J. Filippi, A. Marchionni, F. Vizza, V. Bambagioni "Selective Oxidation of Ethanol to Acetic Acid in Highly Efficient Polymer Electrolyte Membrane-Direct Ethanol Fuel Cells" oral presentation at 216th ECS Meeting, Euro CVD 17 and CVD 17, and the 11th International Symposium on Solid Oxide Fuel Cells (SOFC-XI) 4-9 October 2009 Vienna.

V. Bambagioni, C. Bianchini, J. Filippi, W. Oberhauser, A. Marchionni, F. Vizza, R. Psaro, L. Sordelli, Simonetta Moneti, Vladimiro del Santo "Energy and chemicals from renewable by electrocatalysis" oral presentation at XXXIII Congresso Nazionale S.C.I. Sorrento 5-10 July 2009

